MECHANISM OF ACTION OF THE ZMAB ANTIBODY COCKTAIL

BY

JONATHAN AUDET

A THESIS SUBMITTED TO THE FACULTY OF GRADUATE STUDIES OF

THE UNIVERSITY OF MANITOBA

IN PARTIAL FULFILLMENT OF THE REQUIREMENTS FOR THE DEGREE OF

DOCTOR OF PHILOSOPHY

DEPARTMENT OF MEDICAL MICROBIOLOGY AND INFECTIOUS DISEASES

UNIVERSITY OF MANITOBA

WINNIPEG

ABSTRACT

Ebola virus (EBOV) causes Ebola virus disease (EVD) in humans. Outbreaks of EVD are sporadic and generally happened in Central Africa. These outbreaks often have mortality rates well above 50%. EBOV was not generally considered a major public health issue. However, between 2013 and 2016, an outbreak of EVD caused approximately 28,000 cases and 11,000 deaths in West Africa. This outbreak highlighted the urgent need for vaccines to stop the spread of outbreaks and treatments to reduce the fatality rates.

We have developed a treatment for EVD based on monoclonal antibodies initially isolated from mice. The first version of this treatment, ZMAb, was able to fully protect cynomolgus macaques when the treatment was initiated 24 h. Further work, carried out in partnership with many groups, has led to the development of ZMapp, which fully protected rhesus macaques when the treatment was initiated as late as 5 days post-infection.

The three antibodies from ZMAb were chosen, not because they were better at protecting mice, but because they were neutralizing and better at protecting guinea pigs. While neutralization is a useful mechanism that should be independent of the species receiving the treatment, it may not be the only, or even the most, important mechanism. Understanding which mechanism is involved in protection, can allow us to draw on existing knowledge to optimize the treatment so the main mechanisms can be made more efficient. Additionally, understanding how the antibodies affect the immune response is crucial in increasing our ability to manage outbreaks efficiently.

Using various knock-out mice, neutralization was confirmed to be the main mechanism. Additionally, by studying the immune response of NHPs which survived their challenge, it is possible to suggest that the antibodies neutralize the virus and slow replication. The production of IL-4 by CD4 T cells and the low response of CD8 T cells on Day 21 suggest an immune response that is skewed towards the T_h2 phenotype.

Overall, the results in mice and NHPs support the hypothesis that the antibodies that compose ZMAb and its derivatives work mostly by neutralization rather than by recruiting cytotoxic responses, whether cell- or complement-mediated.

ACKNOWLEDGEMENTS

I will start by thanking Dr Gary Kobinger. First, for taking me on as a student and second for valuable input and a great deal of patience during the completion of the work presented here. I greatly appreciate the advice you provided during those 7 years.

Dr Xiangguo Qiu also deserves many thanks. We have worked closely together from the time I started working in Special Pathogens. You have been a good (co-)mentor over the years as well. I have greatly appreciated your expertise in all things antibody related.

Thank you to my committee members, Drs Blake Ball, Shawn Babiuk, and Cindi Corbett. You have been very supportive and provided excellent advice over the years.

The work presented in this thesis involves much work in high containment, including mouse and primate studies. Such experiments would have been impossible without the help and assistance of a large number of people. Dr Gary Wong was a great help and contributed much time during those experiments. Your insights are also always appreciated. Drs Alex Bello, Hugues Fausther-Bovendo, and Judie Alimonti were a tremendous help as well with the primate studies and the flow cytometry in high containment.

In addition, so many people helped with the studies presented here, and to produce some of the results, such as IgG titers and blood viremia. They include: Hayian Wei (visiting scientist from Henan CDC), Lisa Fernando, Dr Shihua He, Kevin Tierney, Kaylie Tran.

Also, a big thank you to all the people who provided me with regular support (scientific or moral) over the years: Geoff Soule, Anders Leung, Dr Mable Hagan, Charlene Ranadheera, and everyone else in Special Pathogens. I have enjoyed working with you and hope to continue to do so in the future.

I will also thank my family members, my mother Johanne, father Jean, my brother Mathieu, and my grand-mother Pauline, who have provided much support over the years. It's always great talking to you (and visiting).

Table of Contents

Table of tables

Table of figures

List of abbreviations

ABTS	2,2'-azino-bis(3-ethylbenzothiazoline-6-sulphonic acid)
Ad	Adenovirus
Ad5	Adenovirus serotype 5
ADCC	Antibody-dependent cell-mediated cytotoxicity
APC	Antigen-presenting cell
BCR	B cell receptor
BSL4	Biosafety Level 4
CD	Cluster of differentiation
CDC	Center for Disease Control and Prevention
CDR	Complementarity-determining region
CMT	Complement-mediated toxicity
CSCHAH	Canadian Science Center for Human and Animal Health
CX	Complement component X
DC	Dendritic cell
DMEM	Dulbecco's Modified Eagle Medium
DNA	Deoxyribonucleic acid
D-PBS	Dulbecco's phosphate-buffered saline

DRC	Democratic Republic of the Congo
dsRNA	Double-stranded ribonucleic acid
EBOV	Ebola virus
eGFP	Enhanced green fluorescent protein
ELISA	Enzyme-linked immunosorbent assay
EVD	Ebola virus disease
F_{ab}	Fragment, antigen-binding
FBS	Fetal Bovine Serum
F_c	Fragment, crystallizable
FcγR	Fc γ receptor
GEQ	Genome equivalent
GP	Glycoprotein
HIV	Human Immunodeficiency Virus
HLA	Human leukocyte antigen
HPDI	Highest Posterior Density Interval
HRP	Horseradish peroxidase
ICAM	Intercellular adhesion molecule
IFN	Interferon

Ig	Immunoglobulin
IgG	Immunoglobulin G
IgM	Immunoglobulin M
IL	Interleukin
IP	Intraperitoneal(ly)
IRAD	Innate response antagonist domain
ITAM	Immunoreceptor tyrosine-based activation motif
LB	Luria-Bertani
LD_{50}	Median lethal dose
mAb	Monoclonal Antibody
MAC	Membrane attack complex
MA-EBOV	Mouse-adapted EBOV
MLD	Mucin-like domain
NCBI	National Center for Biotechnology Information
NET	Neutrophil extracellular trap
NHP	Non-human primates
NK	Natural Killer
NML	National Microbiology Laboratory

NP	Nucleoprotein
NPC1	Niemann-Pick C1
OD	Optical density
PBS	Phosphate-buffered saline
PCR	Polymerase chain reaction
PFU	Plaque-forming units
PMO	Phosphorodiamidate morpholino oligomers
rhAPC	Recombinant human activated protein C
RNA	Ribonucleic acid
rNAPc2	Recombinant nematode anticoagulant protein c2
RNP	Ribonucleoprotein
RT-qPCR	Reverse-transcription quantitative polymerase chain reaction
sGP	Solube Glycoprotein
siRNA	Small interfering RNA
STAT	Signal transducer and activator of transcription
TACE	TNF-α—converting enzyme
$TCID_{50}$	Median tissue culture infectious dose
Th	Helper T cell

TIM	T cell Ig and mucin domain
TLR	Toll-like receptor
TMB	3,3',5,5'-tetramethylbenzidine
TNF	Tumor necrosis factor
UTR	Untranslated region
VIC	Viral hemorrhagic fever Immunotherapeutic Consortium
VEEV	Venezuelan equine encephalitis virus
VP	Viral protein
VRP	VEEV replicon particles
VSV	Vesicular stomatitis virus
WHO	World Health Organisation
YMH	Yambuku Missionary Hospital

CHAPTER: 1 INTRODUCTION

1.1 Filovirids

Filovirids (family *Filoviridae*) are mononegavirads (order *Mononegavirales*) with an RNA genome that is monopartite, single-stranded, and negative sense. Their genome follows the basic structure 3'-UTR-N-G-L-5'-UTR of mononegavirads. The family *Filoviridae* includes three genera: *Marburgvirus*, *Cuevavirus*, and *Ebolavirus*. (Kuhn et al., 2013)

The genus *Marburgvirus* includes one species (Marburg *marburgvirus*) which contains two viruses: Marburg virus (type species) and Ravn virus. Multiple variants exist for both viruses, but no naturally-occurring strains have been identified yet. The genus *Cuevavirus* includes only one species (Lloviu *cuevavirus*) which contains one virus: Lloviu virus. This virus was sequenced from the remains of a deceased bat found in Spain, but has not been isolated as live replicating virus. No publications have yet claimed to study a live replication-competent isolate of Lloviu virus produced by reverse genetics.

The genus *Ebolavirus* is the most diverse with 5 established species each containing a single virus: *Reston ebolavirus* (Reston virus), *Tai Forest ebolavirus* (Tai Forest virus), *Bundibugyo ebolavirus* (Bundibugyo virus), *Sudan ebolavirus* (Sudan virus), and *Zaire ebolavirus* (Ebola virus (EBOV) (type species). Most of those viruses have multiple variants, but, as with the marburgviruses, no naturally-occurring strains have been identified. Reston virus has caused outbreaks in macaque colonies in the United States, initially in Reston, Virginia, and the Philippines. (Jahrling et al., 1990; Miranda et al., 1999) Despite those outbreaks, no cases of human disease have been recorded, although there was

serological evidence of exposure in the Reston outbreak. Tai Forest virus is known to have caused a single, non-fatal, human infection in a veterinarian who performed an autopsy on an ape carcass in Côte d'Ivoire. Not much is known about the natural range of Tai Forest virus. Bundibugyo virus has caused one outbreak in the Democratic Republic of the Congo since its discovery in 2008 in Uganda. (Kratz et al., 2015; Towner et al., 2008)

Filovirids received their name due to the unique shape of the virions when viewed by electron microscopy, which consists of a long, narrow, often L-shaped particle. The glycoprotein is the only viral protein on the surface of the particle. For ebolaviruses, the 40 kDa viral protein (VP40) forms the matrix lining the inside of the particle. The VP40 gives the ebolavirus particles their filamentous shape, as *trans* expression of VP40 in cells leads to the release of filovirus-shaped particles. The ribonucleoprotein (RNP) complex formed by the viral genome, L (the polymerase), VP30, VP35, NP (the nucleoprotein), and VP24 proteins has a helical structure tightly packed inside the virus particle.

The glycoprotein is the main target of most vaccines, and of antibody-based therapeutics. It is a trimer with each monomer composed of two subunits, GP_1 and GP_2. The GP_1 subunit forms the core of the receptor-binding domain and contains the mucin-like domain (MLD). This MLD is very large and highly disordered. It also tends to be highly immunogenic with a large fraction of the anti-GP antibodies usually directed against this domain. It is also known to be a Toll-like receptor 4 (TLR4), agonist. (Iampietro et al., 2017; Okumura, Pitha, Yoshimura, & Harty, 2010) In many cases, most of the differences between the *gp* genes of different variants are found within this mucin domain. Most of the mucin-like domain is cleaved off in the endosome to allow receptor binding and membrane fusion. After the

cleavage, the remaining GP_1 binds to the L1 loop of the Niemann-Pick C1 (NPC1) protein, which is normally an endosomal cholesterol transporter. (Krishnan et al., 2012) The GP_2 subunit forms the fusion loops holding GP_1, the stalk, as well as the transmembrane domain and the cytoplasmic tail. Upon receptor binding, the fusion loops, which were wrapped around the core, extend into the endosomal membrane and induce membrane fusion.

Ebolaviruses also produce a large amount of a soluble form of GP (sGP). Under normal circumstances, this is the default gene product of the *gp* gene. (Sanchez, Trappier, Mahy, Peters, & Nichol, 1996) Transcriptional editing needs to occur in order to produce the surface protein, GP. This editing takes place at a site which normally has 7 consecutive uracil residues. Approximately 20% of the time, the viral polymerase will add an additional adenine residue to the positive sense RNA yielding the full-length GP. A third transcript can be produced by the addition of 2 adenines, leading to the small secreted GP (ssGP). (Mehedi et al., 2011)

1.2 Ebola virus

1.2.1 History

The first recognized outbreak of Ebola virus disease (EVD) caused by Ebola virus happened in Sudan from June to November of 1976. (World Health Organisation, 1978) During the outbreak, approximately 284 cases were recognized, 151 of which died from the disease (53% case fatality). While the Sudan outbreak was still ongoing an outbreak with patients presenting with similar disease occurred in the Democratic Republic of the Congo (DRC; then Zaire). (Burke, Declerq, & Ghysebrechts, 1978) It would be demonstrated that the two outbreaks were caused by the same agent, Ebola virus. However, subsequent work by

Sanchez et al published in 1996 used the nucleotide sequences of the *gp* gene for the viruses of all outbreaks to date to establish a phylogenetic tree of Ebolaviruses. (Sanchez et al., 1996) Their work suggests that the viruses isolated from the two outbreaks were quite different.

Reports from the first two outbreaks suggest a disease course more predictable and more aggressive than the already-known Marburg virus (discovered in 1967). The main reason for the spread of the disease was suspected to be close contact with (especially nursing of) an infected patient. The normal practice at the epicenter of the Zaire outbreak, Yambuku Missionary Hospital (YMH), was to issue nurses and doctors 5 syringes/needles per day for use in the outpatient clinic, inpatient wards, and the prenatal clinic. The syringes/needles appeared to have been the major method used for administration of drugs at YMH and were rinsed in warm water between patients. Eventually, staff at YMH became ill, with the mission eventually closing due to lack of personnel. The outbreak in Zaire ended a few weeks later.

The report from Sudan also describes extensive transmission to hospital staff and patients.

The next major outbreaks of EVD occurred in Gabon, from the Fall 1994 to early 1997, in three outbreaks.(Georges et al., 1999) The first outbreak started in early December 1994 in gold-panning camps, a total of 49 individuals were infected, with the last case occurring in February 1995. The second outbreak occurred in the spring of 1996, approximately half-way between Makokou and the gold-panning camps where the first outbreak started, 18 people skinned and chopped a chimpanzee cadaver, five of them died. The first cases of the third outbreak were found in October 1996 and the last case was declared on 18 January

1997, with the outbreak declared over in March 1997. The third outbreak caused a total of 60 cases and 45 fatalities.

The next outbreak occurred in DRC in 1995, in what would be the largest outbreak of EVD for the next 19 years. The index case was treated at the Kikwit General Hospital and lead to 13 secondary and tertiary cases, all of whom died. (Khan et al., 1999) By the end of March 1995, many cases of EVD had occurred among patients and staff at both Kikwit II and Kikwit General Hospital. The outbreak then spilled over into the community leading to a total of 315 cases with a reported fatality rate of 81%. The number of nosocomial cases diminished rapidly after the institution of barrier-nursing measures, with only 1 healthcare provider becoming infected. The last case of the outbreak occurred on 16 July.

In the end, the Kikwit outbreak will turn out to be the most lethal outbreak to healthcare providers, as they represented 25% of all cases. While the outbreak was amplified in a hospital, as with the original outbreaks in Sudan and Yambuku, the report mentions that little or no needle reuse occurred in Kikwit II and Kikwit General. This outbreak showed that the attack rate of healthcare workers could be dramatically reduced with proper use of barrier-nursing.

Three separate outbreaks occurred between November 2001 and December 2003 in the Republic of the Congo. Previous outbreaks in Zaire occurred in what is now the DRC. The first outbreak to occur in the Republic of the Congo happened in the region neighboring on Gabon, Cuvette Ouest. (World Health Organization, 2003)

A total of 124 cases (37 laboratory-confirmed) were reported between October 25th, 2001 and March 18th, 2002 in both Gabon and Congo, as the outbreak zone overlapped both

countries. Of all the cases, 97 succumbed to the infection leading to a case fatality rate of 78%.

In December of 2002, a large number of non-human primate and duiker carcasses were found in the districts of Kéllé and Mbomo.(Formenty et al., 2003) By the end of December the CIRMF had confirmed that the animal deaths were due to EBOV. The first human case with symptoms similar to EVD was reported on 21 January 2003.

A new strategy was developed to deal with this outbreak. In the past, the isolation wards were completely walled off from the community and disposal of the bodies of deceased individual was done by cremation. These practices lead to accusations that the medical teams were murdering isolated individuals and the burial practices did not fit well with traditional practices. The outbreak management team recruited members from the communities and from the local Red Cross groups to disseminate public health information, such as symptoms and methods of prevention. They also collaborated with anthropologists to develop isolation and burial practices that would be acceptable to the local populations.

The outbreak was declared over on 7 May 2003, with a total of 143 cases (13 confirmed) and 128 dead.

The third outbreak was declared on November 7th 2003 and the last death was reported on December 3rd 2003. In total there were 35 cases and 29 deaths. (World Health Organization, 2004)

An outbreak started in April of 2007 in the village of Kampungu, DRC. (ProMED-mail, 2007) The outbreak was declared over on 13 November 2007. A total of 264 suspected cases were found, 187 of which are believed to have died from EBOV.

Historically, outbreaks of EVD counted a few hundred cases at most. Many other infectious diseases cause far more cases, and casualties (directly or indirectly), every year. For example, in the year 2000, according to data from the World Health Organization (WHO), there were 77,642 reported deaths due to malaria out of approximately 7.8 million cases, in Africa alone. (World Health Organization, 2015) EBOV and the other filoviruses are relatively minor public health issues by comparison. However, many of the diseases which cause large numbers of cases and deaths in Africa are zoonotic and do not spread well from human to human. There are exceptions, like the Human Immunodeficiency Virus (HIV). Filoviruses are introduced into the population in a zoonotic event, often the consumption of bushmeat, but are then able to spread from human to human. The outbreaks of filoviral diseases also cause very high mortality; on the other hand, the mortality rate of malaria in Africa is about 1%. The main issue has centered around the fear that the filoviruses, including EBOV, do not really have any biological limits to spreading in a human population and, therefore, could cause much larger outbreaks with far more fatalities than zoonotic diseases. A large outbreak of EVD would also have another major consequence, as EBOV is highly virulent, it diverts resource from normal healthcare infrastructure into emergency care and isolation of cases. These resources are not available to deal with less unusual health issues, such as HIV and malaria, thus increasing the indirect loss of life due to the outbreak.

After the 2001 attacks on the World Trade Center, followed, the next week, by the mailing of Anthrax spore-containing letters, bioterrorist attacks became a concern of many governments worldwide. Filoviruses were considered prime pathogens for use in such attacks, as, even if the number of cases were small, the shock effect from the occasional hemorrhage they cause would cause panic. It was in that context that both the United States Department of Defence, and Canada's Department of National Defence started funding research into countermeasures (vaccines and treatments) against filoviruses.

The fears of a large natural outbreak turned into reality in July of 2014. An outbreak of EVD, which had started in Guinea in December 2013, had already spread to neighbouring Sierra Leone and Liberia. The original outbreak had taken the filovirus research community by surprise as all previously recorded outbreaks of EVD due to EBOV happened in Central Africa. By the end of July 2014, according to WHO data collated by the CDC, there had been a total 460 confirmed/probable/suspected cases in Guinea, 329 cases in Liberia, and 533 cases in Sierra Leone. At this point, this outbreak was already the largest outbreak of EVD ever recorded in both the number of cases and the geographical region it affected. By the time the outbreak ended, there would be 28,616 confirmed/probable/suspected cases, including 15,227 laboratory-confirmed cases and 11,310 deaths. All of these numbers only account for the three main countries affected and cases that could be counted, as there was breakdown of the health infrastructure in at least some of the countries. Seven other coutries would face imported and locally acquired EVD cases: Nigeria (20), Senegal (1), Spain (1), the United States (4), Mali (8), the United Kingdom (1), and Italy (1).

Overall, the outbreak highlighted the lack of advanced development–stage vaccines and countermeasures against EBOV. As the outbreak peaked in the fall of 2014, governments, non-governmental organizations, private companies, and the WHO rallied to develop a framework for accelerated clinical testing of vaccines and countermeasures. A number of clinical trials were carried out in Europe and the United States for the initial evaluation of safety of a number of vaccines and treatments. A ring-vaccination trial for the rVSV-ZEBOV vaccine would start recruiting at the end of March 2015 until the end of January 2016. The final report, published in December 2016 reported that the vaccine was 100% efficacious in the context of the trial. (Henao-Restrepo et al., 2017) Over a similar period, March to November 2015, the PREVAIL II trial recruited infected individuals to test the efficacy of a treatment called ZMapp. The final report, published in October 2016, reported that the posterior probability that ZMapp was superior to standard of care was 91.2%. (PREVAIL II Writing Group et al., 2016)

1.2.2 Transmission

It is widely accepted that outbreaks of EVD have a zoonotic origin. The exact nature of the reservoir remains unknown. In some instances, individuals who assisted in the butchering of deceased primates were known to become infected with EBOV. (Georges et al., 1999) In one other instance, wildlife was found to have died off just before an outbreak, with some carcasses confirmed to have infectious EBOV. (Formenty et al., 2003)

Spread between humans has also not been completely elucidated. The most frequent transmission route appears to be contact with bodily fluids, including blood, sweat, and semen(Feldmann & Geisbert, 2011). In outbreaks between 1976 and 1995, attending

physicians and nurses were at very high risk of infection due to close contact with patients. The institution of barrier nursing practices dramatically lowered the risks faced by healthcare staff. During the West Africa outbreak, failure to maintain proper barrier nursing also resulted in healthcare staff being infected in large proportions. Such failures were also likely responsible for some of the transmission chains in developed nations, such as the nurses infected in Texas.

The question of whether EBOV can spread through some form of airborne or aerosol or droplet transmission remains open for debate. (Weingartl et al., 2012) In almost all outbreak cases, some physical contact with bodily fluids or with a surface previously contaminated by bodily fluids can be established. (Roels et al., 1999) Recent experiments using NHPs successfully infected the animals by artificial generation of aerosols. (Jaax et al., 1995; Twenhafel et al., 2013) On the other hand, naïve and infected NHPs in cages that were approximately 0.3 m apart did not provide evidence of transmission. (Alimonti et al., 2014) The most likely scenario is that while aerosols (or droplets) containing otherwise infectious EBOV are indeed infectious, actual infections do not lead to the production of aerosols. This is partly supported by few symptoms that lead to the formation of fine droplets and aerosol such coughing and sneezing; although such symptoms have been observed in pigs. (Nfon et al., 2013) The overall conclusion appears to be that, during an outbreak, EBOV is very unlikely to spread via airborne routes.

1.2.3 Symptoms and clinical manifestation

Once exposed, individuals may start to develop symptoms within 2 to 21 days. (Centers for Disease Control and Prevention, 2014) Many of the symptoms are non-specific.(Burke et

al., 1978; Gatherer, 2014; World Health Organization, 2003) Cases initially present with flu-like symptoms including fever, weakness, headache, muscular pain. This may be accompanied, or followed, by diarrhea and vomiting.

As the disease progresses, signs of coagulopathy become more evident. Survivors tend to have milder coagulation defects, such as conjunctival bleeding and failure to clot after venipuncture. (Mahanty & Bray, 2004) Survivors will start to show improvement around 7-10 days after the onset of symptoms.

Fatal cases may show much more severe signs, such as bloody diarrhea and urine, gingival bleeding, and morbiliform rashes.(Burke et al., 1978; Mahanty & Bray, 2004) As the virus infects hepatocytes, signs of liver damage, such as elevated serum alanine aminotransferase and aspartate aminotransferase, begin to appear.(Burke et al., 1978; Geisbert, Young, Jahrling, Davis, Larsen, et al., 2003) Lymphopenia and thrombocytopenia are also often present in fatal cases. Lymphopenia appears to be due to, at least partially, to the death of lymphocytes during severe disease. (Iampietro et al., 2017)Thrombocytopenia arises from, among other factors, the increased expression of tissue factor on macrophages and monocytes.(Geisbert, Young, Jahrling, Davis, Kagan, et al., 2003) This leads to increased blood clot formation and to disseminated intravascular coagulopathy. Eventually, loss of blood volume and the development of a cytokine storm—the uncontrolled production of large amounts of cytokines by immune cells—lead to death.

1.2.4 Life cycle

Infection of a new cell starts with the virus attaching to the cell surface via one of multiple receptors. The glycoprotein is able to interact with many lectin-binding proteins through

its mucin-like domain. For example, both DC-SIGN (dendritic cell-specific ICAM-3 grabbing non-integrin) and TIM-1 (T cell Ig and mucin domain 1) can be used by the virus as receptors or co-receptors.(Alvarez et al., 2002; Kondratowicz et al., 2011) The virus is taken into the cell by macropinocytosis as well as clathrin-mediated endocytosis.(Aleksandrowicz et al., 2011) At this point the mucin-like domain of GP and a fraction of GP_1 is cleaved off by proteases in the late endosome.(Bornholdt et al., 2016; Marzi, Reinheckel, & Feldmann, 2012) This exposes the NPC1-binding region.(Bornholdt et al., 2016; Wang et al., 2016) Once the GP_1 binds to NPC1, the fusion loops of GP_2 extend into the endosomal membrane and induce fusion.(Watanabe et al., 2000) Gene transcription requires the interaction of NP (bound to the genome), VP35, L, and VP30.(E. M. Mühlberger, Weik, Volchkov, Klenk, & Becker, 1999) The VP35 links NP and L to allow the polymerase to interact with the genome.(E. Mühlberger, 2007) Ebola virus also requires the participation of VP30, although its precise role remains unclear. It is suspected that this role is either to assist with the initiation of transcription or to prevent early termination. Marburg virus is able to perform the transcription and replication phases with only the NP/VP35/L complex, which is more in line with most nonsegmented negative-strand RNA viruses. In both cases, the transcription generates seven monocistronic mRNAs which are capped and polyadenylated by L. The quantity of each mRNA produced in inversely proportional to its location (in the 3' to 5' orientation), with NP having the most mRNA and L the least. Additionally, the polymerase slips in the transcription of the *gp* gene of EBOV (but not Marburg virus) to switch from producing the sGP to the full-length GP.(Mehedi et al., 2011) It has also been found that VP40 and VP24, respectively the major and minor matrix proteins in EBOV, also affect transcription and replication, generally reducing both

as their concentration increases.(Hoenen, Jung, Herwig, Groseth, & Becker, 2010) This is probably used to switch from replication/transcription to packaging and budding. The genome binds with NP and coils itself. VP40 can oligomerize to form rafts underneath the plasma membrane. As the genome-NP interacts with VP35 and VP24, it is directed to the plasma membrane where it interacts with VP40 for packaging. It is actually possible for multiple genomes to be packaged in a single viral particle.(Beniac et al., 2012) The virus then buds and is released to infect a new cell.

1.2.5 Immune evasion

As reviewed in (Audet & Kobinger, 2015), EBOV uses two main methods to escape the immune response. The first mechanism consists of preventing the production of and signaling by interferons (IFNs). The second mechanism uses both the GP and sGP to divert the immune system towards irrelevant targets.

The VP35 protein has been shown to have two important sites for immune suppression in its N-terminal domain. The VP24 protein also has an immunosuppressive site. These sites were termed innate response antagonist domains (IRADs) by Lubaki et al. (Lubaki et al., 2013) The term was suggested because not all three sites are strong suppressors of IFNs, but they all suppress the innate response.

The VP35 has two IRADs, the first is a double-stranded RNA (dsRNA) binding site, the second is a site that can recognize the ends of dsRNA and cap them. The VP35 thus effectively “hides” the dsRNA phases of the virus life cycle, preventing activation of cell defenses such as RIG-I and PKR. (Kimberlin et al., 2010; Leung et al., 2010) The VP24 IRAD has been shown to bind karyopherin-α2 and sequester it to the cytoplasm. Karyopherin-α2

is needed for phosphorylated signal transducer and activator of transcription 1 (STAT1) to be translocated to the nucleus and function as a transcription factor. This prevents the signal from receptors of Type I and II interferons from reaching the nucleus.

The second mechanism for immune evasion is centered around the products of the *gp* gene. The main product, sGP, is secreted in large quantities. It has been shown by Mohan et al to be able to subvert the anti-GP antibody response. (Mohan, Li, Ye, Compans, & Yang, 2012) The sGP does this by being both similar and different from GP. The similarity allows it to bind many of the antibodies directed against the full GP, and since it is present in large quantities, these antibodies will more often bind sGP than GP. The large quantity of sGP also means that B cells which react to it will be expanding to the detriment of B cells specific to GP. The large amount of it, combined with the differences with GP means that it also focuses the antibody response against epitopes not found on the full-length GP.

The other product of the *gp* gene is the full-length spike protein GP (or $GP_{1,2}$). This protein is also involved in immune evasion. First, due to the size of the mucin-like domain, it is able to hide many other proteins on the surface of the cells, including the human leukocyte antigen (HLA-)A, B, and C thus preventing T cells from being activated by infected cells. (Francica et al., 2010) Second, Kühl et al have shown that the GP_2 subunit is able to sequester tetherin into the endoplasmic reticulum, preventing it from interfering with virus budding. (Kühl et al., 2011) Finally, the mucin-like domain is highly immunogenic and less restricted than the rest of the protein, meaning that it can easily accumulate mutations to escape antibody responses.

Another mechanism was recently established. This mechanism represents both a way of escaping the immune system and of causing disease. It had been reported that T cells underwent apoptosis; however, the mechanism by which this happened was not clear. (Bray & Geisbert, 2005) A publication in 2017 suggests that EBOV can activate T cells through their TIM-1 receptors using the phosphatidylserine on the surface of the virus. (Younan, Iampietro, & Nishida, 2017) Signaling through TIM-1 activates T cells in a non-specific manner. This activation of T cells leads to the production and secretion of cytokines, resulting in the "cytokine storm" phenomenon often observed in late stage filovirus infections. Another way EBOV interacts with T cells is by the binding of GP to the TLR4 this activation leads to T cell death by apoptosis and necrosis. (Iampietro et al., 2017)

1.3 Countermeasures against Ebola virus

1.3.1 Vaccines

The first attempt at developing a vaccine against EBOV was published in 1980. (Lupton, Lambert, Bumgardner, Moe, & Eddy, 1980) Lupton et al vaccinated guinea pigs with one or two doses of heat-inactivated or formalin-fixed virus and challenged them 21 days post-immunization or post-boost with 10^4 plaque-forming units (PFU) of EBOV. All vaccinated animals survived while 4 of the 14 controls succumbed to the infection. Attempts to use inactivated vaccines in hamadryad baboons were made in Russia in 1994, but met with, at best, partial success. (Mikhaĭlov, Borisevich, Chernikova, Potryvaeva, & Krasnianskiĭ, 1994)

In 2002, Geisbert et al tested a number of vaccine platforms in non-human primates (NHPs). (Geisbert et al., 2002) Two platforms used inactivated EBOV, either alone or encapsulated in lipid A-containing liposomes. The other two were newer, at least in the

filovirus field, consisting of either Venezuelan equine encephalitis virus (VEEV) replicon particles (VRPs) expressing the EBOV GP and/or NP or of recombinant Vaccinia Virus expressing the EBOV GP. The only immune response reported was virus neutralization. Only animals receiving inactivated virus, with or without lipid A, had neutralizing titers. The authors tested vaccines (not all) in both cynomolgus and rhesus macaques. No cynomolgus macaque survived the challenge, whether vaccinated with VRP-based vaccines, Vaccinia-based vaccines, or inactivated virus (with or without lipid A). One of the two rhesus macaques vaccinated with inactivated virus (no lipid A) did survive the challenge. All control animals, cynomolgus and rhesus, died.

Starting in 1998, a different strategy started to take shape. Xu et al vaccinated guinea pigs with DNA plasmids encoding either the nucleoprotein, the secreted glycoprotein, or the transmembrane glycoprotein. (Xu et al., 1998) They tested two vaccination schedules, the first with vaccines on days 0, 14, 28, 42 and challenge on day 62 and the second with vaccines on days 0, 14, 42, 112 and challenge on day 122. In the first schedule all control-vaccinated animals died, while all the GP- and NP-vaccinated animals survived. The sGP-vaccinated group showed partial protection (5 of 6 survivors). The only experimentally vaccinated animal to succumb to infection had pre-exposure enzyme-linked immunosorbent assay (ELISA) titers of 1:1600, although the antigen is not specified. All the survivors had pre-exposure ELISA titers of at least 1:6400, with some going over 1:25600. The second group (with challenge at day 122) is more informative as to the ELISA titer required for protection. In the GP (3 of 5 survivors) and sGP (3 of 5 survivors) groups, animals with titers below 1:2560 did not survive, and 1 of 3 animals (combined) with titers of 1:2560 survived. All animals with higher titers survived. For the NP-vaccinated group,

only 1 of 4 animals survived, with undetectable ELISA titers. The authors used mixed leukocyte reactions and thymidine incorporation assays to show that the vaccines also elicited T cell responses against the antigens expressed by the plasmids. Due to the nature of the assays requiring spleen removal, they could not be performed on animals that were going to be challenged.

Following in the footsteps of Xu et al, Sullivan et al showed that three plasmid injections (expressing GP) followed by a boost using the human Adenovirus serotype 5 (Ad5) (also expressing GP) could fully protect the 4 cynomolgus macaques that were vaccinated. (Nancy J Sullivan, Sanchez, Rollin, Yang, & Nabel, 2000) Also, a subsequent paper in 2003 showed that a single dose of Ad5-based vaccine alone, expressing both GP and NP, could protect all vaccinated animals. (Nancy J Sullivan et al., 2003) They also showed that, after 28 days, the vaccine induced both antibody production and production of interferon-γ (IFN-γ) from CD8, but not CD4, T cells. These vaccination strategies, in 2000 and 2003, were the first successful vaccinations of NHPs.

In 2005, Jones et al published results showing that using a Vesicular stomatitis virus (VSV) vector, expressing the EBOV GP instead of the VSV G surface protein, could also fully protect NHPs after a single vaccination. (Jones et al., 2005) The VSV vaccine was an attenuated live virus vaccine. The vaccine could still replicate and grow despite having to use a foreign surface antigen, but the growth was much slower and to lower titer than wild-type VSV. This vaccine was facing more potential regulatory issues than the adenovirus-based vaccines. VSV is a pathogen of cattle and causes a disease that resembles Foot and Mouth Disease, which is responsible for economic losses. Some strains of VSV could also be

lethal to cattle. The main worry centered on whether the vaccine could cause disease in cattle and whether it would be shed by vaccinees. A new success for the VSV-based vaccine came in 2007 when Feldmann et al published results showing that the vaccine protected 4 of 8 animals when administered within 30 minutes of infection in a challenge model which normally resulted in 100% lethal disease. (Feldmann et al., 2007) The VSV vaccine also had an important advantage: the Adenovirus serotype 5 used in most Ad-based vaccines is a human adenovirus with high levels of pre-existing immunity in the human population. (Abbink et al., 2007; Nwanegbo et al., 2004) On the other hand, since VSV did not cause (much) disease in humans, pre-existing anti-vector immunity was low. Also, neutralising anti-VSV antibodies would be directed against the VSV G which was not present in the vaccine. (Xiangguo Qiu et al., 2009) During the outbreak of EVD in West Africa, the VSV vaccine would be found to be 100% effective in a ring-vaccination trial. (Henao-Restrepo et al., 2017)

Overall, the VSV vaccine holds great promise to stop outbreaks; its protection appears to set in quickly, in the vaccinated groups of the ring-vaccination trial, no cases emerged more than 7 days post-vaccination. Although, its safety and side-effect profile may prevent the VSV vaccine from being a common or wide-spread vaccine. Early results presented at conferences suggest that the protection may also not be long-lasting after a prime. It is likely that different strategies will emerge with a rapid-onset vaccine like VSV-Ebola used during outbreaks and a different vaccine (such as an adenovirus-based vaccine) used for laboratory and some healthcare workers at risk of occupational exposure, where a longer vaccination schedule with multiple boosts would be acceptable and provide long-lasting immunity.

1.3.2 Correlates of protection

The development of vaccines against EBOV has also triggered the search for correlates and surrogates of protection. Using the definitions developed by Stanley Plotkin (Plotkin, 2010), a correlate of protection is a parameter, such as ELISA titer or IFN-γ production by T cells, which can be measured and is responsible for the protection provided by vaccines. A surrogate of protection is a parameter similar to a correlate, but where the causal link with protection has not been established yet or does not exist at all. The latter case implies that a parameter can correlate mathematically, even very well, with survival but is not the cause of survival; such a parameter is still useful as a purely predictive parameter rather than explicative.

A correlate (or surrogate) of protection would be immensely useful as human clinical trials cannot use the vaccinate-challenge protocol for EBOV. This raises the issue that the best correlate we can develop will come from NHPs, and there is no guarantee that these correlates will hold in humans. Until the clinical trials carried out during the EVD outbreak in West Africa, we did not even know whether vaccines that are protective in NHPs are truly protective in humans. Also, given that only a few trials were able to accrue enough patients or potential cases, the data relating NHP to human efficacy remains sparse. On the other hand, correlates (and surrogates) derived from NHP studies remain the best attempt that can be made at finding a human correlate of protection.

One of the first attempts to summarize the then-known information was made by Sullivan et al (N J Sullivan, Martin, Graham, & Nabel, 2009), going back over data they accumulated from NHP studies, they suggested that immunoglobulin G (IgG) titers above 1:3,700

correlated with all animals surviving. Unfortunately, at titers of 1:3,700 or less, IgG titers alone could not explain all the variation in survival as a number of animals had similar titers but different outcomes. Subsequent work by the same group suggested that IFN-γ production in CD8 T cells were a correlate of protection for their Ad5-based EBOV vaccine. (Nancy J Sullivan et al., 2011)

Given the complexity of immune responses and that the tools we have to experimentally manipulate complex organisms remain blunt, for example knocking out (in mice) or depleting (in NHPs, as Sullivan did) entire cell types, it would be more useful to search for surrogates of protection. An experiment looking for surrogates of protection would not need to eliminate different responses but simply establish a model where the vaccine is partially protective. Then measuring the pre-challenge immune parameters and assessing how well one or more predict survival would provide useful data that could probably be used in human studies.

Such an attempt was made in 2012 by Wong et al. (Wong et al., 2012) They gathered data from multiple NHP studies which used different vaccines and looked for differences in pre-challenge immune parameters between survivors and non-survivors. In many cases, measurements of the IgG response predicted perfectly, or near-perfectly, the survival of the animals; although, neutralizing antibody measurements could not be correlated with survival.

A number of studies were published in 2012 showing that combinations of monoclonal antibodies (mAbs) or purified polyclonal antibodies could protect NHPs in a post-exposure passive transfer setting. (Dye et al., 2012; Marzi, Yoshida, et al., 2012; Olinger et al., 2012;

Xiangguo Qiu, Audet, et al., 2012) These experiments suggest that, in many cases, antibodies may not simply be a surrogate of protection, but a correlate as the treated animals did not have pre-existing immunity to EBOV.

A more recent study also showed that IgG responses were predictive of survival in mice. (Lennemann et al., 2017) The mice were immunized with varying doses of VSVΔG-EBOVGP pseudovirions, bearing a GP with wild-type glycosylation or partially or fully deglycosylated. The authors showed that the survival was dose-dependent, in both prime and prime-boost settings, and that the antibody response was also dose-dependent for all versions of the vaccine tested. They found that the average anti-GP IgG level explained 92% of the survival variation between the groups.

1.3.3 Treatments

1.3.3.1 Immunotherapy

The first attempt to use immunotherapy was carried out in Russia. In 1994, Krasnianskĭĭ et al reported the production of equine hyperimmune serum. (Krasnianskiĭ et al., 1994) In 1995, Borisevich et al described the fractionation of the serum into IgG and reported that it protected 100% of hamadryad baboons exposed to Ebola virus.(Borisevich et al., 1995)

The next use was by Mupapa et al during the 1995 Kikwit outbreak in DRC. (Mupapa et al., 1999) They treated 8 individuals fitting the case definition for EVD and positive for EBOV antigen in the serum with whole blood taken from 5 survivors with anti-EBOV IgG and no detectable antigen. Only 1 of the 8 patients died compared with a fatality rate of 80% for the outbreak overall. It is interesting to note that the individual who succumbed to the infection was treated at the earliest of the 8, this suggests that the other 7 may have already

been past the most lethal time of the disease. There were some issues with the study, including the very small sample size, the absence of any blinding or control group, and, as noted by the authors, that the patients receiving survivor whole blood received better care than others during the outbreak.

In 1996, Jahrling et al reported results from testing a commercially available IgG from horses hyperimmunized against EBOV in cynomolgus macaques. (Jahrling et al., 1996) They observed a slight delay in time to death with the controls dying on Days 6, 6, and 7 whereas the treated animals died on Days 7, 7, 8, 8, 8, and 8. They concluded that higher specific activity and/or better pharmacokinetics would be needed for this approach to work for humans.

In 2002, Parren et al used a neutralizing monoclonal antibody (mAb) (KZ52) isolated from a human survivor of EVD by phage panning to protect guinea pigs pre- and post-exposure. (Parren, Geisbert, Maruyama, Jahrling, & Burton, 2002) This antibody protected 4 of 5 guinea pigs when administered 1 day post-infection. When Oswald et al attempted to use the same mAb to treat NHPs, the results were not as encouraging. (Oswald et al., 2007) The animals were treated with KZ52 on Days -1 and 4. All 4 animals died with 3 animals dying on Day 7 and one on Day 11. Few studies were published afterwards which looked at using antibodies, monoclonal or otherwise, to treat EBOV infections.

In 2012, four independent groups published separate studies showing the protective efficacy of post-exposure antibody treatment. The first study, published in March 2012, showed that polyclonal IgG purified from rhesus macaques which survived an EBOV challenge could protect (3 of 3 survivors) non-immunized macaques against a lethal

challenge when administered 48 h after exposure. (Dye et al., 2012) Similar results were obtained for Marburg virus.

The second study, published in April 2012, was the first to use a combination of neutralizing mAbs (2 in this case). (Marzi, Yoshida, et al., 2012) The mAbs were chimeric antibodies, derived from immunized mice, the variable regions—responsible for binding to the target—were grafted onto the constant regions of human IgG1 by genetic engineering. Three animals received 50 mg of both antibodies (25 mg of each) on Days -1, 1, and 3. One of the animals survived. While this experiment shows partial success the dose was quite low, the weight and age of the animals were not specified, but for the dose to be comparable to other studies, the animals would have had to weigh 2 kg or less.

The third study, published by our group in June 2012 used a combination of three mouse antibodies (called ZMAb) to treat animals starting at 24 h (N = 4) or 48 h (N = 4). (Xiangguo Qiu, Audet, et al., 2012) The treatment dose was 25 mg/kg of mAbs (combined; 8.33 mg/kg/mAb) and the animals received a total of 3 treatments separated by 72 h (Days 1, 4, 7 or 2, 5, 8). All animals receiving ZMAb at 24 h survived the challenge, while two animals who started treatment at 48 h succumbed to the infection. One of the animals treated at 24 h had no detectable viremia by RT-qPCR and only one of the three animals which were positive had detectable virus by median tissue culture infectious dose ($TCID_{50}$). All four animals which received their first treatment at 48 h had detectable virus with only one not having infectious virus by $TCID_{50}$.

The fourth study was published in October 2012 and showed that a combination of three chimeric antibodies (called MB-003) could protect 2 of 3 animals when treatment started

at 48 h. (Olinger et al., 2012) The treatment dose was double that of ZMAb (16.7 mg/kg/mAb) with treatments on Days 2, 6, 8, and 10. Viremia could be detected by reverse-transcription quantitative polymerase chain reaction (RT-qPCR) in all three animals, but none had detectable infectious virus in a plaque assay.

We continued to develop the ZMAb treatment in 2013, showing that a combination of an adenovirus carrying a consensus human IFN-α gene (DEF201) and ZMAb could protect 3 of 4 cynomolgus macaques when the treatment started at 72 h and 2 of 4 macaques when DEF201 was administered at 24 h and ZMAb treatment started at 96 h. (Xiangguo Qiu et al., 2013) Also, the protection of the 72 h treatment combination was 100% (4 of 4) in rhesus macaques.

Around the same time, Pettitt et al showed that MB-003 was able to protect 3 of 6 animals when treatment was initiated after 2 triggers. (Pettitt et al., 2013) The treatment was only initiated after a positive blood RT-qPCR assay for EBOV and fever as detected by telemetric probes.

In 2014, a decision was made to try and combine MB-003 with a chimerized version of ZMAb. MB-003 contained the chimeric antibodies: c13C6, c6D8, and c13F6. ZMAb contained the mouse antibodies: 1H3, 2G4, and 4G7. An initial NHP study of the individual components of MB-003 revealed that protection was almost entirely due to the c13C6 component. (X. Qiu et al., 2014) The components of ZMAb were chimerized (to human IgG1 constant chains) and produced using the same tobacco-based system as MB-003. Further characterization of the various 3-component combinations of c13C6, c1H3, c2G4, and c4G7

in guinea pigs identified two potential cocktails with high protective efficacy: c13C6 + c2G4 + c4G7, and c13C6 + c1H3 + c2G4.

A study comparing both cocktails (N = 6 each) in rhesus macaques showed that the first combination protected 6 of 6 animals while the second protected 5 of 6 animals. Thus, the first combination (c13C6 + c2G4 + c4G7) was named ZMapp and tested for protection at different time points post-exposure. ZMapp was able to protect all animals when treatment started at 72, 96, or 120 h.

1.3.3.2 Other treatments

A number of other treatments have been evaluated for EBOV. One of the first non-IgG-based treatments was the use of IFN-$\alpha 2b$. (Jahrling et al., 1999) Jahrling et al gave 4 cynomolgus macaques daily injections of IFN-$\alpha 2b$ starting 18 h after exposure. The animals died approximately 1 day later, on average, than the 3 controls, suggesting little effect of Type I IFNs on the course of disease.

Another attempt at treatment aimed at preventing the coagulation abnormalities that surface during severe disease. Geisbert et al used recombinant Nematode Anticoagulant Protein c2 (rNAPc2) to counter the elevated procoagulation factors released during EBOV infection. (Geisbert, Hensley, et al., 2003; Geisbert, Young, Jahrling, Davis, Kagan, et al., 2003) A total of 9 animals received a daily dose of rNAPc2 either starting 10 min post-infection and continuing to Day 14 (N = 6) or starting 24 h post-infection and continuing to Day 8 (N = 3). For both treatments, 33% of the animals survived the challenge (1 of 3 and 2 of 6). Their results suggest that managing the symptoms could potentially provide a slight advantage.

A second attempt at remediating the coagulation abnormalities was carried out by Hensley et al using recombinant human Activated Protein C (rhAPC). (Hensley et al., 2007) On the heels of results showing depleted levels of activated protein C (APC) in the blood [Geisbert 2003 JID], Hensley et al wanted to know whether replenishing the stores of APC could help with survival after exposure to EBOV. Eleven animals were placed on a continuous infusion of rhAPC within 60 min of challenge. Consistently with the rNAPc2 results, only 2 of the 11 treated animals survived the challenge. The consistency of the results with rNAPc2 suggests that remediating the coagulation abnormalities is not sufficient to achieve meaningful (i.e. significant, in the vernacular sense) survival.

Later, in 2010, a different approach was attempted. Geisbert et al assessed the efficacy of small interfering RNAs (siRNAs) targeting the EBOV *l*, *vp24*, and *vp35* genes to protect rhesus macaques from a lethal EBOV challenge. (Geisbert et al., 2010) Two treatment regimens were assessed, the first with treatments on 30 min, 1, 3, and 5 days post-challenge (N = 3) and the second with treatments on 30 min and daily on Days 1 to 6 (N = 4). Two of the 3 animals in the 4-treatment group survived and all animals in the 7-treatment group survived. These results were quite encouraging, showing that it was possible to save all animals infected before successful antibody treatments would be found. A version of this treatment was used in a clinical trial in Sierra Leone during the 2014-2016 outbreak which was stopped after three months after reaching a predefined endpoint for futility. (Vogel & Kupferschmidt, 2015)

Also in 2010, Warren et al showed that a different approach to RNA interference, using positively charged phosphorodiamidate morpholino oligomers (PMO *plus*), could provide

partial protection when treatment was administered at 30 min post infection and then daily for 14 days. (Warren et al., 2010) Five of 8 animals survived at the original dose of 40 mg/kg/day. A dose-response study revealed that a similar success rate (3 survivors out of 5) could be achieved with a dose of 28 mg/kg/day. Lower doses resulted in decreased survival.

The next treatment attempts consisted mostly of the antibody-based treatments described earlier. One exception is the development of BCX-4430 (also known as Immucillin-A), which showed great promise in treating Marburg virus-infected cynomolgus macaques, although efficacy against EBOV has not been demonstrated. (Warren et al., 2014)

Overall, antibody-based treatment represented the best option for clinical development as the West Africa outbreak was worsening in mid-to-late 2014. The ZMapp treatment had demonstrated efficacy when the treatment was started as late as Day 5 in rhesus macaques, with a total of only 3 treatments during disease rather than daily doses.

Newer antibody-based treatments are now being developed which can protect against multiple species of ebolaviruses. [Zhao Cell 2017] While researching small-molecules with broad activity spectrum should be important, monoclonal antibody-based treatments should be developed further to provide at least a "stop-gap" measure while more cost-effective options are being researched.

1.4 Immunology

1.4.1 Innate immunity

The immune system is often divided into two arms: the innate immune system and the adaptive immune system. A finer qualification of cells that are part of the immune system,

and a better understanding of the mechanics of various immune responses have come to turn the division into more of a continuum. Traditionally, the innate immune system was considered responsible for the initial, rapid response to invading pathogens. This arm of the immune system generally includes dendritic cells (DCs), macrophages, natural killer (NK) cells, and the various granulocytes (neutrophils, basophils, eosinophils). (Riera Romo, Pérez-Martínez, & Castillo Ferrer, 2016) Some of these, such as DCs and macrophages, are specialized in alerting the adaptive immune system and helping in the development of the adaptive immune response by presenting antigens to T and B cells. Other cells, such as NKs and neutrophil, are efficient at eliminating infected cells and invading pathogens. NKs will kill cells displaying certain distress signals or not displaying certain normal markers; for example, failure to have the HLA-C on the surface of the cell will trigger NKs to kill. (Mandal & Viswanathan, 2015) Some pathogens will take advantage of these mechanisms, the HIV will block the translocation of HLA-A and -B, but not -C, to the membrane thus evading detection and killing of the infected cell. (Zipeto & Beretta, 2012)

Innate immune cells can react to specific pathogens or infected cells once they are coated with antibodies. Various receptors on those cells react to different isotypes of antibodies (IgM, IgA, IgE, IgG) and can direct the cells to produce cytokines or to kill the target cell. (Bruhns & Jönsson, 2015) Pathogens or proteins caught in a network of antibodies are known as immune complexes. These immune complexes can be picked up by a number of innate immune cells including DCs, macrophages and the granulocytes (neutrophils, eosinophils, basophils). DCs and macrophages will release cytokines, migrate to lymph nodes and present antigens from the immune complex. Granulocytes will release cytokines in response to immune complex activation, but also possess effector functions.

1.4.2 Adaptive immunity

1.4.2.1 Antibody response

Antibodies are "Y"-shaped proteins produced by B cells in response to foreign proteins in the body. Each antibody is formed of 2 each of 2 chains (heavy and light). (Presta, 2008) This allows each antibody to bind to two close targets, although both ends have the same specificity.

A schematic representation of an IgG antibody is provided in Figure 1A. The antibody is composed of 6 immunoglobulin (Ig) domains each composed from 2 chains. The Ig domains in the crystallisable fragment (F_c) are made from 2 identical heavy chains (in blue) only. Each heavy chain consists of 4 Ig domains. The N-terminal regions are where the complementarity-determining regions (CDRs) are located and bind to the antigen. The first two Ig domains of the heavy chains bind form their Ig domain with a light chain (in orange). The light chains only contain 2 Ig domains. The most N-terminal Ig domain formed is termed the variable region (V) while the next three Ig domains (1 made from heavy + light chains, 2 from heavy + heavy chains) are the constant regions (named C1-C3 from N- to C-terminal). The two Ig domains formed by heavy and light chains are known as the antigen-binding fragment (F_{ab}). The portion of each heavy chain connecting each F_{ab} to the F_c is known as the hinge. The hinge is where interactions with Fc γ receptors (FcγRs) occur and their sequence and glycosylation affects the affinity of the interactions. The long serum half-life of antibodies (e.g. up to 21 days in humans for IgG1) is mostly due to efficient recycling by the neonatal Fc receptor (FcRn). Interaction of IgG with this receptor occurs between the C2 and C3 domains.

IgG can be cut but by the protease papain to form 2 F_{ab} fragments and one F_c fragment. The F_{ab} fragments thus formed retain the ability to bind to their epitope but lack the ability to interact with FcγRs, C1q, and FcRn leading to an inability to trigger any F_c-based mechanism of action and a dramatically reduced half-life.

B cells are cells of the immune system which spend their early development in the bone marrow, as opposed to T cells which spend their early development in the thymus. (K. Murphy, 2012) After B cells leave the bone marrow, they circulate in the lymph tissue looking for antigens which bind to their B cell receptor (BCR). If such an antigen is found, the B cell will remain in the lymph node and start dividing. Some daughter cells will produce IgM antibodies, consisting of 5 linked antibodies (pentameric antibodies). These IgM have a low affinity and specificity for the target antigen, but can effectively trigger the complement pathway. Meanwhile, the daughter cells which remain in the lymph node will undergo expansion and rapid somatic mutations (termed somatic hypermutation) in the V regions (specifically in the CDRs). Cells bearing mutations which increase specificity and affinity are given survival and expansion signals. Eventually, the cells carrying BCR specific to the antigen will undergo antibody class-switching from IgM to IgA, IgE, or various classes of IgG depending on the immune mediators (cytokines and chemokines) present in their environment. After class-switching, the B cells will expand and form memory B cells, which will return to the bone marrow for long-term “storage” and plasma cells which will produce very large amounts of their antibody.

1.4.2.1.1 Neutralization

Antibodies have two main ways of effecting anti-pathogen activity. The first, explored here, is by neutralizing the pathogens. The second class of mechanisms requires interaction of the F_c portion of an antibody to trigger various immune functions.

Neutralization occurs when an antibody prevents a pathogen (generally a virus for this mechanism) from binding to and infecting a target cell. (K. Murphy, 2012) A number of mechanisms can be involved in neutralization. The simplest mechanism consists of the antibody occupying a space where its bulk ends up between the viral attachment protein and its cell-surface receptor. This mechanism is termed steric hindrance. This is likely to be the mechanism used by both 1H3 (in ZMAb) and c13C6 (in ZMapp) as these antibodies bind at the top of the glycoprotein and would be sticking out from GP. (Murin et al., 2014; Tran et al., 2016)

The other mechanism by which antibodies neutralize viruses consists of stabilizing the structure of the fusion protein (GP_{cl} for EBOV) into its pre-fusion structure and preventing membrane fusion. This is the mechanism involved in neutralizing antibodies targeting the fusion peptides of the influenza hemagglutinin and the envelope of HIV. (Khanna, Sharma, Kumar, & Rajput, 2014; Montero, van Houten, Wang, & Scott, 2008). Murin et al and Tran et al show that the antibodies 2G4 and 4G7 bind to a region of GP_1 near the base of the protein where the GP_1 contacts with the GP_2 fusion loops. The antibodies are able to bind to the cleaved GP (GP_{cl}) and prevent the unfolding of the fusion loops into the endosomal membrane. They do this without preventing endosomal entry and processing, and without blocking the interaction of GP_{cl} with the NPC1 endosomal receptor.

1.4.2.1.2 Other mechanisms

Neutralization is a useful property for therapeutic antibodies to have as this mechanism is, generally, species-agnostic. It is useful to prevent further spread of the virus or pathogen, but does not contribute, on its own, to clearing infected cells. However, antibodies can trigger a number of other immune pathways, depending on the immune cells they interact with. (Bruhns & Jönsson, 2015; Kapur, Einarsdottir, & Vidarsson, 2014; X. Liu, Pop, & Vitetta, 2008; K. Murphy, 2012)

Two of the most common ways antibodies help to rid the body of pathogens are antibody-dependent cell-mediated cytotoxicity (ADCC) and complement-mediated toxicity (CMT; more accurately called antibody-dependent complement-mediated cytotoxicity, which also abbreviates to ADCC).

ADCC occurs when many antibodies bind to their target on the surface of a cell. As NK cells, mostly, patrol tissues, the antibodies interact with the Fcγ receptors (FcγRs), more specifically FcγRIII on NK cells, on the surface of the cells. When a large number of FcγRs bind antibodies close together (cross-linking), a signaling cascade activates the cell, stimulating it to release cytotoxic granules containing granzyme B and perforin towards the target cell and/or to release IFN-γ and other pro-inflammatory cytokines to attract immune cells and promote their cytotoxic activity. The FcγRIII cannot signal on its own as it does not contain an immunoreceptor tyrosine-based activation motif (ITAM). An adapter protein containing an ITAM interacts with FcγRIII to initiate signalling; this adapter is called the Fc receptor γ subunit (FcR γ subunit). The rough outline of the structure is presented in Figure 1B.

The complement cascade starts in a similar manner, with a large number of antibodies binding to the surface of a cell. The complement is generally present in the serum and the extracellular medium. The complement component C1 will bind to the antibodies; the change in conformation activates subcomponents to catalyze the cleavage of components C2 and C4. Two products (C2a and C4b) assemble to form the C3 convertase which cleaves component C3. The C3b product, known as the C5 convertase, continues the reaction by cleaving C5 which will continue the cascade. Eventually, multiple subunits of the component C9 are inserted into the cell membrane where they form the membrane attack complex (MAC), effectively creating holes in the membrane and killing the cell.

Another way that antibodies can interact with the immune system is by forming immune complexes with the pathogens. An immune complex is a network of antibodies and pathogens bound together in a large structure. These structures can be detected by DCs, macrophages, and granulocytes by some of the antibodies binding to the FcγRs on the surface of these cells. DCs and macrophages will process the contents of immune complexes and present antigens to T cells as well as release various cytokines to activate and direct the immune response. Granulocytes can also secrete cytokines and perform some effector functions, such as the production of neutrophil extracellular traps (NETs) by neutrophils, which can trap and damage extracellular pathogens.

Figure 1: Schematic structure of IgG and FcγR.

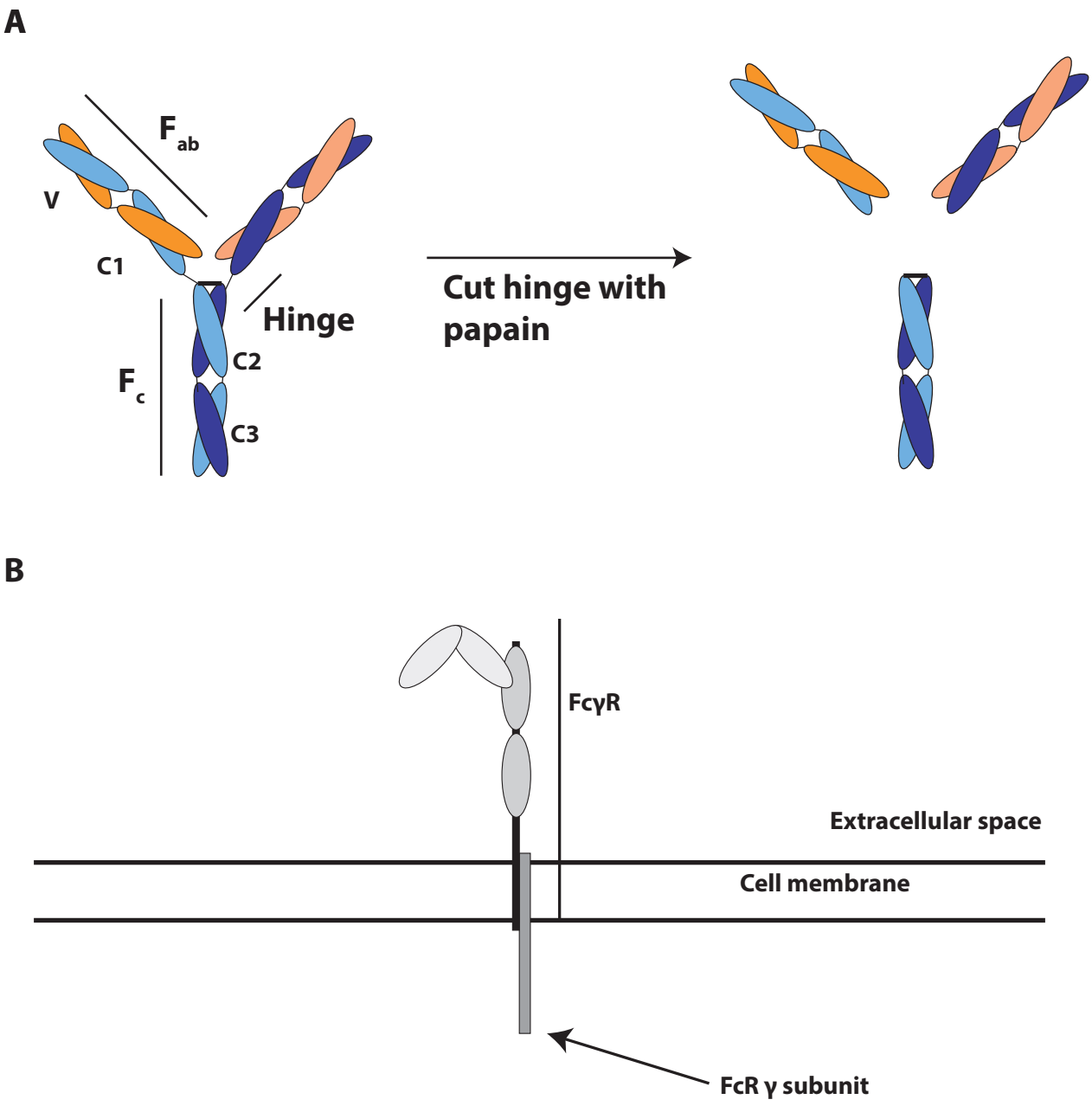

A) Schematic representation of an IgG antibody. The antibody consists of Variable regions (V) supported by three pairs of Constant regions (C1-C3). The F_{ab} fragment is composed of both light (orange) and heavy (blue) chains. The F_c fragment is composed of heavy chains only. The F_{ab} and F_c are linked by the hinge region. Cutting of the hinge with papain releases the two F_{ab} fragments from the F_c fragment. B) Schematic representation of an FcγR with the receptor itself anchored in the membrane. The receptor interacts with the FcR γ subunit, which contains an ITAM, in order to transmit signals inside the cell.

1.4.2.2 T cell response

T cells are immune cells which spend part of their development in the thymus. During this stage, they will favor one of two co-receptors, CD4 or CD8. (K. Murphy, 2012)

1.4.2.2.1 CD4 T cells

CD4 T cells tend to be involved as "managers" of adaptive immune responses. They are activated by binding to peptides presented on molecules of the major histocompatibility complex (MHC)-II, which is only expressed on antigen-presenting cells (APCs). (K. Murphy, 2012) Naive CD4 T cells will then differentiate based on signals received from the APCs to produce a number of cytokines to initiate, maintain, and downregulate the immune response. Mature CD4 T cells have been subdivided into many different roles. Helper T cells (T_h) produce varying patterns of cytokines.

The two most studied helper profiles are the T_h1 and T_h2 profiles. (Annunziato & Romagnani, 2009; Mahnke, Brodie, Sallusto, Roederer, & Lugli, 2013; K. Murphy, 2012; Raphael, Nalawade, Eagar, & Forsthuber, 2015) T_h1 cells produce IFN-γ and interleukin (IL-)2 in response to stimulation. The IFN-γ induces a number of response in immune and non-immune cells which enhance the ability of the immune system (and the body in general) to fight off intracellular pathogens, such as viruses. T_h1 cells develop when CD4 T cells are activated by APCs in the presence of cytokines like IL-12. Such CD4 T cells will also provide enhancing signals to APCs to allow them to induce the maturation of naïve CD8 T cells. Cytokines like IL-2, IFN-γ, and TNFα can also enhance the killing activity of CD8 T cells and NK cells. These cytokine can also increase the phagocytic activity of macrophages. Additionally, IL-2 acts as an expansion signal for T cells.

The T_h2 profile is considered to be related to immune responses against extracellular pathogens. These cell secrete cytokines such as IL-4 and IL-5 which can promote, among other things, the development and expansion of B cells. The cytokines secreted by T_h2 cells can also stimulate the activity of eosinophils and neutrophils which can phagocytose extracellular pathogens caught in immune complexes with IgG. Macrophages exposed to cytokines secreted by T_h2 cells take on a role related to wound healing rather than immunity.

CD4 T cells can also differentiate into other effector categories. T_h17 cells are often related to the response to mucosal pathogens and, in some cases, to self-antigens. T_h9 and T_h22 cells also exist, with less well-defined roles. T_{reg} cells are CD4 T cells with anti-inflammatory activity. These cells can reduce the activation of other T cells they come in contact with and secrete high levels of IL-10 which has anti-inflammatory activity.

A few points are important to keep in mind. First, immune responses are complex and almost never consist of cells from a single profile. T cells will mature based on the local cytokine environment, which can be drastically different from the overall or serum profile. Second, while the T_h2 response is associated with (and often thought of as) the "humoral" response, most profiles will lead to the production of antibodies. Even T_h1-dominant responses can lead to very high antibody titres. The polarization of the environment around maturing B cells also affects isotype switching. As the B cells undergo recombination away from IgM, different cytokine profiles lead to different isotypes. For example, a T_h2 profile is more likely to lead to the production of IgE antibodies which are involved in allergy. Third, while the response have prototypical contexts (T_h1 =

intracellular, T_h2 = extracellular, T_h17 = mucosal, etc.), such contexts are useful because they represent average responses and allow us to set some initial expectations. For example, Marzi et al demonstrated that antibodies were key to the protection against lethal disease after vaccination with VSV-Ebola and challenge. [Marzi et al] They also showed that depletion of CD8 T cells did not reduce protection. Because viruses are intracellular pathogens, a cell-mediated (T_h1) response would be expected to play a fairly important role; however, both T_h1 and T_h2 responses lead to antibody production. In this context, discussions of T_h1 vs T_h2 responses are meant to reflect the overall polarization of the immune response, not to imply that only one of the profiles exists or matters.

1.4.2.2.2 CD8 T cells

CD8 T cells tend to have two main activities: they produce T_h1-related cytokines and/or kill cells. (K. Murphy, 2012) Naive CD8 T cells require a stronger signal from APCs in order to mature, generally requiring the APCs to have received stimulation signals from a CD4 T cell (known as "licensing"). CD8 T cells react to peptides presented by proteins from the MHC-I complex. These proteins are expressed by all nucleated cells. CD8 T cells perform surveillance of nucleated cells for peptides related either to mutations (i.e. preventing the development of cancer) or to infection. When a CD8 T cell finds a cell presenting a peptide it is capable of reacting to, it will release cytokines or kill the cell, or both.

1.5 Rationale

Antibody-based treatments have been widely used in the treatment of cancer for many years. Much knowledge has been accumulated on mutations that can be used to enhance various effector functions of monoclonal antibodies. By understanding the mechanisms

required for the components of the ZMAb cocktail to work, it may be possible to eventually enhance its effectiveness. Additionally, the knowledge gained from the mechanisms involved in mediating the protection of ZMAb and its derivatives can help to understand the disease itself and to focus future research into developing mAb-based treatments against related pathogens.

The study, here, of the mechanisms of protection in both mice and NHPs also helps to confirm that the mechanisms are likely to be the same in humans. Finally, understanding the important functions of the antibodies can help with gaining a better understanding of antibodies as surrogates or correlates of protection.

1.6 Hypothesis

The hypothesis around which this work is centered is that:

Neutralization is the main mechanism of action of the ZMAb cocktail and its derivatives.

In order to shed light on this hypothesis, the following objectives will be studied:

1. **Properties of the antibodies investigated.** Evaluate some of the basic properties of the antibodies, such as their sequence and germline origin and their ability to neutralize EBOV.
2. **Mechanisms of action required for protection in mice.** Establish the essential mechanisms required for the three antibodies composing ZMAb to protect mice. The mechanisms studied will be: neutralization, antibody-dependent cell-mediated cytotoxicity, and triggering of the complement cascade.

3. **Immune responses in NHPs treated with the antibodies.** Evaluate the immune responses of survivor NHPs treated with different versions of the ZMAb treatment. Understanding how the various treatments affect the developing immune response may allow us to verify whether the antibodies interact more with NK cells than in mice and confirm whether the mechanism of action is similar. Interaction with NK cells would lead to the production of IFN-γ and, most likely, a T_h1-skewed response.

CHAPTER: 2 MATERIALS AND METHODS

2.1 Biosafety

All experiments involving the use of live versions of EBOV (wild-type, mouse-adapted, or expressing the enhanced green fluorescent protein (eGFP)) were carried out in the Biosafety Level 4 (BSL4) laboratory of the National Microbiology Laboratory of the Public Health Agency of Canada located at the Canadian Science Center for Human and Animal Health (CSCHAH).

2.2 Cells and viruses

Vero E6 cells were grown in Dlbecco's Modified Eagle Medium (DMEM; HyClone) supplemented with 10% Fetal Bovine Serum (FBS; HyClone). The cells were passaged when they reached 80-100% confluence.

The virus used for the mouse studies was the mouse-adapted Ebola virus (MA-EBOV) (Ebola virus USAMRIID/BALB/c-lab/COD/1976/Mayinga-MA-p3). The challenge virus for the NHP studies was Ebola virus H.sapiens-tc/COD/1995/Kikwit-9510621 (EBOV) (order *Mononegavirales*, family *Filoviridae*, species *Zaire ebolavirus*; GenBank accession no. AY354458) obtained from the Centers for Disease Control and Prevention (Atlanta, GA), passaged twice on Vero E6 cells cultured in complete minimal essential medium. The reporter virus used for neutralization experiments was Ebola virus NML/H.sapiens-lab/COD/1976/Mayinga-eGFP-p3 (EBOV/May-eGFP) (derived from an Ebola virus, family *Filoviridae*, species *Zaire ebolavirus*;GenBank accession no. NC_002549), which encodes the

enhanced green fluorescent protein (eGFP) reporter gene between the NP and VP35 open reading frames.(Ebihara et al., 2007)

2.3 Antibody F_{ab} production

F_{ab} fragments were produced using the Pierce Fab Production and Purification Kit (Fisher Scientific). Briefly, each mAb (0.5 ml at 8 mg/ml) was buffer exchanged into Fab digestion buffer using a Zeba desalting spin column. The mAbs were then incubated with immobilized papain for 5 h at $37°C$ with continuous rotation. The mixture was spun out of the incubation column and incubated with immobilized Protein A for 10 min. The flowthrough was collected, as it contains the F_{ab} and buffer exchanged into Dulbecco's phosphate-buffered saline (D-PBS) (HyClone) 5 times using a 15 ml Centricon (MWCO 3,000 Da). The retentate was filter-sterilized using a 0.22 μm syringe-filter. The concentration was measured by absorbance at 280 nm and calculated as 1 mg/ml = 1.4 OD.

2.4 Antibody germline determination

2.4.1 Sequencing of hybridomas

RNA was isolated from the hybridomas for 1H3, 2G4, and 4G7 using a Qiagen RNeasy mini kit starting from 10^7 cells. Reverse transcription was performed using the Improm II reverse transcription kit (Promega) with 150 ng of random hexamers and 1 μg of RNA, following manufacturer's instructions. PCR amplification was based on the procedure and primers from Tiller 2008. The Phusion enzyme was used for PCR amplification (ThermoScientific). The resulting amplicons were run on a 1% agarose gel and extracted using the QIAquick Gel Extraction kit (Qiagen). The purified amplicons were cloned into the pJet vector using the CloneJet kit (ThermoScientific) and transformed into competent cells.

The transformants were grown overnight at 37°C on Luria-Bertani (LB) agar containing 100 $\frac{\mu g}{ml}$ ampicilin (Sigma-Aldrich). Twenty colonies were screened by polymerase chain reaction (PCR) using the DreamTaq Green enzyme with PCR program: 95°C for 3 min; followed by 30 cycles of: 95°C for 30 s, 55°C for 30 s, 72°C for 30 s; and a final extension of 5 min at 72°C. The amplicons were visualized on a 1% agarose gel. Twelve colonies with amplicons of the proper size were grown overnight at 37°C in LB broth containing 100 $\frac{\mu g}{ml}$ ampicilin. Plasmid DNA was extracted using a MiniPrep kit (Qiagen) and sent to DNA core for Sanger sequencing using vector-specific primers provided by the manufacturer. The resulting sequences were aligned to incomplete reference sequences using DNASTAR Lasergene SeqMan (v 10). The new consensus containing the Framework 1 sequence were exported as FASTA files.

2.4.2 Germline matching

The nucleotide sequences were run through the IgBlast tool of the NCBI to search the mouse germline gene library. The databases queried were the NCBI mouse databases (for V, D, and J genes), with all other options being the default options.(Ye, Ma, Madden, & Ostell, 2013)

2.5 In vitro experiments

2.5.1 Neutralization of EBOV-eGFP

Two-fold dilutions of antibodies were performed in plain DMEM (HyClone) in 2 ml deep-well blocks. EBOV/May-eGFP was added to each appropriate well at 100 PFU/well, for the total number of well of a 96-well plate that will be infected with a specific mixture. The antibodies and virus were allowed to incubate for 1 h at 37°C with 5% CO_2. The mixture

was added to Vero E6 cells plated the day before to reach 80% confluence, at 100 μl/well. The cells were incubated for 1 h at 37°C with 5% CO_2. The mixture was removed and 100 μl of DMEM 2% FBS was added. The plates were incubated for 48 h at 37°C with 5% CO_2. The plates were fixed using 10% neutral-buffered formalin (Fisher Scientific) by signed-off personel as per PHAC CL4 procedures. The plates were read using an AID iSpot FluoroSpot Reader System.

2.5.2 ELISA

2.5.2.1 Semi-quantitative assay

Half-area 96-well RIA/EIA plates (Corning) were coated with 30 μl of recombinant transmembrane domain-deleted EBOV-GP (IBT Bioservices) at 1 μg/ml overnight at 4°C. The plates were blocked for 2 h at 37°C with 100 μl of 5% Skim Milk (Difco) in PBS (NML Media service). The serum samples were diluted to the starting concentration (1:100, 1:1000, or 1:8000) in 2% Skim Milk in PBS. The blocking buffer was removed from the plates and 30 μl of diluted samples were added to the first row, in triplicate. The Day 0 sample was run on every animal's plate at the same starting dilution as the other samples on the plate. The other wells received 30 μl of 2% Skim Milk in PBS and serial 1:2 dilutions were performed down the plate with a multi-channel pipettor, with 8 mixes per dilution. The plates were incubated at 37°C for 2 h. The plates were then washed 6 times with PBS 0.1% Tween-20 (Fisher) using a Bio-Tek ELS405TS. The secondary antibody, anti-human IgG conjugated to HRP (KPL), was applied to the plates (30 μl per well, 0.5 μg/ml in 2% Skim Milk) for 1 h at 37°C. The plates were washed 6 times and 30 μl of 2,2'-azino-bis(3-ethylbenzothiazoline-6-sulphonic acid) (ABTS) substrate (KPL) was added. The reaction

was allowed to occur at room temperature for 30 min and the plates were read at 405 nm using a VersaMax reader (Molecular Devices).

The titer was the last dilution where a sample had an average optical density (OD) more than 3 standard deviations higher than the corresponding dilution of Day 0 serum.

2.5.2.2 Quantitative assay

The plates were sealed with fresh adhesive film at every step. Half-area 96-well RIA/EIA plates (Corning) were coated with 30 μl of recombinant transmembrane domain-deleted EBOV-GP (IBT Bioservices) at 1.25 μg/ml overnight at 4°C. The plates were blocked for 2 h at 37°C with 100 μl of 5% Skim Milk (Difco) in PBS (NML Media service). The serum samples were diluted at 1:100 and 1:1000 in 2% Skim Milk in PBS. The standard was diluted at 1:100 and then 11 1:2.5 serial dilutions to obtain 12 standards. The blocking buffer was removed from the plates and 30 μl of diluted samples were added. The plates were incubated at 37°C for 2 h. The plates were then washed 4 times with PBS 0.1% Tween-20 (Fisher) using a Bio-Tek ELS405TS. The secondary antibody, mouse monoclonal anti-Rhesus IgG conjugated to HRP, was applied to the plates (30 μl per well, 0.5 μg/ml in 2% Skim Milk) for 1 h at 37°C. The plates were washed 4 times and 50 μl of 3,3',5,5'-tetramethylbenzidine (TMB) substrate (ThermoFisher) was added. The reaction was allowed to occur at room temperature for at least 30 min and the plates were read at 650 nm using a VersaMax reader (Molecular Devices). Samples were re-run until they met the following condition: 1) the 1:100 dilution has higher signal than the 1:1000 (except for samples where 1:100 is too strong and turns green); 2) variation between replicates satisfied: $-0.4 \leq \ln(\frac{Rep1}{Rep2}) \leq 0.4$.

2.5.3 Cytokine measurement

Cytokines in NHP serum samples were measured using the U-PLEX TH1/TH2 Combo NHP assay (Meso Scale Diagnostics) following manufacturer's instructions, with a sample incubation time of 2 h. Cytokine quantification from the standard curve was performed as described in the "Statistical analyses"/"ELISA and cytokine measurements" section. The standard curve was expanded from the manufacturer's recommendation to the following: the standard was reconstituted in 150 μl of Diluent 43 and run undiluted and with ten 4-fold dilutions (in Diluent 43) and Diluent 43 alone (for a total of 12 standard samples, run in duplicate).

2.6 In vivo experiments

2.6.1 Mouse protection studies

The *in vivo* mouse studies were performed in accordance with Canadian laws, and recommendations of the Canadian Council on Animal Care. The protocol (H-14-001) was approved by the Animal Care Committee of the CSCHAH. All experiments involving live Ebola virus were carried out in the Containment Level 4 laboratory at the National Microbiology Laboratory of the Public Health Agency of Canada.

2.6.1.1 $F_CR\gamma$ subunit KO

Four to 8 weeks old mice carrying a knocked-out form of the $F_CR\gamma$ subunit, in a C57BL/6 background, were obtained from Taconic. Normal C57BL/6 (4-8 weeks old) mice were also obtained from Taconic at the same time. The knock-out mice were kept in sterile caging. The mice were transferred to cages in BSL4 (6 mice per cage) and allowed to acclimatize for 7 days, with food and water provided *ad libitum*. The mice were observed daily to ensure their health status and to top up food and water. Cages were changed weekly or

more as needed. The mice were anesthetized with inhalational isoflurane and challenged intraperitoneally (IP) with $1000 \times LD_{50}$ (median lethal dose) of MA-EBOV diluted in 100 μl of DMEM (Hyclone). On day 2, the animals were treated intraperitoneally with 100 μg of the specified mouse antibody in 100 μl of commercial, sterile D-PBS (HyClone) or 100 μl of D-PBS alone. (1 cage per antibody per background) The animals were scored daily starting on day 1. Group weights were recorded every day until day 14. On day 28, the surviving animals were euthanized with an overdose of isoflurane followed by cervical dislocation. Animals which reached the endpoint score (3) or lost > 20% of their initial body weight were euthanized by the same process.

2.6.1.2 $Nfil3^{-/-}$ mice

Four to 8 weeks old mice carrying a knocked-out form of the transcription factor Nfil3 were obtained from Dr Sam Kung at the University of Manitoba and were from a C57BL/6 background. The knock-out mice were kept in sterile caging. Similarly aged normal mice were obtained from Charles River as normal controls. The mice were transferred to cages in BSL4 (6 mice per cage) and allowed to acclimatize for 7 days, with food and water provided *ad libitum*. The mice were observed daily to ensure their health status and to top up food and water. Cages were changed weekly or more as needed. The mice were anesthetized with inhalational isoflurane and challenged intraperitoneally with $1000 \times LD_{50}$ of MA-EBOV diluted in 100 μl of DMEM (Hyclone). On day 2, the animals were treated intraperitoneally with 100 μg of the specified mouse antibody in 100 μl of commercial, sterile D-PBS (HyClone) or 100 μl of D-PBS alone. (1 cage per antibody per background) The animals were scored daily starting on day 1. Group weights were recorded every day until day 14. On day 28, the surviving animals were euthanized with an

overdose of isoflurane followed by cervical dislocation. Animals which reached the endpoint score (3) or lost > 20% of their initial body weight were euthanized by the same process.

2.6.1.3 C3-depleted mice

Forty-eight BALB/C mice, 6-8 weeks old, were obtained from Charles River. The mice were randomly assigned to cages (6 mice per cage) and transferred to BSL4. They were allowed to acclimatize for 7 days, with food and water provided *ad libitum*. The mice were observed daily to ensure their health status and to top up food and water. Cages were changed weekly or more as needed. The depleted mice were kept in sterile caging. The mice were anesthetized with inhalational isoflurane and injected intraperitoneally with 10 U of Cobra Venom Factor on day -1. On day 0, the mice were anesthetized with inhalational isoflurane and challenged intraperitoneally with $1000 \times LD_{50}$ of MA-EBOV diluted in 100 μl of DMEM (Hyclone). On day 2, the animals were treated intraperitoneally with 100 μg of the specified mouse antibody in 100 μl of commercial, sterile D-PBS (HyClone) or 100 μl of D-PBS alone. (1 cage per antibody per background) The animals were scored daily starting on day 1. Group weights were recorded every day until day 14. On day 28, the surviving animals were euthanized with an overdose of isoflurane followed by cervical dislocation. Animals which reached the endpoint score (3) or lost > 20% of their initial body weight were euthanized by the same process.

2.6.1.4 $C1q^{-/-}$ mice

Four to 8 weeks old mice carrying a knocked-out form of the common γ-chain, in a C57BL/6 background, were obtained from Jackson Labs. The knock-out mice were kept in sterile caging. Normal C57BL/6 (4-8 weeks old) mice were also obtained from Jackson Labs

at the same time. The mice were transferred to cages in BSL4 (6 mice per cage) and allowed to acclimatize for 7 days, with food and water provided *ad libitum*. The mice were observed daily to ensure their health status and to top up food and water. Cages were changed weekly or more as needed. The mice were anesthetized with inhalational isoflurane and challenged intraperitoneally with 1000 × LD_{50} of MA-EBOV diluted in 100 μl of DMEM (HyClone). On day 2, the animals were treated intraperitoneally with 100 μg of the specified mouse antibody in 100 μl of commercial, sterile D-PBS (HyClone) or 100 μl of D-PBS alone. (1 cage per antibody per background) The animals were scored daily starting on day 1. Animal weights were recorded every day until day 14. On day 28, the surviving animals were euthanized with an overdose of isoflurane followed by cervical dislocation. Animals which reached the endpoint score (3) or lost > 25% of their initial body weight were euthanized by the same process.

2.6.1.5 F_{ab} protection study

Seventy BALB/C mice, 6-8 weeks old, were obtained from Charles River. The mice were randomly assigned to cages (5 mice per cage) and transferred to BSL4. They were allowed to acclimatize for 7 days, with food and water provided *ad libitum*. The mice were observed daily to ensure their health status and to top up food and water. Cages were changed weekly or more as needed. On Day 0, all mice were challenged with 1000 × LD_{50} of MA-EBOV diluted in 100 μl of DMEM (HyClone) via an intraperitoneal injection. On Day 2 in the morning, the mice received 100 μl of treatment or D-PBS intraperitoneally. The treatment was either 150 μg (1.5 mg/ml) of mouse 1H3, 2G4, or 4G7 or 100 μg (1 mg/ml) of F_{ab}s of the same antibodies. In the afternoon of Day 2, the mice receiving F_{ab} received a second dose. These mice received 2 doses per day on Days 3 and 4 as well. Weight was measured

for each animal from Day 1 to Day 14. The animals were scored daily. On day 28, the surviving animals were euthanized with an overdose of isoflurane followed by cervical dislocation. Animals which reached the endpoint score (3) or lost > 25% of their initial body weight were euthanized by the same process.

2.6.2 NHP studies

All NHPs were obtained from reputable suppliers (see experiment-specific details for supplier). The NHPs were allowed to acclimatize to BSL4 holding facilities for 10 days before the beginning of any experimental manipulation. The animals received commercial monkey chow, treats, vegetables, and fruits daily as well as water *ad libitum*. Environmental enrichment consisted of commercial toys and visual stimulation. On Day 0, all subjects were challenged with 1000 PFU of EBOV/Kikwit in 1 ml DMEM. At the appropriate times, the animals received a 5-ml bolus administered slowly via the saphenous vein, which consisted of a mix of EBOV-GP-specific mAbs diluted in commercial D-PBS (Gibco). Animals were scored daily (observed twice daily) for disease progression using a scoring sheet for signs including attitude, activity level, posture, abnormal breathing, stool (quantity and solidity), bleeding, rashes, and petechia among other factors. Weight and temperature were measured on sampling and treatment days. For exams and treatments, the animals were anesthetized using ketamine hydrochloride (6-8 mg/kg) via intramuscular injection using a 23 or 25 gauge needle (3/8-1 inch). Anesthesia was maintained using isoflurane at 3.5-5% for induction, and maintenance at 2.5-3.5% carried by 100% oxygen. For animals which met the humane endpoint (score > 25; score > 20 for the control), euthanasia was carried out by either: 1) intravenous or intracardiac injection of 100 mg/kg of pentobarbital following an intramuscular injection of 10 mg/kg of

ketamine hydrochloride; or 2) femoral or intracardiac exsanguination under isoflurane anesthesia following an injection of 25-50 mg/kg ketamine hydrochloride. On the last day of the experiment surviving animals were euthanized as above. Room temperature was maintained between $19 - 24°C$, with relative humidity at 45-60%, illumination at approximately 323 lux. The light/dark cycle was a 12-hour split. All NHP experiments were reviewed and approved by the Animal Care Committee of the Canadian Science Center for Human and Animal Health (CSCHAH).

2.6.2.1 Experiment 1

Nine male and female cynomolgus macaques were obtained from the Health Canada Animal Resources Division. The initial weights ranged from 2.5 to 4.9 kg. The animals were randomized into two treatment groups (N = 4 each) and 1 control animal. The experimental treatment consisted of a mixture of three mouse monoclonal antibodies directed against the EBOV GP called ZMAb (composed of 1H3, 2G4, 4G7), at a combined dose of 25 mg/kg. All animals were challenged on Day 0. The first experimental group received the treatment on Days 1, 4, and 7. The second experimental group received the treatment on Days 2, 5, and 8. The animals were also sampled on Days 14, 21, and 28. Blood was collected on exam days for serum separation (~1-2 ml of whole blood) for blood biochemistry analysis and measurement of antibodies by ELISA.

2.6.2.2 Experiment 2

Twelve male and female cynomolgus macaques were obtained from Primus Bio-Resources. The initial weights ranged from 2.1 to 5.9 kg. The animals were randomized into two treatment groups (N = 4 each) and two control groups (N = 2 each). The first treatment group received a combination of ZMAb (50 mg/kg) with $10^9 PFU/kg$ of Ad-IFN on Day 2

and ZMAb (50 mg/kg) alone on Days 5 and 8. Ad-IFN consists of an adenovirus vector carrying a gene to express human consensus IFN_{α}. The second treatment group received a combination of ZMAb (50 mg/kg) with $10^9 PFU/kg$ of Ad-IFN on Day 3 and ZMAb (50 mg/kg) alone on Days 6 and 9. Blood and serum were collected on Days (depending on treatment) 0, 1, 3, 4, 6, 7, 9, 10, 14, 21, 28. On Day 21, 5-7 ml (depending on animal weight) of EDTA-Blood was collected for isolation of PBMCs for flow cytometry. The mouse antibodies were produced by the Biotechnology Research Institute. (Xiangguo Qiu et al., 2013)

2.6.2.3 Experiment 3

Six male and female rhesus macaques were obtained from Primus Bio-Resources. The initial weights ranged from 3.1 to 5.0 kg. The animals were randomized into two groups, one treated (N = 4) and one control (N = 2). The treated animals received a combination of ZMAb (50 mg/kg) with $10^9 PFU/kg$ of Ad-IFN on Day 3 and ZMAb (50 mg/kg) alone on Days 6 and 9. The mouse antibodies were produced by the Biotechnology Research Institute. (Xiangguo Qiu et al., 2013) Blood and serum were collected on Days (depending on treatment) 0, 3, 6, 9, 14, 21, 28. On Day 21, 5-7 ml (depending on animal weight) of EDTA-Blood was collected for isolation of PBMCs for flow cytometry.

2.6.2.4 Experiment 4

Fourteen male and female rhesus macaques were obtained from Primgen (USA). The initial weights ranged from 4.1 to 9.6 kg, the animals were 4-8 years old. The animals were assigned to groups to have balanced sex and weights between groups. Three groups were formed, two treatment groups (N = 6) and one control group (N = 2). The back-titration on the challenge material was 2512 PFU per animal. The first treatment group was treated

with ZMapp1 on Days 3, 6, and 9. The second treatment group was treated with ZMapp2 on Days 3, 6, and 9. ZMapp1 consisted of human-mouse chimeric (c) antibodies c13C6, c2G4, and mouse 4G7 (the chimeric antibody was not available in sufficient quantity). ZMapp2 consisted of c13C6, c1H3, and c2G4. The chimeric antibodies and 4E10 were produced by Kentucky BioProcessing in tobacco plants, under GMP conditions. (Olinger et al., 2012) The mouse 4G7 was produced by the Biotechnology Research Institute. (Xiangguo Qiu et al., 2013) Blood and serum were collected on Days (depending on treatment) 0, 3, 6, 9, 14, 21, 28. On Days 0 and 21, 5-7 ml (depending on animal weight) of EDTA-Blood was collected for isolation of PBMCs for flow cytometry. The survivors were euthanized on Day 28.

2.6.2.5 Experiment 5

Twenty-one male and female rhesus macaques were obtained from Primgen (USA). The initial weights ranged from 2.5 to 3.5 kg, the animals were 2 years old. The animals were assigned to groups to have balanced sex and weights between groups. Three groups were formed, three treatment groups (N = 6) and one control group (N = 3). The back-titration on the challenge material was 628 PFU per animal. All treated animals received ZMapp (c13C6, c2G4, c4G7; 1:1:1). The treated groups were treated on Days: 3, 6, 9; or 4, 7, 10; or 5, 8, 11. The chimeric antibodies were produced by Kentucky BioProcessing in tobacco plants, under GMP conditions. (Olinger et al., 2012) Blood and serum were collected on Days (depending on treatment) 0, 3, 4, 5, 6, 7, 8, 9, 10, 11, 14, 21, 28. On Days 0 and 21, 5-7 ml (depending on animal weight) of EDTA-Blood was collected for isolation of PBMCs for flow cytometry. The survivors were euthanized on Day 28.

2.6.3 Flow cytometry

Peripheral blood mononuclear cells were isolated by Ficoll (GE Life Sciences; for rhesus macaques) or 60% Percoll (GE Life Sciences; for cynomolgus macaques) centrifugation. The blood was diluted 1:1 with D-PBS and layered on the density medium (15 or 4.5 ml depending on the blood volume). The blood was spun at 700 x g for 40 min without brake. The interphase was collected using transfer pipettes. The cells were washed with DPBS and spun at 400 x g for 10 min. The pellet was resuspended in 1 ml of RPMI 1640 (HyClone) with 10% FBS, 10 mM L-glutamine (Gibco), 50 μM β-mercaptoethanol (cRPMI). A cell sample was diluted 1:10 in D-PBS containing 100 μg/ml propidium iodide (Molecular Probes) and 5 μg/ml acridine orange (Molecular Probes). The cells were counted using a Cellometer Auto 2000 (Nexcelom).

The cells were plated at 5×10^5 cells per well and rested overnight. The cells were then stimulated with media or peptide pools (2 μg/ peptide) with 0.25 μg of Brefeldin A (GolgiPlug; BD Biosciences), 0.3 μl of monensin (GolgiStop; BD Biosciences), and 5 μl of anti-CD107a (H4A3; BioLegend) Brilliant Violet 421 for 5 h. The cells were washed with 1 ml of PBS and spun at 400 x g for 10 min. The cells were incubated with 5 μl of Human TruStain FcX (BioLegend) for 10 min prior to staining. The surface stain included anti-CD3 (SP34-2; BD Biosciences) Alexa Fluor 700, CD4 (L200; BD Biosciences) PerCP-Cy5.5 and CD8 (RPA-T8; BioLegend) PE-Cy7. Surface staining was carried out in D-PBS 2% FBS for 20 min at room temperature in the dark. One milliliter of D-PBS 2% FBS was added and the cells were spun at 300 x g for 10 min. The supernatant was discarded and the cells were resuspended in 400 μl of Cytofix/Cytoperm (BD Biosciences) for 30 min at room temperature in the dark. The cells were spun at 500 x g for 10 min and the supernatant was

discarded. The samples were transferred into clean tubes, resuspending the cells with 400 μl of Cytofix/Cytoperm. The tubes were removed from CL4 following standard procedures and were not opened for at least 30 min (generally overnight). The samples were transferred to a deep-well plate and washed twice with 1 ml of PermWash (BD Biosciences) with spins at 500 x g for 10 min. Intracellular staining was performed in PermWash with antibodies to IFN-γ (B27; BioLegend) APC, IL-2 (MQ1-17H12; BioLegend) Alexa Fluor 488, and IL-4 (8D4-8; BioLegend) PE. The staining proceeded for 30 min at 4°C in the dark. The cells were washed twice with PermWash and resuspended in 250 μl of PBS 1% Formaldehyde. The samples were run on a BD LSR II flow cytometer.

2.6.4 Flow cytometry gating

Flow cytometry gating was performed using the openCyto package in Microsoft R Open 3.3.3 which is based on R 3.3.3. (Finak et al., 2014; R Core Team, 2017) All experiments which are compared together are gated based on the same markers. First, the media-only samples are gated down to the single cytokine/activation marker gates. Second, the stimulated samples are gated down to the CD4 and CD8 populations. Third, the single cytokine/activation marker gates are copied from the media-only into the appropriate stimulated samples. Fourth, both media-only and stimulated samples are gated down to the combination gates of the cytokines/activation markers. This process ensures that the location of the thresholds for determining the number of responding cells in stimulated samples are based on the media-only samples.

2.7 Statistical analyses

2.7.1 Bayesian statistics and notation

In Frequentist statistics, probabilities represent long-run frequencies of a parameter. In Bayesian statistics, probabilities can be interpreted as uncertainty regarding the value of a parameter. Bayesian statistics use Bayes' formula to calculate the probability of different values of a parameter given the assumed model. Bayes' formula is :

$$p(\theta|Data) = \frac{p(\theta) \times p(Data|\theta)}{p(Data)}$$

Where θ is one or more parameter(s) (e.g. mean, variance, regression coefficients, etc), p(θ) is a probability distribution describing the information we have on the parameters before having seen the data (the **prior**), p(Data|θ) is the probability of the data given values of the parameters (the **likelihood**), p(Data) is the probability of the data independently of any value of the parameters, and p(θ|data) is the distribution representing the uncertainty on the parameters after having observed the data (the **posterior**). The analytical solutions to this equation exist only for trivial models. One frequent reason for this is that p(Data) cannot be defined properly, i.e. it is difficult to express the probability of some data arising independently of the parameters. This term (p(Data)) only serves as a normalizing factor (forces the area under the curve of the posterior to integrate to 1) and does not affect the shape of the posterior. Modern computers use variants of an algorithm called Markov Chain Monte Carlo (MCMC) to draw sample values from the posterior distribution. These samples can be used to estimate the properties of the posterior. MCMC and its variants (such as Hamiltonian Monte Carlo

(HMC), used here) do not require the computation of the normalizing term, they make use of the following proportionality:

$$p(\theta|Data) \propto p(\theta) \times p(Data|\theta)$$

The effect of Bayes' Theorem is illustrated in Figure 2. Here a model is used to infer the concentration of a cytokine in samples (colored points) based on a standard curve (black points). The prior is illustrated as the wide, purple distribution at the bottom. It is important to note that the distributions are not to scale, for example the rightmost sample (red) should have a distribution that spikes to a height of ~15 while the prior, because it is so wide, should be barely visible as it is too close to the axis. The prior, here, has two functions, it provides the range of *a priori* possible results (most of the concentrations covered by the curve) and prevents very low or very high samples from going to $\pm\infty$ which would make computations very difficult and would not provide useful information.

Figure 2: Reassignment of probability during bayesian modelling.

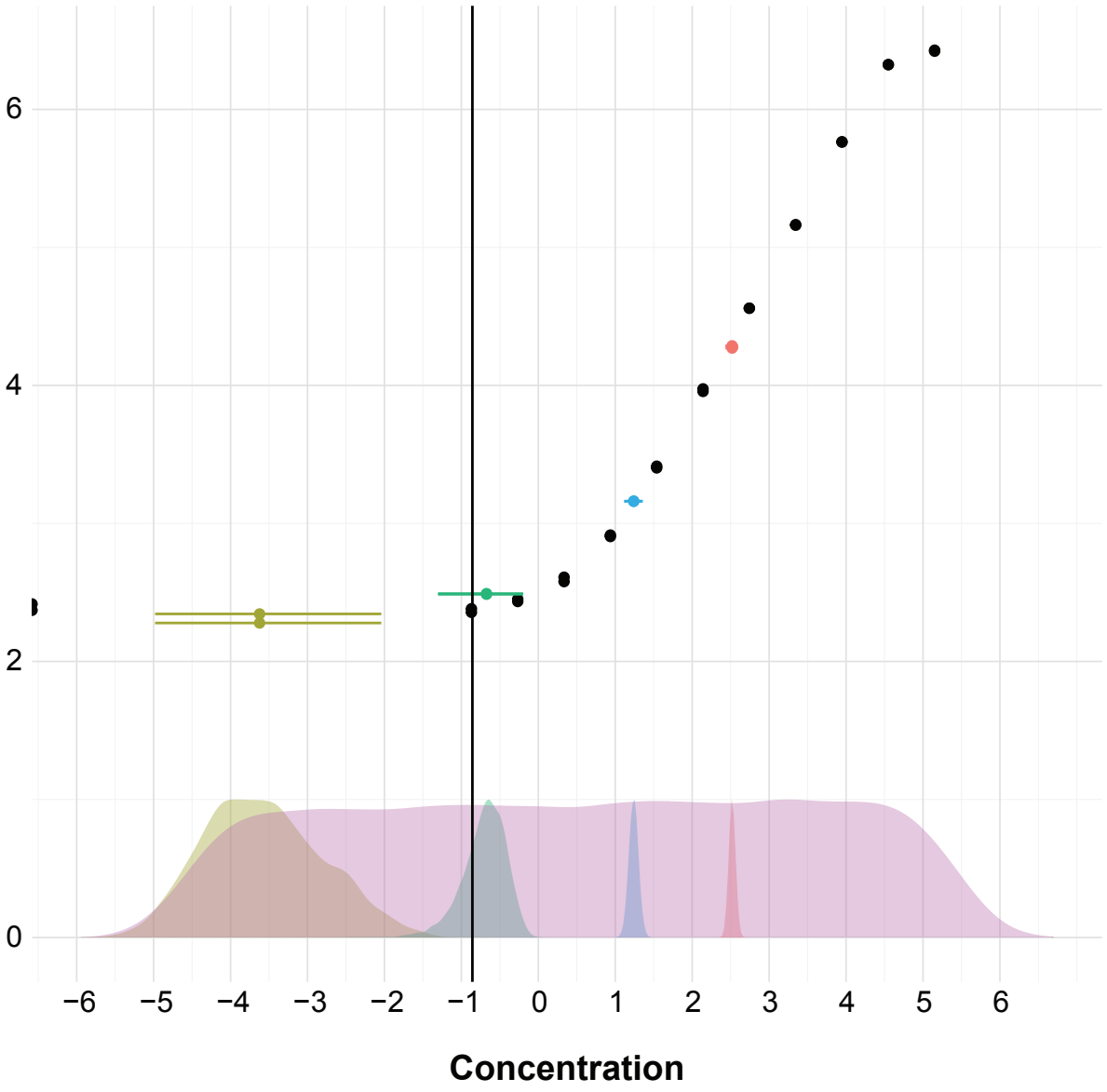

The purple density distribution at the bottom represents the prior for all cytokine samples. The green, teal, blue, and red distributions represent the posterior densities obtained from the model for samples that are, respectively, below the limit of detection, just above the limit of detection, just above the "turn" of the standard, and close to the middle of the standard. The black points represent the standard, for reference. The concentration is in $\log_{10}$(pg/ml).

Depending on the data, the probability in the prior is reassigned to the values most consistent with the data. For points located in the linear region of the curve (red and blue) the probability mass is reassigned to a very narrow interval as the data is only consistent with a few concentrations, due to the slope of the curve. As the signal diminishes and moves towards the bottom plateau of the curve, the probability mass is reassigned to wider intervals of concentrations as the variation between replicates becomes more important compared to the signal and the slope of the curve gets close to 0. The two points for the yellow sample have visibly different signal, this would lead the points to have very different concentrations; however, the information passed into the model identifies them as coming from the same sample. The corresponding sample is thus given a very uncertain posterior distribution that represents a form of weighted average between the two replicates. Any point left of the black line would have a wide posterior distribution for two reasons, beyond it, the curve is mostly flat meaning that a small change in signal is a large change in concentration and because there is no standard data available and as we move farther from the last standard point, the uncertainty in the location of the curve increases.

The use of Bayesian statistics has a number of advantages. First, because the models have to be written for each application and because the prior is part of the calculations, the assumptions the model makes are explicit (assuming the model code is available). These assumptions can be verified or even modified to see their effect on the conclusions. The use of the prior also allows the inclusion of external information that might come from basic features of the data (e.g. absorbance data is always between 0 and 4) or from prior experiments and experience. The priors can also be used to regularize the estimation. That is, they can be more or less concentrated around “neutral” or conservative values (if such

values exist). For example, the prior on a regression coefficient can be concentrated around 0 (e.g. N(0, 1)) such that the data has to be very strong for the coefficient to take on large values. Otherwise, the prior will pull the estimated coefficient towards 0. This prevents the models from being overly enthusiastic about the data and generally has advantages when attempting to use the model to predict future data. (McElreath, 2015, Chapter 6)

Second, the posterior represents a simple concept, the probability of different values of the parameters after seeing the data (and, always, assuming the priors and the model). This posterior distribution can be used to estimate, for example, the probability that two means are different without requiring reference to a null hypothesis or to repeated sampling. For example, a p-value of 0.021 on a T-test would be interpreted as: "If the two means are exactly equal, we would expect to see a T value at least this large only 2.1% of the time over an infinite number of experiments." Whereas, a Bayesian result could be interpreted as: "According to this model, there is a 97.9% probability that mean 1 is greater than mean 2." With the second being the probability that is generally of interest.

Third, due to the use of bespoke models in Bayesian statistics, the models can be "generative", that is to say that they can be made to capture (at least some of the) processes by which the data comes to be. For example, a standard curve made by serial dilution of a concentrated standard may not have exactly the nominal concentration at each point, due to both random (instrument accuracy) and technical errors. Bayesian models can easily incorporate such aspects of the data to provide a more honest appraisal of the uncertainty around estimates based on such a curve.

Fourth, if multiple groups or categories are included in the same model, for example in a multilevel model, there is no need to correct for multiplicity. Multilevel models "shrink" the estimates towards the overall mean so that more (or better) data is needed to have an estimate that is very different from the others.

2.7.1.1 Notation

Variables that are measured (e.g. OD, luminescence, weight, etc.) or fixed (e.g. concentration) are labelled using their symbol, e.g. optical density as OD and concentration as Conc or C. For variables that are unknown but represent quantities in equations, a name will be used, e.g. Bottom and Span in logistic curves. For unknown variables that represent distributional parameters (e.g. mean, standard deviation, probability), lowercase greek letters will generally be used. The "~" (tilde) symbol reads as "is distributed as". Shorthand and parameterizations for distributions are as follows:

Table 1:Distributions used and parameterizations

Distribution Name	Shorthand	Parameterization	Parameters
normal	N	$N(\mu, \sigma)$	μ = mean, σ = standard deviation
multinomial	MultiNom	$MultiNom(p_1 \ldots p_k)$	k = number of categories, p_k = probability of that category such that $\sum_{i=1}^{k} p_i = 1$
dirichlet	Dir	$Dir(\alpha_1 .. \alpha_k)$	k = number of categories, α_k = weight of that category

2.7.2 Survival analysis

The log-rank test was used to determine significance in survival experiments between the wild-type and modified mice treated with the same antibody. A p-value less than 0.05 is considered significant. The analysis was carried out in R 3.4.1 using the *survival* package.

2.7.3 Quantitative ELISA and cytokine measurements

The model used to estimate the concentrations of IgG in the quantitative ELISA and the cytokine concentrations is based on a dilution-assay model designed by Gelman et al. (Gelman, Chew, & Shnaidman, 2004) The model was adapted for use in the current assays and recoded in Stan. (Stan Development Team, 2013, 2016)

The model uses the measured signal (called y, OD_{650} or $\ln(Light\ Units)$) to determine the log of the concentration ($\ln(\theta)$). Each well has a measurement that is part of a dilution series (there are D dilutions [called d] numbered 1…D for each sample), which has replicates (there are K replicates per dilution [called k] numbered 1…K). We have I samples [called i] numbered 1…I. So there are approximately $I \times D \times K$ measurements, but not all samples have the same number of dilutions. The total number of y's is N with each read labelled as y_n for n in 1…N. The samples are run on plate p for p in 1…P and the parameters of the curve are determined for each plate.

$$y_n \sim N(\mu_n, \sigma_y)$$

The mean μ_n is defined using the following equation (a 4-parameter logistic curve):

$$\mu_n = B_{p_n} + \frac{S_{p_{i[n]}n}}{(1 + e^{(\ln(x_{i[n]}) - \ln(EC_{50}{}_{p_n}))) \times H_{p_n}})}$$

The parameters are modeled as multilevel, ensuring that they are consistent plate-to-plate, but allowing variation:

$$S_p \sim N(\mu_S, \sigma_s)$$

$$B_p \sim N(\mu_B, \sigma_B)$$

$$\ln(EC_{50_p}) \sim N(\ln(\mu_{EC_{50}}), \sigma_{EC_{50}})$$

$$\ln(H_p) \sim N(\ln(\mu_H), \sigma_H)$$

The priors on the hyperparameters (e.g. μ_B and σ_B) are tailored to each case (IgG or cytokines) as the properties of the curves are very different. For the cytokines, the prior for $\ln(\mu_{EC_{50}})$ is centered on the average of the log concentration of the standard curve, since different cytokines have standards with different ranges.

The concentration of each sample is modeled, with a mixture prior taking a vector of means (generally integer values from a to b). The result is something like the purple distribution in Figure 2.

$$\ln(\theta_i) \sim \prod_{m=a}^{b} \frac{N(m, 2)}{(b-a)+1}$$

When sample i is the standard (assumes a 1% error on the quantification of the standard provided by the company):

$$\ln(\theta_i) \sim N(\ln(\mu_{Std}), 0.01)$$

Each measurement has an error on the concentration, based on pipetting and other errors. So the error increases with additional dilutions:

$$\ln(x_{i[n]}) \sim N((\ln(\theta_{i[n]}) + \ln(dilution_n)), 0.05 + 0.01 * d_n)$$

For the cytokine measurement, each plate has samples with only buffer (called Std_0) to establish the baseline of the curve:

$$Std_{0_{p,k}} \sim N(B_p, \sigma_y)$$

2.7.4 Neutralization quantification

The 2-parameter curve fit to the neutralization data was fit in GraphPad Prism 5. The data was fit to a 4-parameter curve with the Top fixed to 100 and the Bottom fixed to 0, this ensures that partial curves (like for 4G7) do not result in incorrect values of the median inhibitory concentration (IC_{50}) and that the IC_{50} is the concentration where 50% of the virus is neutralized. The data was not aggregated before fitting the regression.

2.7.5 Flow cytometry analysis

For each sample, the counts of CD4 and CD8 T cells in each of the combination gates are exported. We assume that there is a vector of true frequencies for each group. In this context, all the counts (separately for CD4 and CD8) for each animal are considered as a single data point. By using counts, rather than transforming them into proportions, we preserve the information about the total number of T cells (CD4 or CD8) that were measured. The number of cells measured is important because with low frequencies, some samples may not have enough events to detect the presence of a specific activation pattern. The vector $\overrightarrow{c_a}$ is a vector containing the counts for all 16 activation patterns (for either CD4 or CD8) for an animal. The vector $\overrightarrow{f_g}$ is a vector containing the frequency of each activation pattern for a group of animals. The index g_a is the group of animal a.

$$\overrightarrow{c_a} \sim MultiNom(\overrightarrow{f_{g_a}})$$

Which we can rewrite (more explicitly):

$$(c_1, \ldots, c_{16})_a \sim MultiNom(f_{1_a}, \ldots, f_{16_a})$$

The frequencies for each group are the only parameters of the model. They are given a flat prior on the probabilities scale [0, 1] using the Dirichlet distribution.

$$(f_1, \ldots, f_{16})_g \sim Dir(1,1,1,1,1,1,1,1,1,1,1,1,1,1,1,1)$$

2.8 Availability of data and code

All data and code used here are available at https://gitlab.com/jonaudet/ThesisCode. FCS files of the flow cytometry data are located on FlowRepository.org

CHAPTER: 3 RESULTS

3.1 Antibody characterization

The data presented in this section is adapted from Audet et al. (Audet et al., 2014)

3.1.1 Germline sequence comparison

The sequences of the variable regions of the components of ZMAb were determined in order to confirm that they were unique antibodies. Those sequences were used to determine the germline genes from which the antibodies derived to ensure that they were not clonally related. The sequences for the light and heavy chains were obtained for all three hybridomas. The amino acid sequences of the variable regions are reported in Figure 3. While all three sequences are fairly divergent in their heavy chain sequences, 2G4 and 4G7 share very similar light chain sequences (Figure 3B). The light chains of 2G4 and 4G7 share approximately 84.5% overall homology at the amino acid level, and 67% homology when looking only at the complementarity-determining regions (CDRs).

Figure 3: Amino acid sequences of the three antibodies composing ZMAb.

Alignments of the amino acid sequences of the three antibodies which are in ZMAb, 1H3, 2G4, and 4G7. The boxes highlight the positions of the complementarity-determining regions as reported by IMGT DomainGapAlign. A) Alignment of the heavy chaing sequences. B) Alignment of the light chain sequences.

(Adapted from Audet et al 2014, Sci Rep under CC-BY licence.)

The nucleotide sequences were then entered into the IgBlast tool of the NCBI. The top 3 germline line genes for each antibody are reported in Table 2.

Table 2: Germline sequences associated with the mouse antibodies composing ZMAb

Chain	Antibody	Top V genes	Top D genes	Top J genes	% Similarity to closest V gene
H	1H3	VHSM7.a3.93 SM7.3.54 SM7.2.49	DSP2.2 DSP2.3 DSP2.4	JH2 JH4 JH3	97.6
H	2G4	VHJ606.a6.127# J606.1.79 VH22.1	DSP2.5 DSP2.7 DSP2.8	JH4 JH2 JH3	97.6
H	4G7	J558.12 J558.1 J558.11	DFL16.1 DFL16.2 DFL16.1j	JH3 JH2 JH4	96.3
L	1H3	at4 aq4 ab4	----	JK2 JK1 JK5	100
L	2G4	12-46 12-41 12-44	----	JK2 JK1 JK5	97.9
L	4G7	12-44 12-41 12-46	----	JK4 JK2 JK3	97.9

For the heavy chains, all three antibodies appear to have derived from different families of germline V genes. 1H3 and 2G4 appear to have derived from a related family of D genes (DSP2.X) with 4G7 getting its D region from a different family. The J regions appear quite homogeneous; however, only 4 separate joining (J) region genes exist in the NCBI database. For the light chains, antibodies 2G4 and 4G7 share the same top three closest V genes, albeit in a slightly different order. 1H3 appears to come from a separate family and also has 100% similarity with the closest germline gene (at4). The J regions are also similar, as

there are only 5 separate genes in the NCBI database. Although both 1H3 and 2G4 have the same germline genes in the same order. Overall, all three antibodies are indeed different and developed from different combinations of germline genes.

3.1.2 Cross-inhibition

An ELISA was used to evaluate the extent to which the antibodies of ZMAb can cross-inhibit each other. This allows us to know whether we should expect competition between the components of ZMAb. The ELISA made use of chimeric antibodies and the mouse antibodies. The plates were coated with sucrose-purified virus, blocked, and incubated with the mouse antibodies, including an anti-Marburg virus GP antibody as negative control. The plates were then washed and incubated with the same concentration of mouse-human chimeric antibodies. The detection antibody was an anti-human IgG polyclonal antibody, because an anti-mouse IgG antibody could have reacted to the mouse regions of the chimerics. Table 3 shows the reduction in signal (average of three technical replicates) from each pair of mAbs. Each antibody was its most potent competitor, as expected, and the anti-Marburg virus antibody 3H1 induces no decrease in signal. 2G4 and 4G7 show high levels of competition with each other. Overall, the antibodies 2G4 and 4G7 do inhibit each other, whereas 1H3 appears to bind in a completely different area.

Table 3: Cross-inhibition of the antibodies in ZMAb

		Signal from*		
		1H3	**2G4**	**4G7**
Blocking mAb	**1H3**	60	104	97
	2G4	96	64	66
	4G7	91	44	41
	3H1	114	102	106

* Numbers represent % of maximal signal left.

3.1.3 Neutralization

The antibodies in ZMAb were chosen, in part, because they were neutralizing, it will be useful for reference during the study of the mechanisms of action to have a good estimate of the ability of each antibody to neutralize EBOV/May-eGFP. Neutralization was evaluated by incubating 100 PFU of EBOV/May-eGFP with serial dilutions of the respective antibodies for 1 h at 37°C. Then, the mixture was used to infect Vero E6 cells for 1 h at 37°C. The medium was replaced and the plates were incubated for 48 hrs before formalin fixation. Plaques were counted using an AID ELISpot reader with GFP reading capabilities. The results are presented in Figure 4. Both 2G4 and 4G7 were highly neutralizing with $IC_{50}s$ of 0.157 $\frac{\mu g}{ml}$ (95% CI: 0.136-0.1822) and 0.109 $\frac{\mu g}{ml}$ (95% CI: 0.056-0.212), respectively (Figure 3). 1H3 was substantially less efficient at neutralization, with an IC_{50} of 39.98 $\frac{\mu g}{ml}$ (95% CI: 26.57-60.16). This is consistent with previous reports. (Xiangguo Qiu, Fernando, et al., 2012)

3.2 Mouse mechanisms of action

3.2.1 Fcγ subunit KO

The importance of ADCC, one of the main F_c-mediated effector mechanisms, was evaluated using two different models. In the first model, the mice bear a knock-out mutation preventing the expression of the FcR γ subunit. This subunit is crucial to initiate the signalling cascade after antibodies bind to the FcγR. C57BL/6 mice with a knocked-out FcR γ subunit (KO; N = 6 per group, N = 3 for 4G7) were challenged with $1000 \times LD_{50}$ EBOV/Mayinga-MA via IP injection on Day 0 and treated with 100 μg of the mouse mAbs on Day 2. Normal C57BL/6 mice (WT; N = 6 per group) were challenged and treated following the same schedule. The animals were group-weighed from Day 1 to Day 13.

The PBS-treated animals died on similar days irrespective of their knock-out status (Figure 5A). The 1H3-treated animals all survived, independently of their knock-out status (Figure 5B). For the 2G4-treated animals, one KO animal died on Day 7 for a final survival rate of 83% (95% CI: 58.3-100%) (Figure 5C). The log-rank test for comparing survival curves yielded a p-value of 0.317. All 4G7-treated animals survived the challenge (Figure 5D).

Figure 4: Neutralizing activity of the mAbs against EBOV/Mayinga-eGFP.

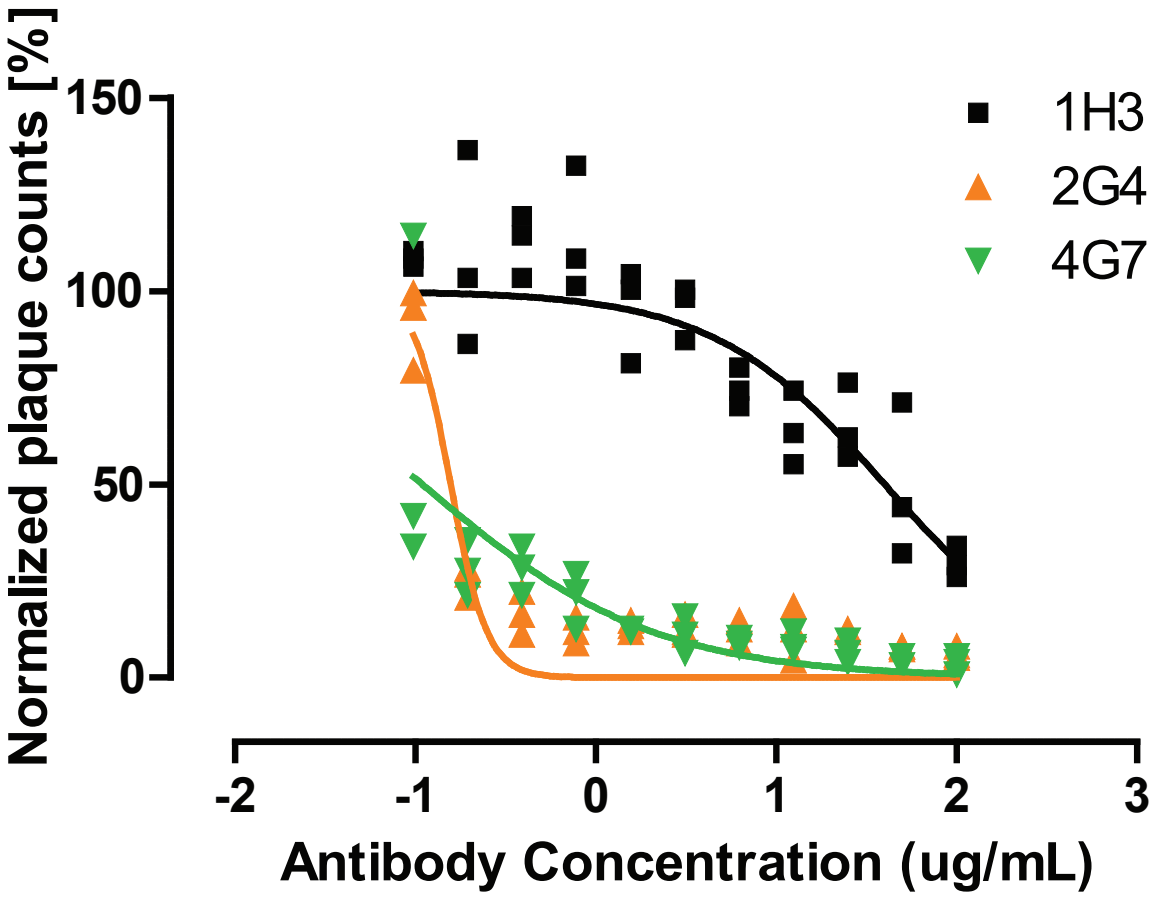

Neutralizing activity of 1H3 (black squares), 2G4 (orange "up" triangles), and 4G7 (green "down" triangles) against EBOV/Mayinga-eGFP. The appropriate concentrations of each antibody were incubated with 100 PFU of the virus for 1 h. The mixture was put on cells for 1 h, then removed. The cells were incubated in fresh medium for 48 h, then fixed with 10% buffered formalin. The fluorescent plaques were counted using a iSpot FluoroSpot Reader System. Counts were normalized so 100% corresponds to wells with no mAb. Data adapted from Audet et al 2014, Sci Rep.

The PBS-treated KO animals lost weight at generally the same rate as the WT animals, although the few animals which died later kept losing substantial weight (Figure 5E). For the animals treated with 1H3, the KO animals lost about 10% of their initial bodyweight, on average, around Day 3, but recovered rapidly to a weight gain by Day 13 (Figure 5F). The WT animals treated with 1H3 did not lose weight, on average, but also did not gain weight during the weighing period. Both groups of animals treated with 2G4 lost weight during the experiment (Figure 5G). The WT group lost up to 20% of their initial bodyweight, on average, versus 10% for the KO group. The animals treated with 4G7 also lost weight during the experiment, albeit less than the 2G4-treated animals (Figure 5H). The WT animals still lost a little bit more weight, on average, than the KO animals; ~8% for the WT and ~6% for the KO.

3.2.2 Nfil3 KO

In order to strengthen the results from the γ-chain knock-out mice, we used C57BL/6 mice in which the *nfil3* gene has been knocked-out (KO). This transcription factor is necessary for the development of NK cells, as such these mice do not have NK cells which are the main effectors of ADCC. This experiment was run in parallel with the γ-chain knock-out mice, thus the same WT animals are used as controls. All animals were challenged with $1000 \times LD_{50}$ EBOV/Mayinga-MA via IP injection on Day 0 and treated with 100 μg of the mouse mAbs on Day 2.

The PBS-treated KO animals (N = 4) died slightly earlier than the WT (N = 6) (Figure 6A). The KO animals died on Days 7 and 8, whereas the WT animals died on Days 7-9. The log-rank test for comparison of survival curves yielded a p-value of 0.141.

Two KO animals treated with 1H3 (N = 6) did not survive the challenge for a final survival rate of 67% (95% CI: 37.9-100%) (Figure 6B). The log-rank test for comparison of survival curves yielded a p-value of 0.138. All KO animals treated with 2G4 (N = 6) survived the challenge (Figure 6C). Since all the WT animals survived as well, no p-values or confidence intervals can be calculated. Four of the 5 KO animals treated with 4G7 did not survive the challenge (Figure 6D) while all WT animals did. The final survival rate for the KO animals is 20% (95% CI: 3.46-100%) and the log-rank test for comparison of survival curves yields a p-value of 0.0072.

The KO animals treated with PBS lost less of their bodyweight than the WT animals, despite the fact that all of them succumbed to the infection (Figure 6E). The KO animals only lost about 13% of their initial bodyweight, on average, versus just under 20% for the WT animals. The KO animals treated with 1H3 lost about 8% of their bodyweight, on average, by Day 8 (Figure 6F) while the WT animals did not lose weight. While the KO animals treated with 2G4 all survived the challenge, the KO mice lost about as much weight as the WT, just under 20% on average (Figure 6G). In this case the KO animals appear to have lost their weight with a slight delay compared to the WT mice. The KO animals also did not recover their weight by Day 14, while the WT animals had gained weight at that point. The 4G7-treated KO mice lost slightly more weight than the WT mice (Figure 6H), about 11% by Day 8 vs 8% for the WT mice. The increase in weight on Day 10 is probably due to the lone survivor not losing much weight.

Figure 5: Survival and weight loss of wild-type and common γ-chain knock-out mice treated with ZMAb.

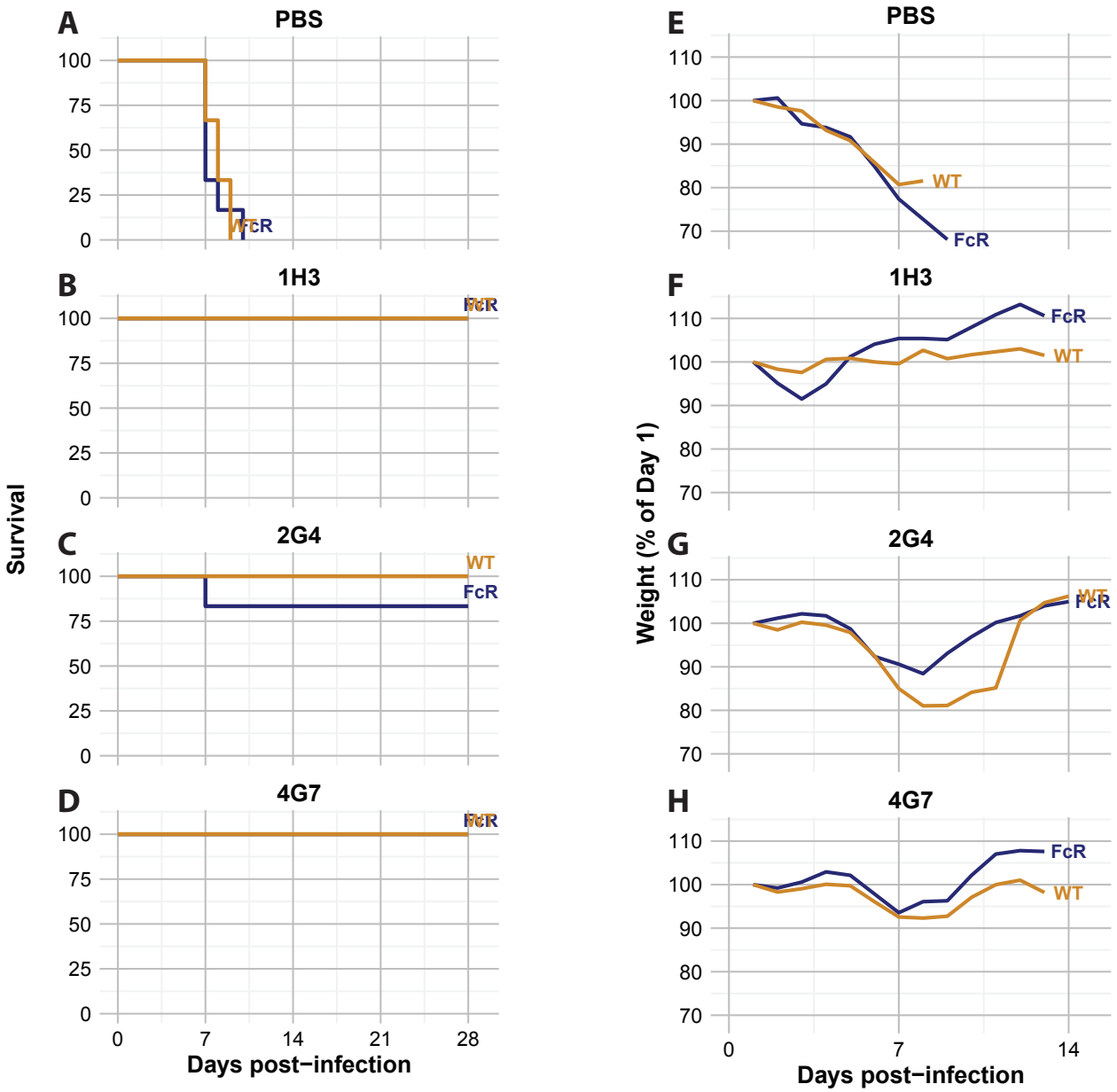

Survival and weight change of mice challenged with 1000 x LD_{50} of EBOV/Mayinga-MA on Day 0 and treated with ZMAb on Day 2. The wild-type animals (WT) are in gold and the animals knocked-out for the common γ-chain (FcR) are in blue. A) Survival curve of PBS-treated animals. B) Survival curve of 1H3-treated animals. C) Survival curve of 2G4-treated animals. D) Survival curve of 4G7-treated animals. E) Weight loss curve of PBS-treated animals. F) Weight loss curve of 1H3-treated animals. G) Weight loss curve of 2G4-treated animals. H) Weight loss curve of 4G7-treated animals.

Figure 6: Survival and weight loss of wild-type and Nfil3$^{-/-}$ mice treated with ZMAb.

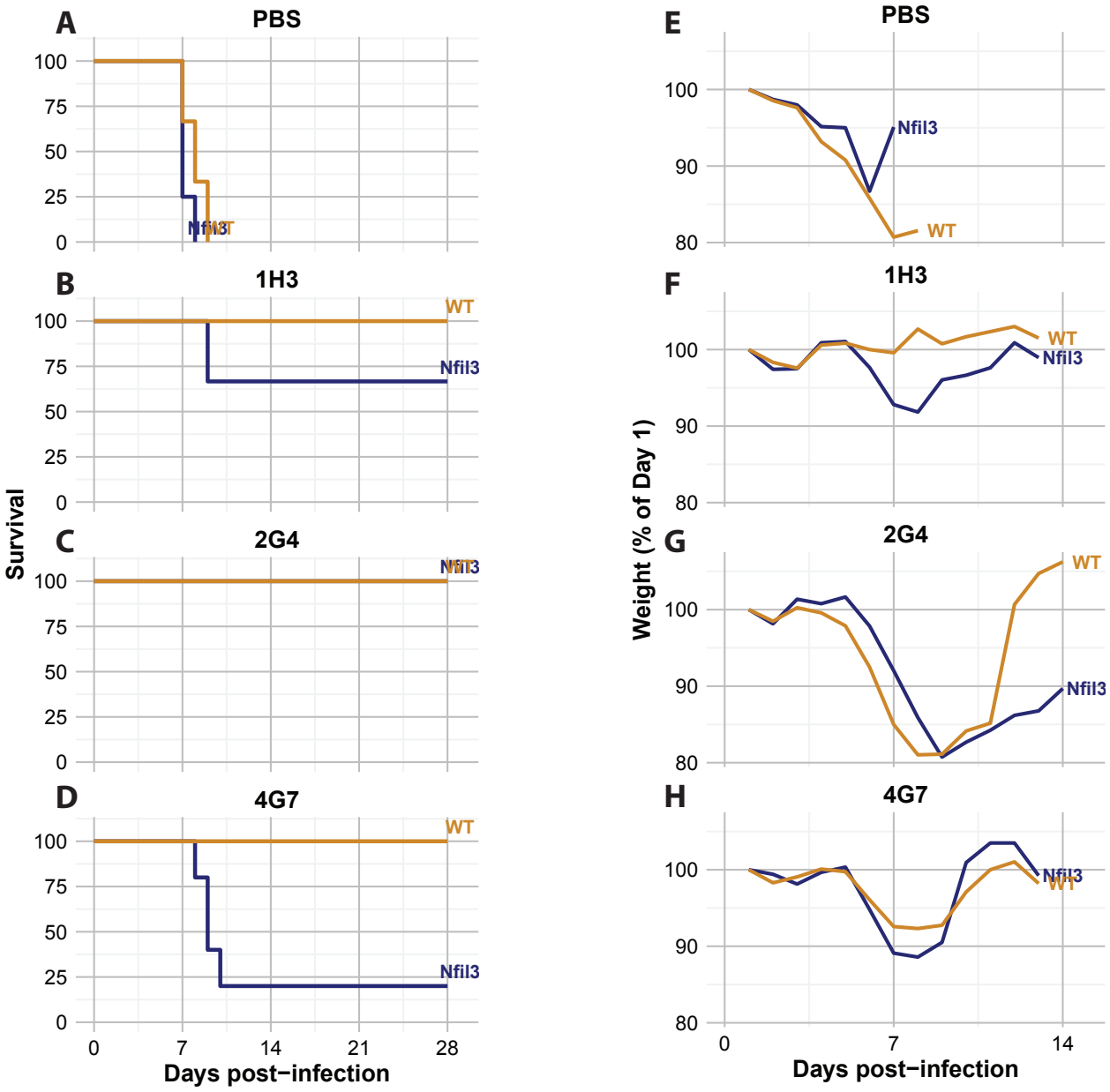

Survival and weight change of mice challenged with 1000 x LD_{50} of EBOV/Mayinga-MA on Day 0 and treated with ZMAb on Day 2. The wild-type animals (WT) are in gold and the animals knocked-out for Nfil3 (Nfil3) are in blue. A) Survival curve of PBS-treated animals. B) Survival curve of 1H3-treated animals. C) Survival curve of 2G4-treated animals. D) Survival curve of 4G7-treated animals. E) Weight loss curve of PBS-treated animals. F) Weight loss curve of 1H3-treated animals. G) Weight loss curve of 2G4-treated animals. H) Weight loss curve of 4G7-treated animals.

Overall, ADCC appears to play at best a minor role in the protective efficacy of 1H3 and 2G4. However, 4G7 may require NK cells to be completely effective; also, the results may not be completely contradictory between the FcR γ subunit and NK cell knock-out models as the smaller sample size for FcR γ subunit may hide a decrease in efficacy.

3.2.3 C1q KO

C1q is an important protein in the complement system. The complement system can kill invading pathogen and infected cells when antibodies mark them and allow C1q to bind. This initiates a cascade of proteases which will lead to the formation of a pore through the membrane and, eventually, cell death. The complement can also enhance the ability of cells like macrophages to phagocytose and destroy infected cells and invading pathogens. In order to understand the effect of the complement, mice which in which the gene for the C1q protein was knocked out (KO) and normal controls (wild-type; WT) were infected and treated under similar conditions.

C1q KO mice and WT controls were infected with $1000 \times LD_{50}$ MA-EBOV via IP injection on Day 0 and treated with 100 μg of the mouse mAbs on Day 2. The animals were weighed and scored daily until Day 14 and checked daily until Day 28. All animals alive on Day 28 were euthanized by anesthetic overdose and cervical dislocation.

For both KO and WT control animals (receiving only D-PBS), all animals died on days 6, 7, and 8 with nearly completely overlapping curves (Figure 7A). The log-rank test for comparing two survival curves yields a p-value of 0.82, which is consistent with the visual assessment that any difference would be substantially smaller than the current sample size

(N = 6 per group) can discriminate. This suggests that the absence of C1q does not appreciably change the normal course of the disease in mice.

Only one animal died in each group (KO and WT) treated with 1H3, on Day 8 for WT and on Day 9 for the KO group yielding identical survival proportions of 83% (95% CI: 58.3-100%) and a log-rank test with a p-value of 0.949 (Figure 7B). For 2G4, both groups (KO and WT) had complete protection (Figure 7C). In this context, no confidence interval or p-values can be calculated. Antibody 4G7 protected 5 of 6 WT animals and all 6 KO animals yielding a survival proportion of 83% (95% CI: 58.3-100%) for the WT group and 100% (CI cannot be calculated) and a p-value for the log-rank test of 0.317 (Figure 7D). In every case the lack of C1q does not appear to have a measureable effect on survival.

Weight loss was also similar between the groups (Figure 8). For the control group, some of the WT animals only started losing weight after Day 5; whereas, the other animals were losing weight by Day 3. For antibodies 1H3 and 2G4 (Figures 8B & C) both the average weights and the individual weights are indistinguishable between the WT and KO groups. For 4G7, the KO group does appear to have lost a little bit more weight in the average, although the individual curves for that group show large amounts of variation. One animal lost about 15% of its bodyweight and had not recovered by day 14, but others recovered and put on weight faster than any WT animal.

Overall, removal of the C1q component appears not to have a large effect on protection mediated by the components of ZMAb.

Figure 7: Survival of wild-type and C1q knock-out mice treated with ZMAb.

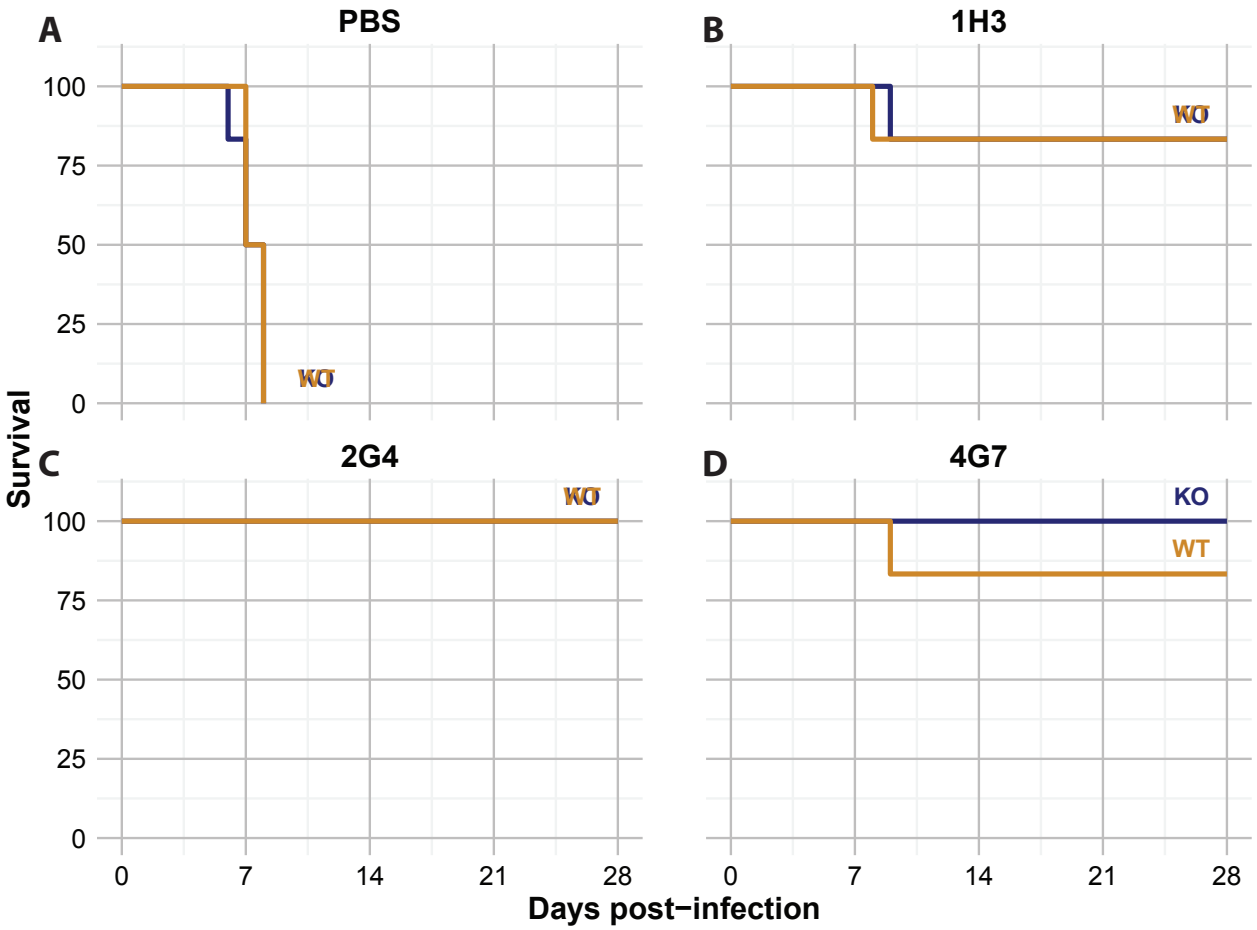

Survival of mice challenged with 1000 x LD_{50} of EBOV/Mayinga-MA on Day 0 and treated with ZMAb on Day 2. The wild-type animals (WT) are in gold and the animals knocked-out for C1q (KO) are in blue. A) Survival curve of PBS-treated animals. B) Survival curve of 1H3-treated animals. C) Survival curve of 2G4-treated animals. D) Survival curve of 4G7-treated animals.

Figure 8: Weight loss of wild-type and C1q knock-out mice after treatment with ZMAb components.

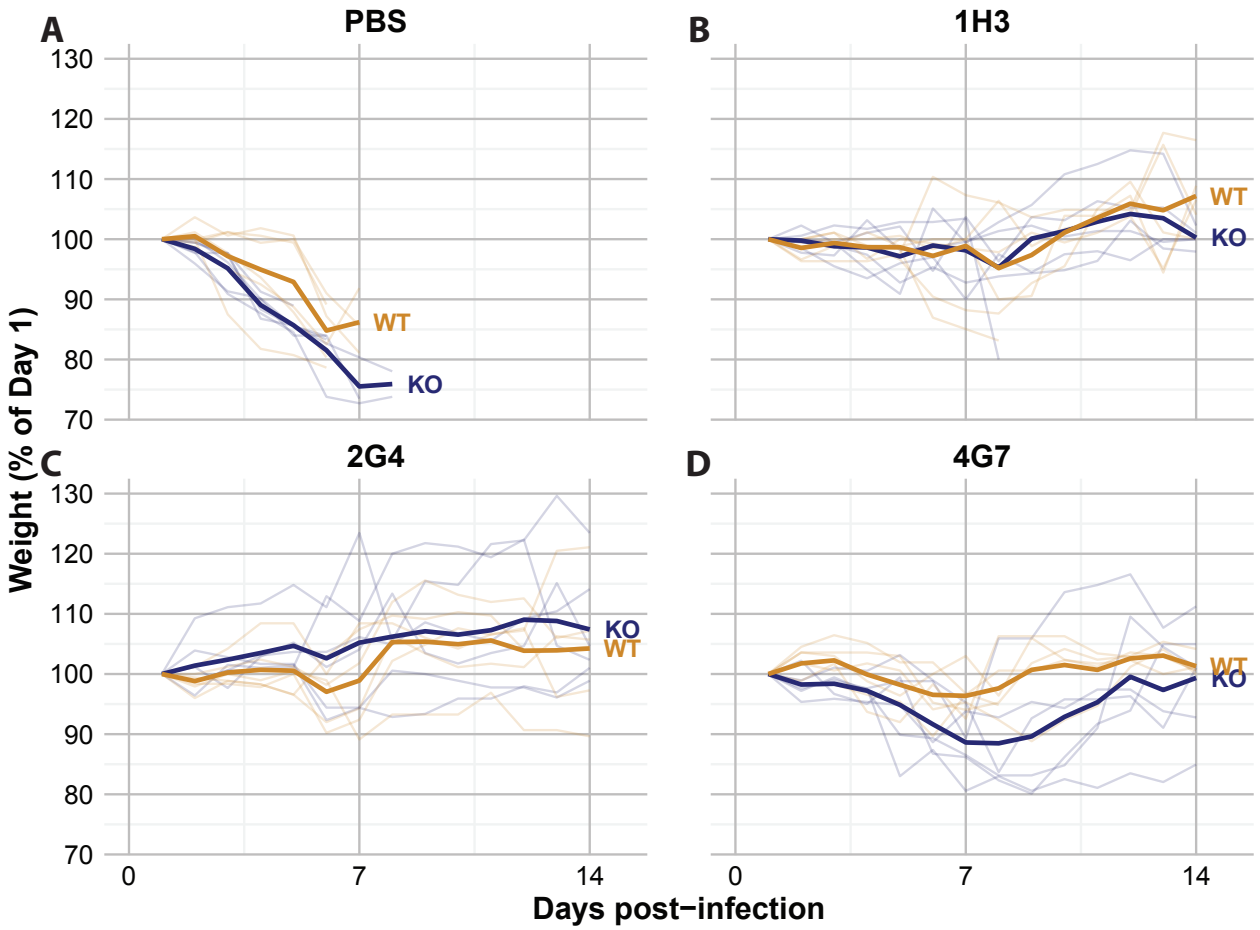

Weight loss of mice challenged with 1000 x LD_{50} of EBOV/Mayinga-MA on Day 0 and treated with ZMAb on Day 2. The wild-type animals (WT) are in gold and the animals knocked-out for C1q (KO) are in blue. The light and thin lines represent individual animals, the thick lines represent daily averages for each group. A) Weight loss of PBS-treated animals. B) Weight loss of 1H3-treated animals. C) Weight loss of 2G4-treated animals. D) Weight loss of 4G7-treated animals.

3.2.4 C3-depleted mice

In order to confirm the results from the C1q knock-out mice and to confirm that the antibodies do not (somehow) indirectly induce complement activation, the efficacy of the antibodies was tested in mice in which the components of the complement downstream of C3 were depleted. Balb/c mice were depleted in complement using cobra venom factor injected IP (N = 8 per group). Control mice were infected at the same time with $1000 \times LD_{50}$ of MA-EBOV on Day 0 (N = 5 per group). Complement-depleted PBS-treated animals died slightly later than the non-depleted controls, on Days 8 through 11 rather than 8 through 9 (Figure 9A). The log-rank test for comparison of survival curves was not significant, with p = 0.17. For 1H3 and 2G4-treated animals, all animals whether complement-depleted or not survived the challenge (Figures 9B and C). Because no animals died in any of the treatments, no p-value or confidence interval can be computed. For 4G7, surprisingly, one non-depleted animal died leading to an 80% observed survival rate (95% CI: 51.6-100%) (Figure 9D). The log-rank test for comparing survival curves yielded a p-value of 0.206.

The PBS-treated non-depleted animals lost up to 25% of their initial bodyweight, whereas the complement-depleted animals only lost 15-20% of their initial bodyweight, on average (Figure 9E). As for survival, the animals treated with 1H3 and 2G4 followed the same pattern of uninterrupted weight gain (Figures 9F and G). The non-depleted animals treated with 4G7 did lose approximately 5% of their initial bodyweight, although this might be due mostly to the animal that died (Figure 9H). On the other hand, the complement-depleted animals treated with 4G7 appear to have had no weight loss, on average.

Overall, the results from complement depletion agree with those of the C1q knock-out mice and support the hypothesis that the complement does not play an important role in mediating the protection provided by the ZMAb antibodies.

3.2.5 Fab fragment protection

In order to remove all other mechanisms of action and evaluate the protective effect of neutralization alone, F_{ab} fragments were generated from each mAb using the Pierce F_{ab} Production and Purification Kit (Fisher). The mice (Balb/c, N = 10 per group) were infected with 1000× LD_{50} EBOV/Mayinga-MA on Day 0. They were treated by IP injection (100 μl) with either: 1) D-PBS alone on Day 2; 2) whole IgG (1 group per mAb) on Day 2; or 3) F_{ab} fragment (1 group per mAb) twice per day (morning and afternoon) on Days 2, 3, and 4. The animals were weighed daily from Day 1 to Day 14. The animals were scored and observed daily from Day 0 to 28.

The control animals died on Days 5-8 as is usual (Figure 10A). The F_{ab} of 1H3 protected 2 of 10 treated animals as opposed to complete protection with the full IgG (Figure 10B). Survival with the F_{ab} was 20% (95% CI: 5.79-69.1%) and 100% with the IgG (no CI). The log-rank test for the comparison of survival curves yielded a p-value of 0.000272. The F_{ab} of 2G4 protected 5 of 10 treated animals while the full IgG protected all treated animals (Figure 10C). Survival with the F_{ab} was 50% (95% CI: 26.9-92.9%) and 100% with the IgG (no CI). The log-rank test for the comparison of survival curves yielded a p-value of 0.012. The F_{ab} of 4G7 protected 6 of 10 treated animals as opposed to the complete protection of the full IgG (Figure 10D). Survival with the F_{ab} was 60% (95% CI: 36.2-99.5%) and 100% with the IgG (no CI). The log-rank test for the comparison of survival curves yielded a p-

value of 0.0295. One animal treated with the 4G7 F_{ab} died on Day 4, which is unusual in mice. This animal appeared well before treatment in the morning of Day 4, but was found dead within a few minutes of being returned to its cage. It is possible that the injection caused internal damage that lead to the animal's death. However, since this could not be verified, the animal was not removed from the study.

Figure 9: Survival and weight loss of wild-type and C3-depleted mice treated with ZMAb.

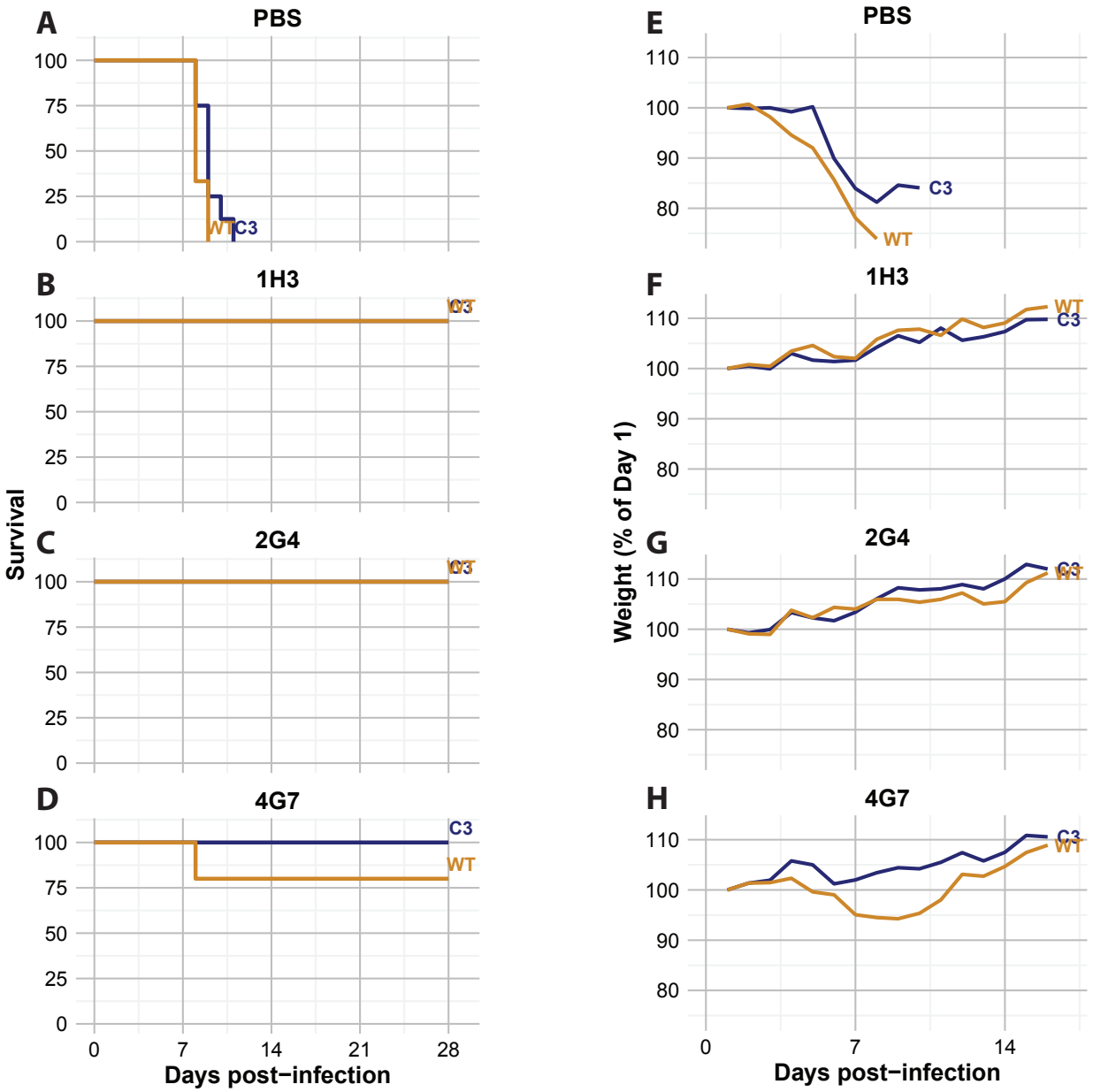

Survival and weight change of mice challenged with 1000 x LD_{50} of EBOV/Mayinga-MA on Day 0 and treated with ZMAb on Day 2. The wild-type animals (WT) are in gold and the animals depleted in C3 (C3) are in blue. A) Survival curve of PBS-treated animals. B) Survival curve of 1H3-treated animals. C) Survival curve of 2G4-treated animals. D) Survival curve of 4G7-treated animals. E) Weight loss curve of PBS-treated animals. F) Weight loss curve of 1H3-treated animals. G) Weight loss curve of 2G4-treated animals. H) Weight loss curve of 4G7-treated animals.

The control animals started to lose weight around Day 4 and kept losing weight until they were euthanized (Figure 11A). The animals treated with 1H3 lost about 5% of their bodyweight on average, but with much variation (Figure 11B). One animal lost no weight and two animals lost approximately 15% of their bodyweight before recovering. The animals treated with the 1H3 F_{ab} all lost at least 10% bodyweight and some of the non-survivors lost more than 15%. Both survivors recovered by Day 14. Most animals treated with 2G4 only lost weight compared to the weight gained after Day 0, coming back down to 100% around Day 9 and coming back up by Day 14 (Figure 11C). One animal did lose approximately 20% of its bodyweight, but recovered by Day 14. Some of the non-survivors treated with F_{ab} 2G4 lost over 20% of their initial body weight. The survivors only lost about 5%, on average. Most animals treated with 4G7 stopped gaining weight, but none lost significant amounts of weight (Figure 11D). On average, the animals treated with F_{ab} 4G7 lost about 10% of their body weight both for survivors and non-survivors. Overall, in every case, the F_{ab}-treated animals generally lost more weight on average than the IgG-treated animals.

Figure 10: Survival of mice treated with full IgG or F_{ab} fragments.

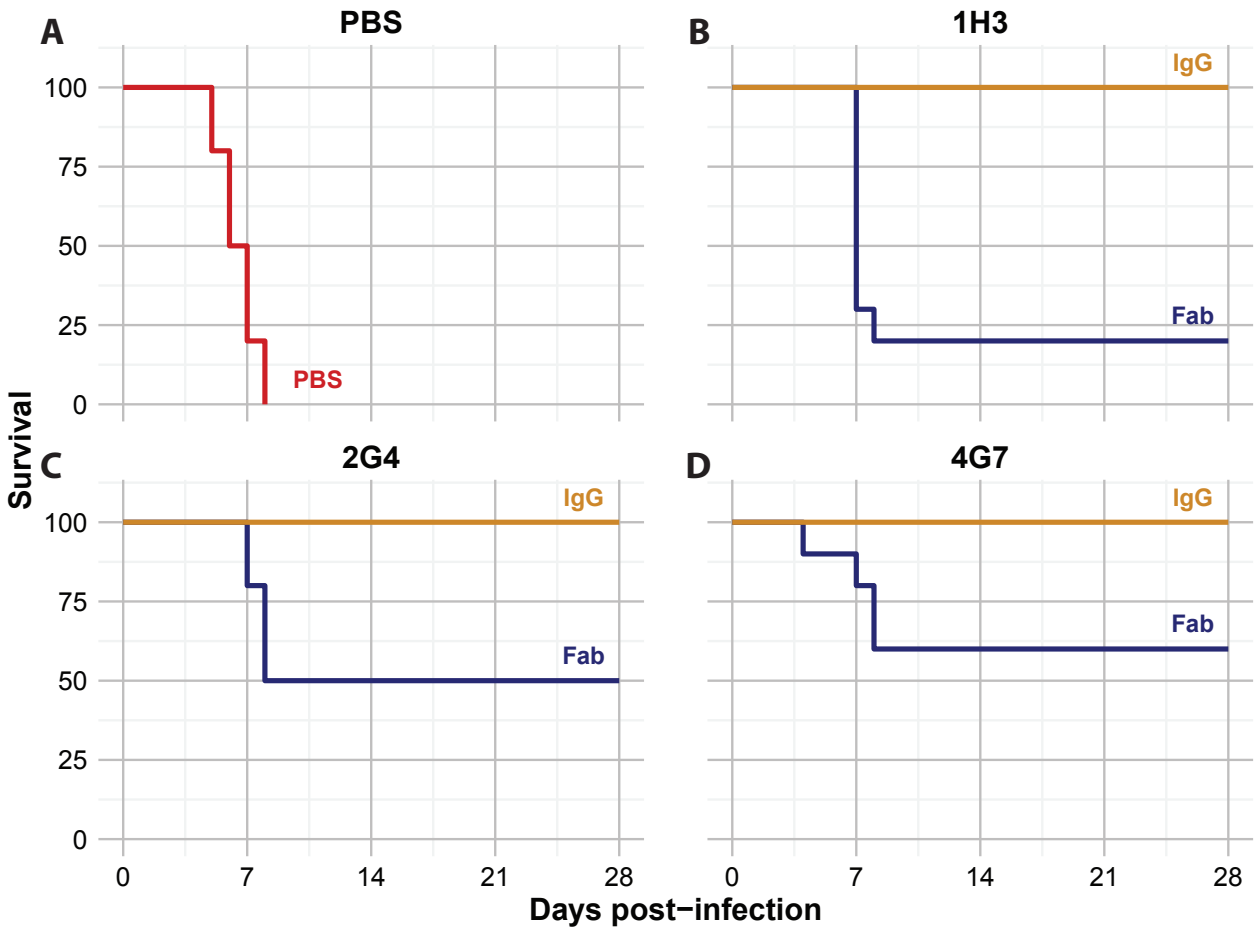

Survival of mice challenged with 1000 x LD_{50} of EBOV/Mayinga-MA on Day 0 and treated with ZMAb on Day 2. The animals treated with full IgG (IgG) are in gold and the animals treated with F_{ab}s (Fab) are in blue. A) Survival curve of PBS-treated animals. B) Survival curve of 1H3-treated animals. C) Survival curve of 2G4-treated animals. D) Survival curve of 4G7-treated animals.

Figure 11: Weight loss of mice treated with full IgG or F_{ab} fragments.

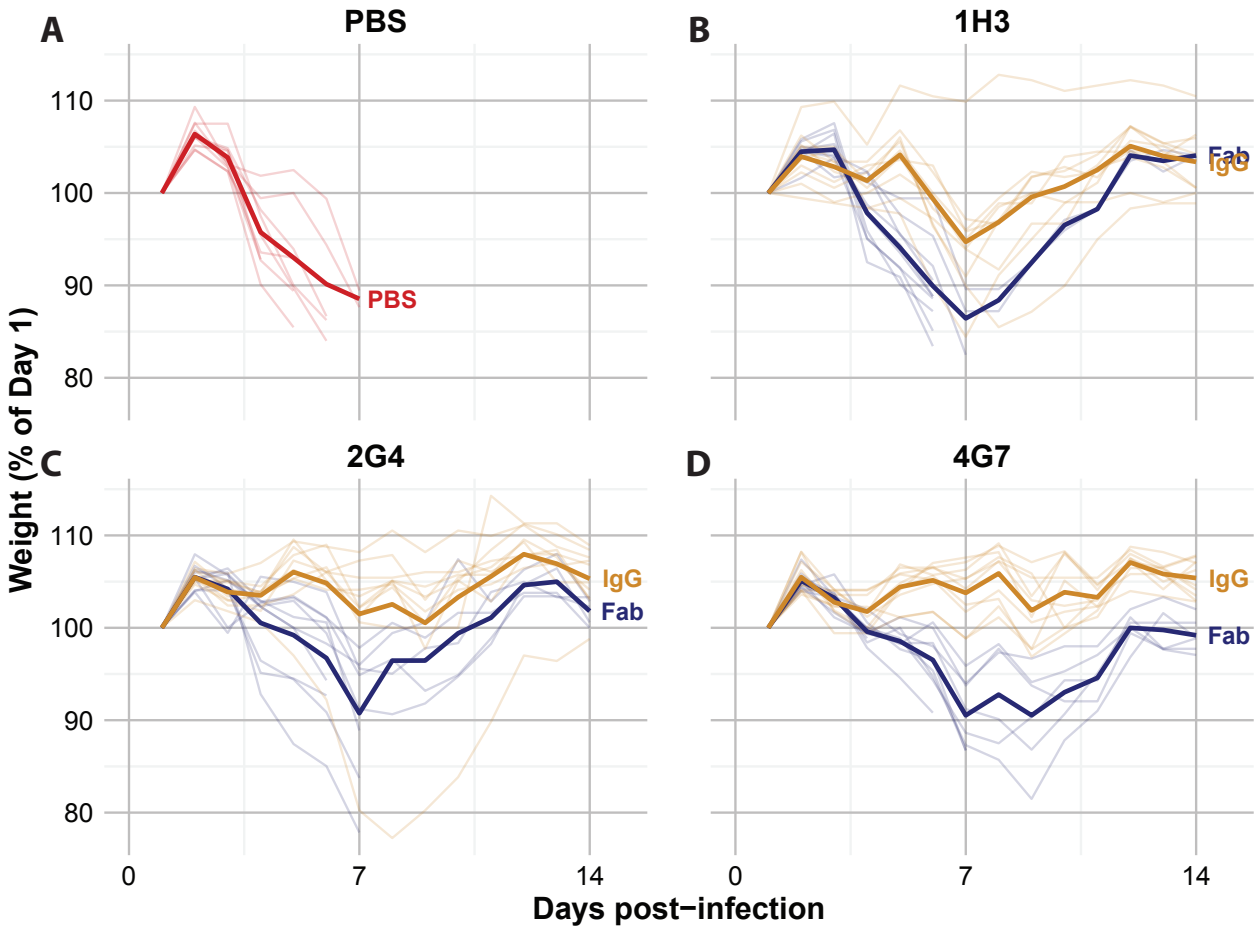

Weight loss of mice challenged with 1000 x LD_{50} of EBOV/Mayinga-MA on Day 0 and treated with ZMAb on Day 2. The animals treated with full IgG (IgG) are in gold and the animals treated with F_{ab}s (Fab) are in blue. The light and thin lines represent individual animals, the thick lines represent daily averages for each group. A) Weight loss of PBS-treated animals. B) Weight loss of 1H3-treated animals. C) Weight loss of 2G4-treated animals. D) Weight loss of 4G7-treated animals.

3.3 NHP immune responses

The immune responses of NHPs which survived the challenge after receiving a version of ZMAb (ZMAb, ZMAb + DEF201, ZMapp1, ZMapp2, and ZMapp) were profiled using three methods. First, the levels of 9 cytokines involved in the T_h1—T_h2 balance were measured in serum samples to obtain a complete profile of the challenge. The cytokine secretion patterns of CD4 and CD8 T cells were measured on Day 21, in response to peptides from the glycoprotein. Finally, the antibody response is measured using two different assays.

The animals treated with ZMAb + DEF201 are included for two reasons. First, they allow us to compare the results in cynomolgus macaques and rhesus macaques since we have 1 group of each species which received the same treatment. Second, depending on the strength of the effect of DEF201, we can get some measure of the effect of the chimerization of the antibodies. Since we know that mouse antibodies (ZMAb) do not interact well with primate FcγRs, we can suggest that if the immune response induced by ZMapp (a chimeric cocktail) is very different, then either ZMapp interacts with the primate immune system in a very different way than ZMAb or DEF201 has a very strong effect.

Since DEF201 expresses IFN-α, we would expect to see that the groups receiving it have a T_h1-skewed cytokine profile and T cell response. For the groups receiving ZMAb + DEF201 to have cytokine and T cell response profiles similar to other groups requires two things: 1) DEF201 must have a negligible effect on the immune response; and 2) ZMAb and ZMapp must interact with the immune system in a similar way.

For all figures related to the immune responses of NHPs (Figures 11-24), individual animals always have the same color within each group.

3.3.1 Viral loads during challenge

The viral loads of the animals that survived their challenge are presented in Figure 12 for reference purposes. The data were adapted from (Xiangguo Qiu et al., 2013) and (X. Qiu et al., 2014). The viral load is reported based on the PCR assays rather than $TCID_{50}$ assays as this measurement should track more closely with the antigen load due to virions in the blood.

Two of the animals treated with ZMAb + DEF201 at 48 h had no detectable viral loads. The third animal had detectable viremia on Days 6 and 9, peaking just under 3 logs, and returned to undetectable levels on Day 16. All three animals treated with ZMAb + DEF201 at 72 h had detectable viremia starting on Day 3. One animal only had detectable viremia on Day 3 with a viremia just above 4 logs which returned to background by Day 6. Another animal also peaked on Day 3 with approximately 6 logs of viremia which returned to background on Day 16. The third animal peaked on Day 6 at 4 logs and returned to background on Day 9. The rhesus macaques treated with ZMAb + DEF201 at 72 h all had a similar pattern of viremia. The animals had detectable viremia from Day 3 to Day 9 with lower viremia on Day 6 and peaks between 2.5 and 3.5 logs. One of the animals did remain around 2 logs. The control animals infected at the same time died on Day 6 (N = 2 for cynomolgus macaques) and on Days 6 and 9 (N = 2 for rhesus macaques).

Four of the rhesus macaques treated with ZMapp1 had detectable viremia starting on Day 3. Of these animals, two peaked on Day 6 and returned to background on Day 9. One also peaked on Day 6 and returned to background on Day 14. Another animal peaked on Day 9 and returned to background on Day 21. This animal reached a peak of just over 10^5

genome equivalents (GEQ)/ml. One animal had no detectable viremia for the entire duration of the challenge. The last animal had detectable viremia only on Day 6. The five rhesus macaques which were treated with ZMapp2 had detectable viremia on Day 3. Three of those animals peaked on Day 3 and returned to background on Day 9 or 14. One animal peaked on Day 6 and also returned to background on Day 14. The fifth animal peaked on Day 9 and quickly returned to background on Day 14. The control animals for this experiment died on Days 6 and 7; additionally, the animal treated with ZMapp2 which succumbed to infection died on Day 9.

All animals treated with ZMapp at 72 h had detectable viremia on Day 3. One animal peaked on Day 6 with a viremia of almost 10^7 GEQ/ml and returned to background on Day 14. Two other animals peaked on Day 6 just under 10^5 GEQ/ml and returned to background on Days 14 and 21. A fourth animal also peaked on Day 6 at about $10^{2.5}$ GEQ/ml and returned to background on Day 9. One animal peaked on Day 3 at 10^4 GEQ/ml and returned to background on Day 9. The sixth animal peaked on Day 9 at 10^4 GEQ/ml and returned to background on Day 14.

All animals treated with ZMapp at 96 h peaked on Day 4 or 7. Most animals peaked at viremia levels of 10^5-10^6 GEQ/ml except one which peaked at 10^4 GEQ/ml on Day 4. Two animals returned to bacakground on Day 10, including the animal with lower viremia. Three other animals returned to background on Day 14 and one on Day 21.

Four of the animals treated with ZMapp on Day 5 had detectable viremia on Day 3. All animals reached peak viremia on Day 5 with two animals over 10^6 GEQ/ml and the other

four between $10^{4.5}$ and $10^{5.5}$ GEQ/ml. The four lower animals returned to background by Day 11. The other two animals returned to background on Days 14 and 21.

The control animals for this experiment died on Days 4, 8, and 8.

Overall, most animals had detectable viremia by Day 3. The viremia peaked on Days 3-9 and was cleared by Day 14, except for 4 animals which cleared their viremia on Day 21.

Figure 12: Viral loads of NHPs during challenge

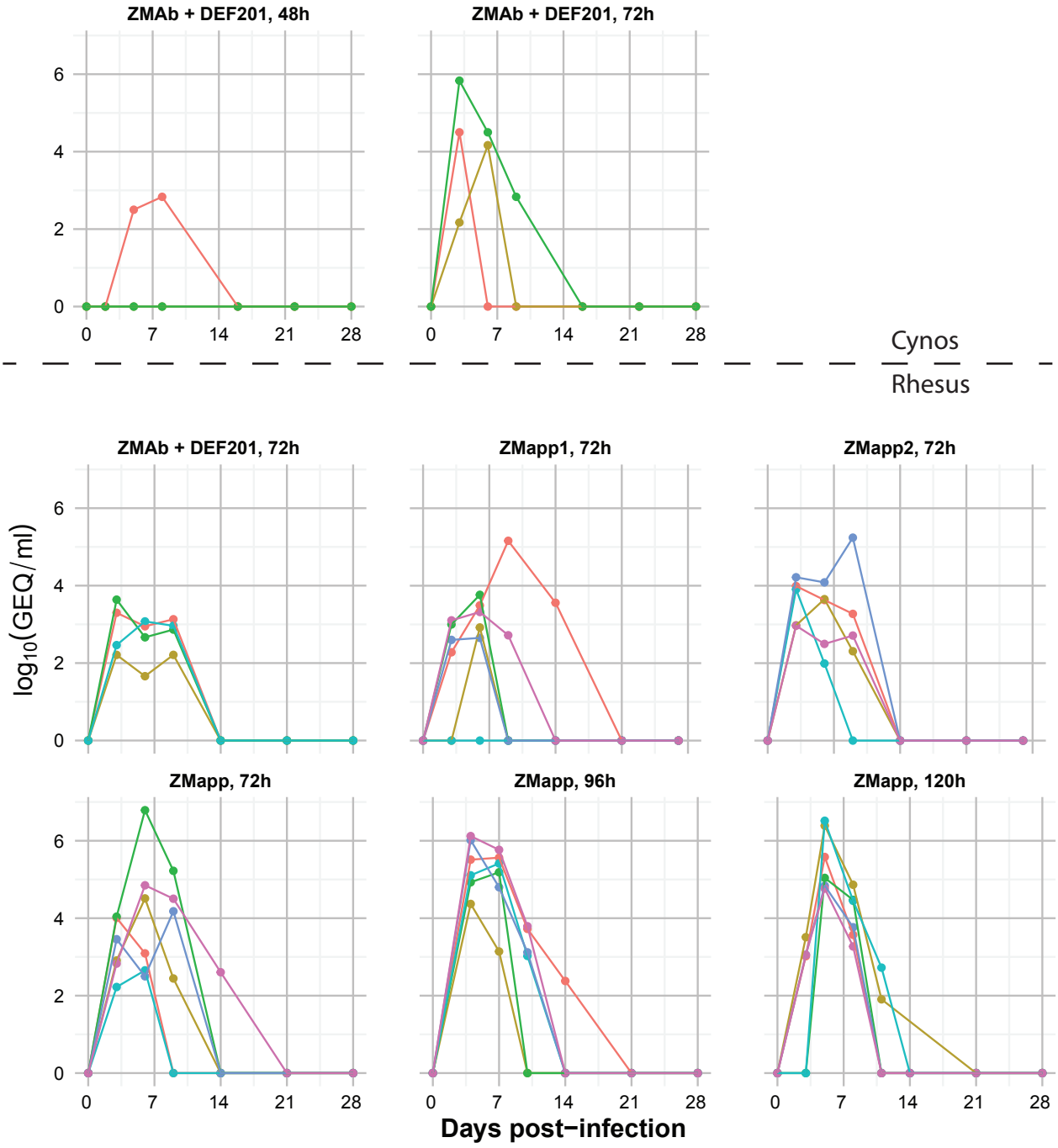

Viral loads of NHPs during their challenge. The viral load was measured using an RT-qPCR assay for the *gp* gene (cynomolgus macaques and rhesus treated with ZMAb + DEF201) or the *l* gene (all other rhesus macaques). The figure presents data adapted from Qiu et al, STM 2013 and Qiu et al, Nature 2014.

3.3.2 Cytokine responses

Measuring serum cytokines is a practical way of obtaining a systemic-level image of the current status of the immune response. Here, nine cytokines are studied because they reveal some of the overall balance between the T_H1 and T_H2 responses that are generally the dominant responses to infection. By measuring cytokine levels at various time points, it is possible to obtain an understanding of how the overall immune response changed during the challenge.

The concentration of 9 different cytokines was assessed in the serum from every available time point for each NHP. The 9 cytokines were: IFN-γ, IL-10, IL-12p70, IL-1β, IL-2, IL-4, IL-5, IL-8, and tumor necrosis factor (TNF)-α. The quantification was done using the TH1/TH2 NHP Cytokine kit from Meso Scale Discovery. Unfortunately, the cynomolgus macaques (which all received ZMAb) developed an anti-mouse IgG antibody response which interferes with the assay. This leads to all animals appearing to have increasing levels of all measured cytokines until Day 28. In the cases of animals which were re-challenged, the measured cytokines were still as high at the beginning of re-challenge as they were on Day 28. For the above reasons, the data from cynomolgus macaques will not be presented.

The calculation from light units to pg/ml is done using a standard curve and a Bayesian model; this allows the incorporation of a dilution error on the increasing dilutions of the standard and provides estimates for all samples. In the event that a sample is in one of the flat regions, either at the top or the bottom, the estimate of the concentration will have wide error bars. The error bars represent the 95% Highest Posterior Density Interval (HPDI), which is the interval with a 95% chance of containing the "true value". Because the

procedure always provides an estimate of the concentration, the limit of quantification should be thought of as the point below which quantification has substantial uncertainty, leading to intervals that can be as much as 4 logs in width.

This uncertainty is represented in two ways in the figures: first, all points have error bars to show the 95% HPDI; second, because the error bars can overlap and be difficult to visualize, the points are made to be more transparent as the uncertainty grows. The lines in the graphs always relate the best estimates of each animal.

Because the standard curve becomes essentially flat below the limit of quantification, the measurement (i.e. light units) only helps to define an upper limit to the concentration. The posterior distribution (e.g. the yellow distribution in Figure 1) averages over a likelihood (not represented) that extends from negative infinity (on the log-scale, 0 pg/ml) to the maximum concentration that can lead to the amount of signal measured. At this point, only the prior distribution (in purple in Figure 1) prevents the value from going to negative infinity. In this context, the lower end of the uncertainty and the estimate itself are likely to be affected (to some degree) by changes in the prior, although the upper end of the uncertainty will remain more stable. In Supplementary Figure 1, it is possible to observe that for values above the limit of quantification, the Bayesian approach used here and the results calculated by the software provided by Meso Scale Discovery are in near-perfect accordance. Values at or below the limit of quantification have a large discrepancy as the uncertainty in the curve drags the best estimates towards a concentration of 0 pg/ml (negative infinity on those graphs). Since the classical regression does not account for the uncertainty in the curve to affect the interpolated concentrations (the concentrations are

calculated from the best-fit parameters only), the values are estimated much higher. Also, the classical regression will not calculate the estimated concentration for some very low measurements, whereas the Bayesian regression will adjust the regression to allow some kind of value to be given to all measurements (which makes sense since the measurement was made, it must be possible).

Overall, values with very wide uncertainty intervals (very transparent) should be thought of more as placeholders than actual concentrations, the data does not allow a clear determination between 0 and some other very small value. Large changes in this range (e.g. 2 or more log-units) may reflect true changes but that remains uncertain. Estimates of increases will be based on the point estimates but those points will generally be described as (and should be thought of as) simply "below the limit of quantification".

The data presented in the figures represents curves that have been "centered" vertically so that overall trends may be made apparent. The correction is done by choosing the 4 lowest values of each animal (curve) and using them to calculate the animal's and the group's mean "baseline", on the log scale. The difference between an animal's baseline and that of its group is used to shift its concentrations up or down so that all animals in the group have the same baseline mean. For this reason the results below report the relative increases (e.g. 1 log), the relative location of the points within a curve is maintained.

3.3.2.1 IFN-γ

As expected during a viral infection, the levels of IFN-γ varied during the challenge (Figure 13). In general, the levels peaked around Days 3-8, increasing by anywhere from 0 to almost 5 logs. The response then returned to baseline, in most cases, by Day 14. Rhesus

macaques treated with both ZMAb and DEF201 took slightly longer to return to baseline, by Day 21 (Figure 13A). These animals also peaked quite early, three peaked on Day 3 and one on Day 6. The smallest increase was just over 2 logs and the largest was about 4.

The animals treated with ZMapp1 had a similar range of increase (Figure 13B). Four of these animals peaked on Day 3, one had two peaks on Days 3 and 8, and one peaked on Day 8. They returned to baseline by Day 14.

The animals treated with ZMapp2 showed more variability in the intensity and timing of their response (Figure 13C). Four of the five animals peaked around Day 8 and the other around Day 14. Some animals also had much weaker response, increasing by only about 1 log and remaining below the lower limit of quantification (as observed by the large error bars).

The three groups of animals treated with the final ZMapp product show interesting trends (Figure 13D-F). The animals treated at 72 h post infection are similar to the ZMapp1 animals, although they appear to peak more around Days 5 and 8, with only one animal peaking on Day 3. The total intensity and the duration of the high-IFN-γ phase increase as treatment is delayed. This is most obvious when treatment occurs at Day 5 (120 h), where all animals reach concentration clear of the background variation on Days 0, 11, 14, 21, and 28. Some animals in the 96 and 120 h treatment groups have an increase as strong as 5 logs.

Figure 13: Interferon γ concentration in the serum of Rhesus macaques after challenge with EBOV/Kikwit and treatment with monoclonal antibodies

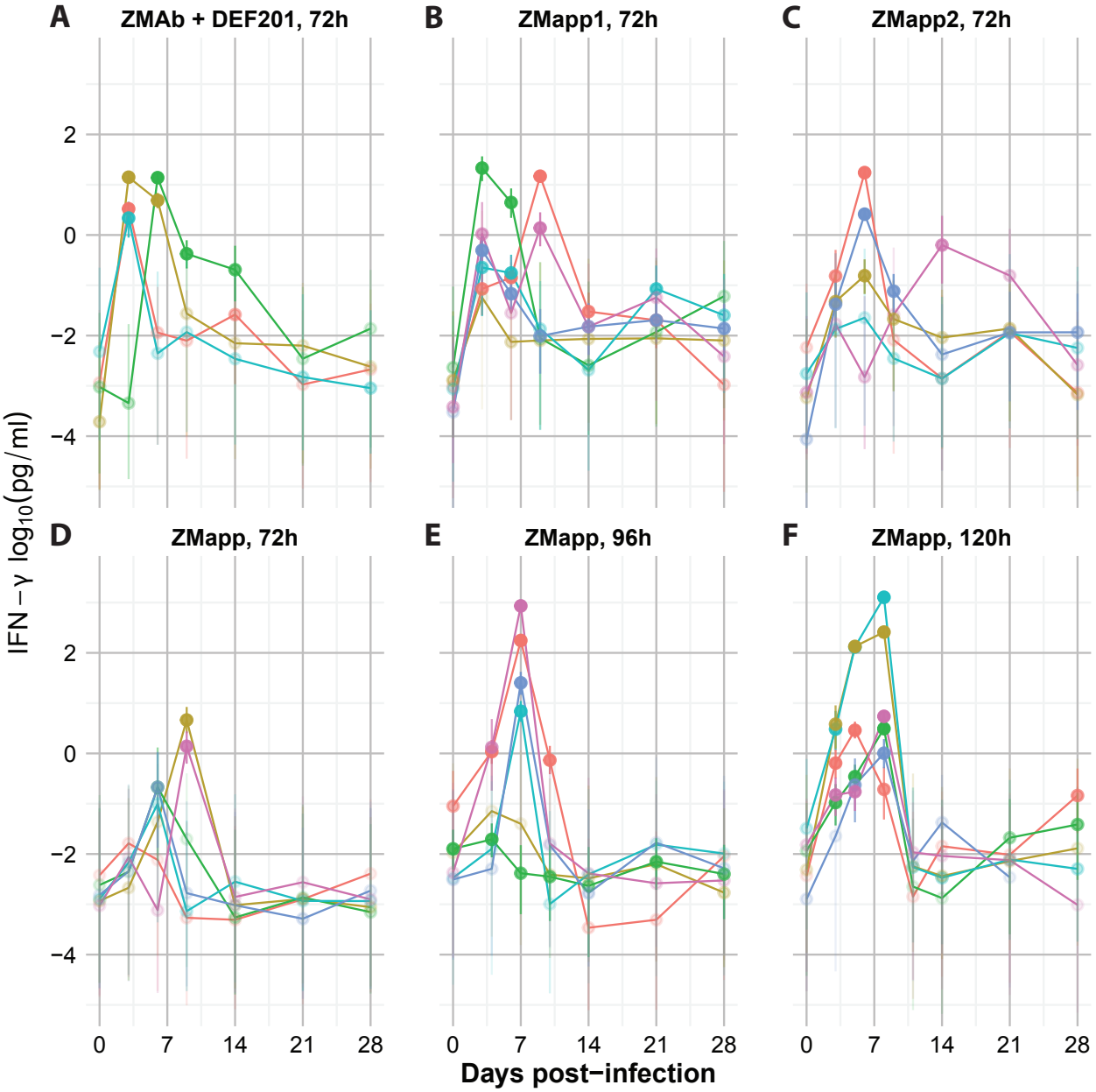

Concentration of interferon γ were estimated using an electrochemiluminescent assay. The limit of quantification was about 0.100 pg/ml. The concentrations are calculated from a standard curve using a bayesian multilevel model. The error bars represent the 95% HPDI for the sample. The individual curves were vertically centered for each group using the 4 lowest values (”baseline level”) of each animal’s curve. The transparency of the points reflects the uncertainty of each value, more transparent points have very wide error bars, more opaque points have shorter error bars and are, therefore, more accurate and reliable. The colors within each group represent different animals.

Figure 14: Interleukin 1β concentration in the serum of rhesus macaques after challenge with EBOV/Kikwit and treatment with monoclonal antibodies

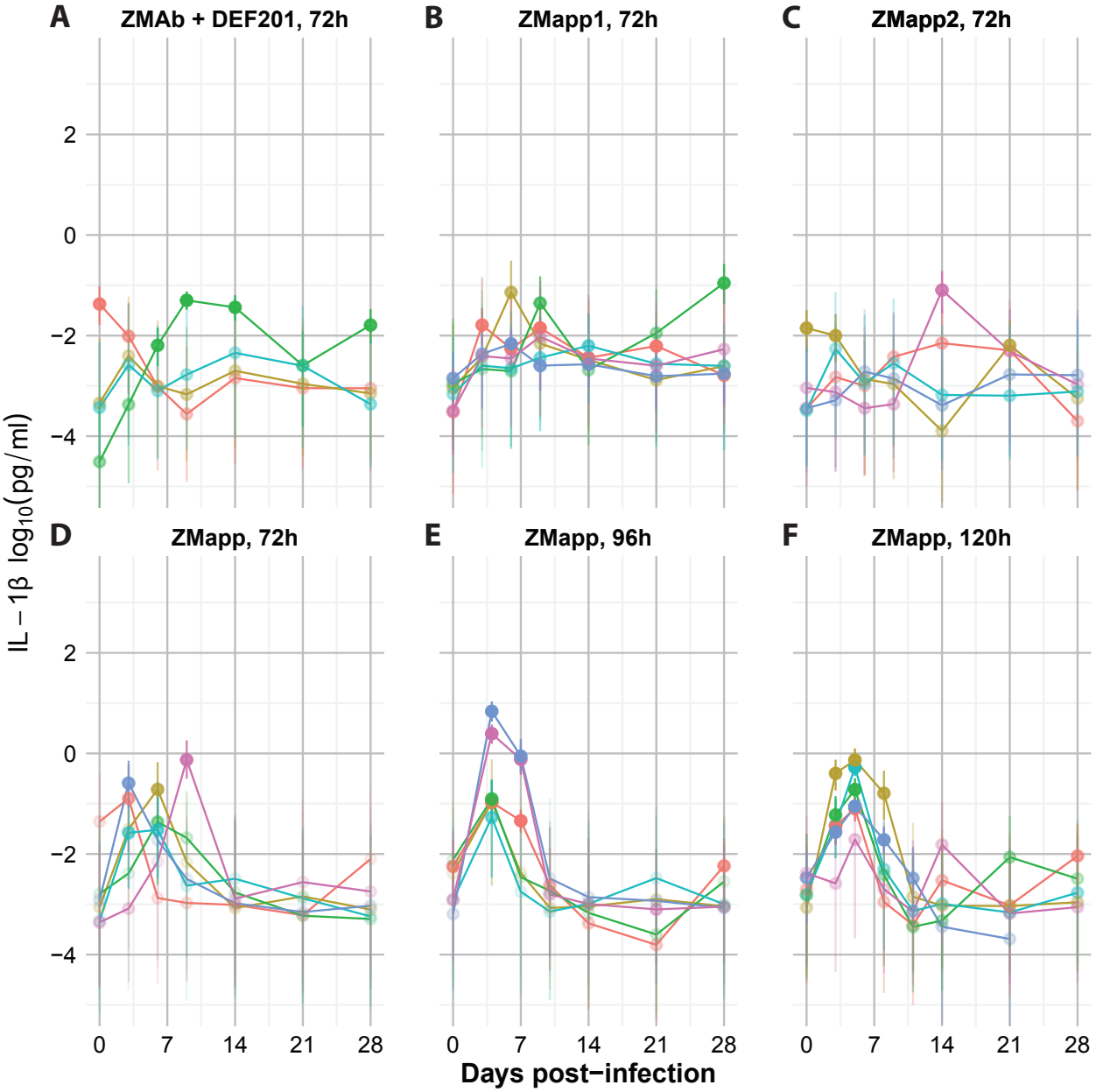

Concentration of interleukin 1β were estimated using an electrochemiluminescent assay. The limit of quantification was about 0.031 pg/ml. The concentrations are calculated from a standard curve using a bayesian multilevel model. The error bars represent the 95% HPDI for the sample. The individual curves were vertically centered for each group using the 4 lowest values (”baseline level”) of each animal’s curve. The transparency of the points reflects the uncertainty of each value, more transparent points have very wide error bars, more opaque points have shorter error bars and are, therefore, more accurate and reliable. The colors within each group represent different animals.

3.3.2.2 IL-1β

The cytokine IL-1β followed kinetics that were generally quite different from IFN-γ (Figure 14). Most animals in the ZMAb + DEF201, ZMapp1, and ZMapp2 groups did not show much change during the challenge (Figure 14A-C). One animal in the ZMAb + DEF201 group did have an increase of about 3 logs which decreased, but did not return to baseline by Day 28. One animal in the ZMapp1 group had an increase of 2 logs by Day 28. Finally, one animal in the ZMapp2 group had an approximately 2.5-log increase on Day 14, which returned to baseline by Day 28.

The animals treated with ZMapp did show changes in IL-1β during the challenge (Figure 14D-F). Surprisingly, the animals treated at 72 h with ZMapp show an increase between 1.5 and 3 logs with peaks between Days 3 and 9, while none of the ZMapp1-treated animals showed similar kinetics despite the treatments being extremely similar (ZMapp1 used the mouse 4G7 rather than the chimeric in ZMapp). The animals treated at 96 h showed a more unified pattern with all animals reaching the peak on Day 4. For three animals, the peak appears longer-lasting than the animals treated at 72 h. The intensity of the increase is also greater with a range of 2 to 4 logs. Two animals treated at 96 h appear to have had an increase in IL-1β between Days 21 and 28.

The animals treated at 120 h did not have stronger increases than the animals treated at 96 h, with a range of increase of about 0.5 to 3 logs for the peak between Days 3 and 8. Two animals from the 120 h group had increases on Days 14 or 21 (purple and green lines); although, the animal in purple never reached a concentration that is above the high uncertainty range (it always remained below the limit of quantification, which is at about

-1.5 $log_{10}(\frac{pg}{ml})$). Two of the animals had peaks that were relatively flat, lasting from Day 3 to Day 8.

3.3.2.3 IL-2

The kinetics of IL-2 were quite varied between the different treatments (Figure 15). The animals treated with ZMAb or ZMapp1 or ZMapp2 had increasing levels of IL-2 during the challenge (Figure 15A-C). The animals treated with ZMAb + DEF201 generally started showing increased levels of IL-2 around Day 6. The concentration of IL-2 remained high until Day 28, when it was still about 1 to 4 logs higher than on Day 0. The animals treated with ZMapp1 and ZMapp2 followed similar kinetics but with many animals showing earlier increases where IL-2 concentration were rising or high on Day 3, before any treatment was administered. The increase in IL-2 is also more consistent and substantial in the ZMapp1 and ZMapp2 groups, where Day 28 concentrations are approximately 3 to 6 logs higher than the Day 0 concentrations.

These kinetics are virtually non-existent in the ZMapp-treated animals (Figure 15D-F). The animals treated with ZMapp at 72 h generally remained in the low-precision area of the standard curve, making it difficult to differentiate between actual trends and noise. Four of the animals in this group (teal, blue, purple, and green) appear to have had a decrease in IL-2 between Days 0 and 3. Three of those (blue, purple, and green) increased by Day 6 along with the yellow animal. The teal animal remained low until it increased on Day 14. The red animal remained relatively low and only started increasing around Day 21.

Figure 15: Interleukin 2 concentration in the serum of rhesus macaques after challenge with EBOV/Kikwit and treatment with monoclonal antibodies

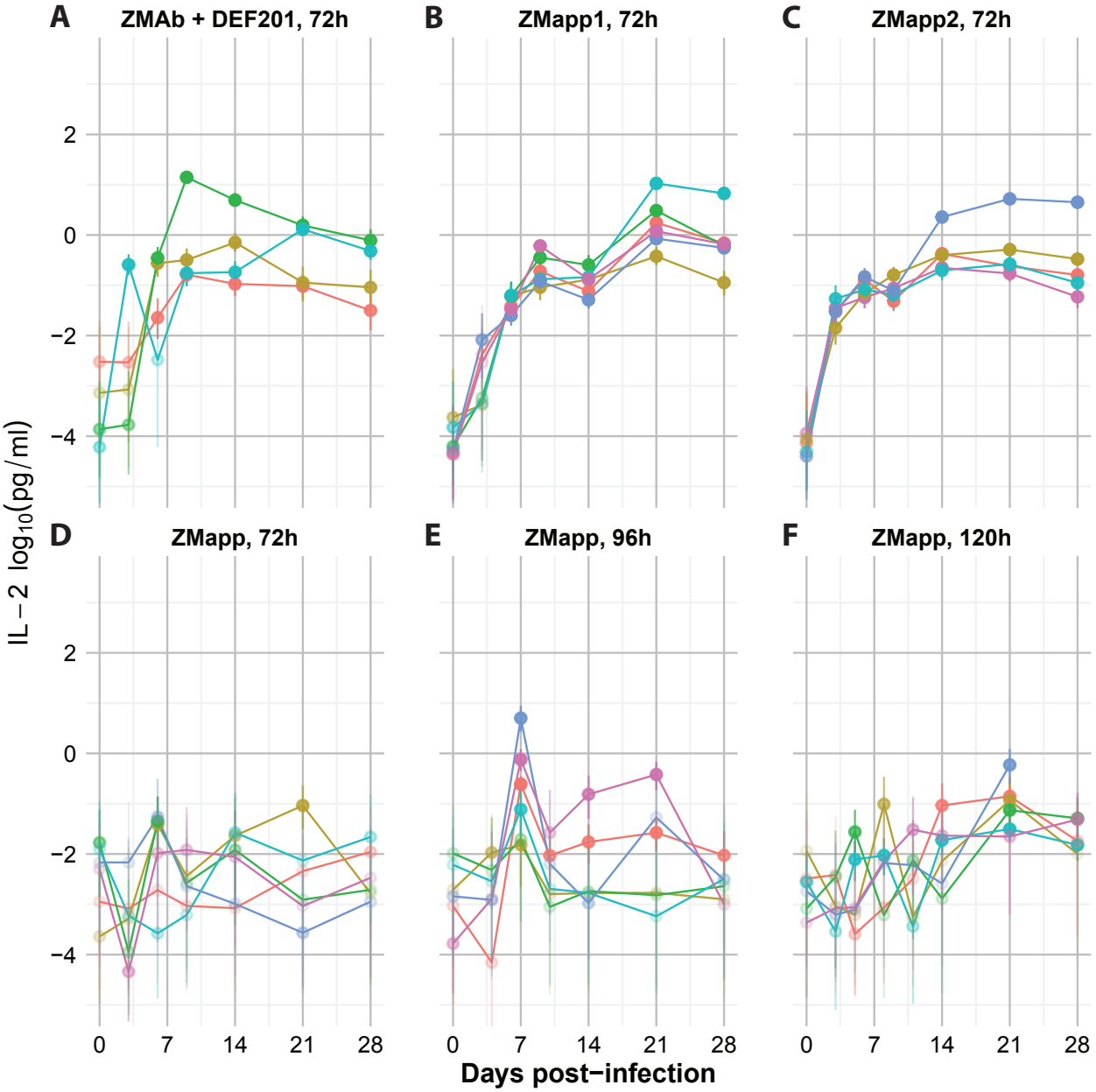

Concentration of interleukin 2 were estimated using an electrochemiluminescent assay. The limit of quantification was about 0.063 pg/ml. The concentrations are calculated from a standard curve using a bayesian multilevel model. The error bars represent the 95% HPDI for the sample. The individual curves were vertically centered for each group using the 4 lowest values (”baseline level”) of each animal’s curve. The transparency of the points reflects the uncertainty of each value, more transparent points have very wide error bars, more opaque points have shorter error bars and are, therefore, more accurate and reliable. The colors within each group represent different animals.

The animals treated at 96 h had different kinetics than were seen before. Four of these animals (blue, purple, red, and teal) had a peak of IL-2 around Day 7 and three of them (blue, red, purple) had a secondary peak on Day 21. The green and yellow animals did not have much change between Days 0 and 7, but did decrease by about 1 log on Day 10. The teal animal also decreased on Day 10 and its IL-2 concentration remained low until Day 28, similar to the yellow and green animals. The purple animal also decreased substantially on Day 28.

Two of the animals treated at 120 h (green and yellow) to have few patterns during the first half of the challenge, the concentration of IL-2 oscillates up and down in the low-precision space of values. These two animals rejoin the others on Days 21 and 28. The teal and purple animals appear to mostly increase from Day 0 to Day 28 with the purple animal stabilizing around Day 11 and the teal animal around Day 14. The red animal initially dips on Day 5 and then increases through Day 21 and goes back down by 1 log on Day 28. The blue animal increases through Day 21. While the early kinetics of IL-2 production in the animals treated at 120 h is different from ZMapp1 and ZMapp2, they are somewhat consistent in being elevated after Day 14.

3.3.2.4 IL-4

In many cases, IL-4 showed a high level of within-group variation in concentration kinetics (Figure 16). All animals treated with ZMAb + DEF201 showed an increase in IL-4 on Day 6 and three continued to increase on Day 9 (Figure 16A). All animals slowly returned near their Day 0 levels by Day 28.

Figure 16: Interleukin 4 concentration in the serum of rhesus macaques after challenge with EBOV/Kikwit and treatment with monoclonal antibodies

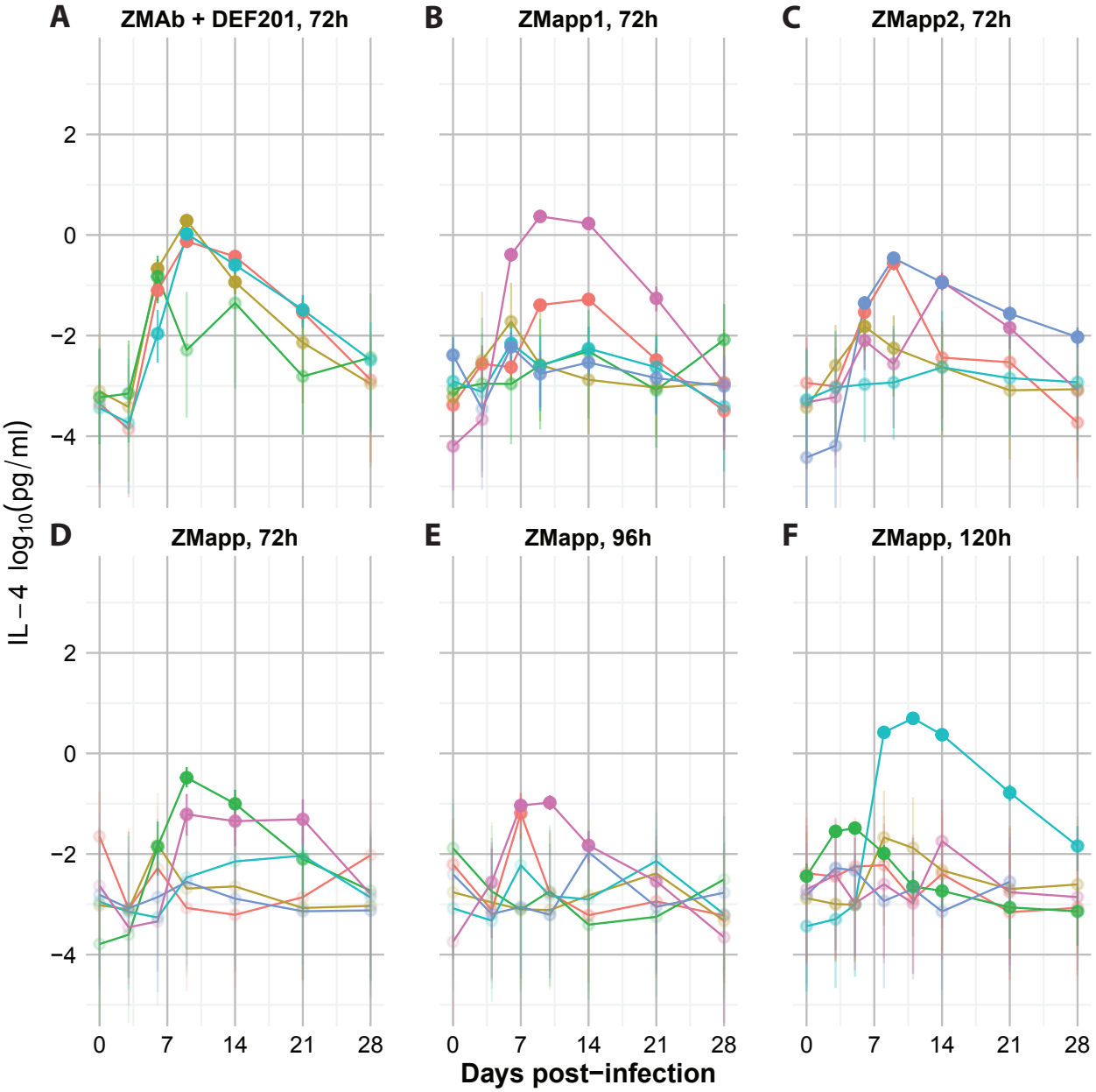

Concentration of interleukin 4 were estimated using an electrochemiluminescent assay. The limit of quantification was about 0.016 pg/ml. The concentrations are calculated from a standard curve using a bayesian multilevel model. The error bars represent the 95% HPDI for the sample. The individual curves were vertically centered for each group using the 4 lowest values (”baseline level”) of each animal’s curve. The transparency of the points reflects the uncertainty of each value, more transparent points have very wide error bars, more opaque points have shorter error bars and are, therefore, more accurate and reliable. The colors within each group represent different animals.

The animals treated with ZMapp1 showed more variation in IL-4 kinetics (Figure 16B). Two animals (red and purple) had IL-4 concentrations measureable in the more precise section of the standard curve. The concentration of IL-4 in the red animal peaked on Day 14 with a 2-log increase in IL-4 over Day 0 and returned to baseline on Day 28. The purple animal peaked on Days 9 and 14 with a > 4-log increase over Day 0 and also returned near baseline by Day 28. The other animals did not have much of an increase in IL-4 during the course of the challenge.

In the animals treated with ZMapp2, one animal (teal) did not have much change in concentration and remained below the limit of quantification for the entire period (Figure 16C). The yellow animal had a slight increase on Day 6 (about 1.5 log), but the concentration did not rise to levels that could be quantified with precision. The teal and red animals both peaked on Day 9 with a 4-log increase (teal) and a 2.5-log increase (red). Both declined substantially by Day 28 with red returning to baseline while teal was still measureable with precision. The blue animal peaked later, on Day 14, with an approximately 2-log increase and returned to baseline by Day 28.

Two animals in the ZMapp 72 h group showed increases above the limit of quantification, green and purple (Figure 16D). The green animal peaked on Day 9 with an increase of about 3.5 logs and then went back to background. The purple animal increased on Day 9 and remained stable until Day 21, it returned to baseline by Day 28. The teal and red animals appear to have increases on Days 21 and 28, respectively, but still remain in the low precision range.

Four of the animals treated at 96 h did not show much change in serum IL-4 during the challenge, oscillating in the low precision range (Figure 16E). The red animal had an IL-4 peak on Day 7 then returned to baseline. The purple animal peaked on Days 7 and 10 with a 3-log increase, approximately, before returning to baseline by Day 28.

The group of animals treated at 120 h also had 4 animals which remained below the limit of quantification (Figure 16F). The curve for the green animal shows a slight increase, about 1 log, around Days 3 and 5. Despite all the points on the curve being above the limit of quantification, its flatness means the centering makes it look like the response is low. Although the change from baseline was, indeed, small suggesting that while the concentration was higher, the challenge and treatment did not affect it very much. The teal animal had the largest increase of the ZMapp-treated animals with a 4-log increase between Days 8 and 14 and returned close to baseline by Day 28.

In all cases except the green animal treated at 120 h, the large increases always happen after the first treatment which suggests that the treatment might be related to the change in IL-4 concentrations.

3.3.2.5 IL-5

In general, IL-5 concentrations tended to oscillate near the limit of quantification (Figure 17). In the ZMAb + DEF201 group, most animals had measureable levels of IL-5 between Days 6 and 14 (Figure 17 A). The yellow animal peaked on Day 6 with an increase of slightly less than 1 log and then returned to baseline around Day 21. The red animal peaked on Days 9 and 14, with a similar increase and also returned to baseline by Day 21. The green animal peaked on Day 14 with minor peaks on Days 6 and 28. The maximum

increase from Day 0 was about 3.5 logs. The teal animal may have had a decrease in IL-5 on Days 3 to 9; however, all its values, except for the peak on Day 14, are in the low-precision range. The maximum increase from Day 0 for this animal is about 1 log.

Two of the animals treated with ZMapp1 which did have a change in IL-5 (teal and yellow) peaked on Day 6 with increases of 2.5-3 logs compared to Day 0 (Figure 17B). The teal animal remained at the same levels until Day 28 while the yellow animals returned to baseline on Day 9. The purple animal did not have IL-5 concentrations above the limit of quantification during the entire challenge. The green animal fluctuated substantially during the early phase, see-sawing over 2 logs until Day 9, then increasing slowly until Day 28. The red animal had slowly increasing IL-5, peaking on Day 14 with a 1.5 log increase over Day 0 which then declined back to baseline by Day 28.

For the animals treated with ZMapp2, only the teal and blue animals showed interesting increases over the Day 0 values, with an about 1.5-log increase on Day 9 in both cases (Figure 17C). The teal animal returned to baseline on Day 14, the blue animal's IL-5 levels decreased slowly until Day 28. The red animal appears to have oscillated around the limit of quantification leading to see-saw patterns with most time points in the low-precision range below the limit of quantification. The yellow animal appears to have a peak around Day 9, but never quite crosses the limit of quantification. Finally, the green animal never moves from baseline and remains below the limit of quantification.

Figure 17: Interleukin 5 concentration in the serum of rhesus macaques after challenge with EBOV/Kikwit and treatment with monoclonal antibodies

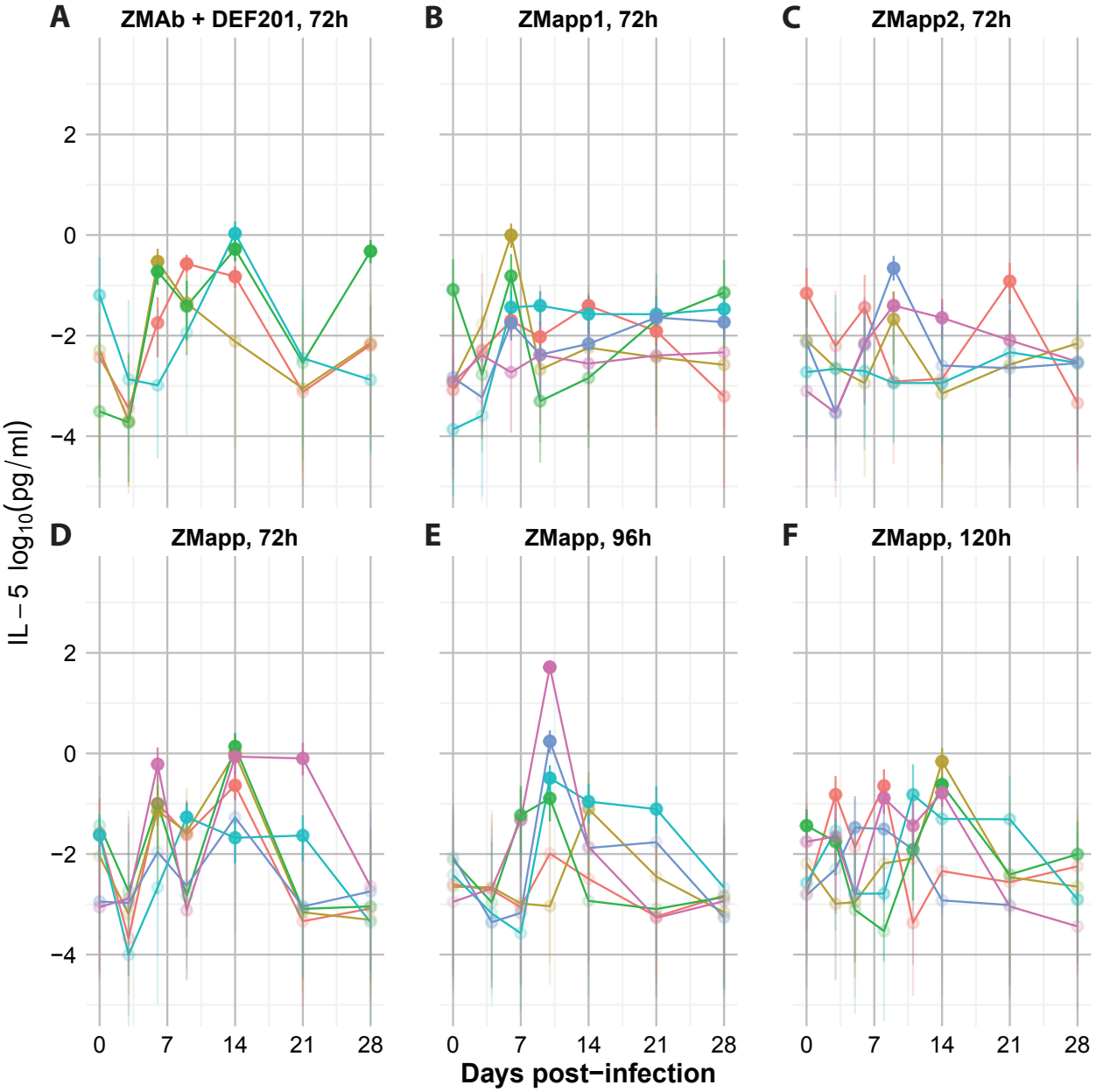

Concentration of interleukin 5 were estimated using an electrochemiluminescent assay. The limit of quantification was about 0.033 pg/ml. The concentrations are calculated from a standard curve using a bayesian multilevel model. The error bars represent the 95% HPDI for the sample. The individual curves were vertically centered for each group using the 4 lowest values (”baseline level”) of each animal’s curve. The transparency of the points reflects the uncertainty of each value, more transparent points have very wide error bars, more opaque points have shorter error bars and are, therefore, more accurate and reliable. The colors within each group represent different animals.

Most of the animals treated with ZMapp at 72 h follow a similar pattern, albeit with different intensities (Figure 17D). The teal animal appears to have a marked decrease of IL-5 on Day 3, when, despite much uncertainty, the uncertainty intervals for Day 0 and 3 are non-overlapping. This animal then recovers and remains close to the limit of quantification until Day 21. The other five animals, generally, show some decrease on Day 3 (1-2 log), and increase on Day 6 (1-3 log), a decrease on Day 9 (0.5-3 log), and a final increase on Day 14 (1-3 log), followed, for four of them, byt a return to baseline on Day 21. The purple animal only returns to baseline on Day 28.

The animals treated at 96 h also show a pattern, with five animals peaking around Day 9 and then generally decreasing by Day 14 or 21 (Figure 17E); although, the red animal never passes above the limit of quantification. The purple animal displays the largest increase in IL-5 in the entire data set, with a difference of 5 logs between Day 0 and the peak on Day 9. The teal animal decreases more slowly after the Day 9 peak, only returning to background on Day 28. The yellow animal, unlike the others, peaks on Day 14.

The animals treated at 120 h show a high level of variability in the kinetics of IL-5 production (Figure 17F). The red animal had quantifiable IL-5 on Days 3 and 8, then returned to baseline with a possibly strong decrease on Day 11. The yellow animal peaked on Day 14, with an increase of 2 logs over the Day 0 concentration, and then returned to baseline. The green animal had a considerable decrease in IL-5 between Day 0 and Day 8 (~2 logs) and then peaked on Day 14 slightly above the Day 0 level and returned to baseline on Day 21. The teal animal jumped around below the quantification limit until Day 8, then peaked on Day 11 (less than 2 logs above Day 0) before decreasing slightly on Days

14 and 21 and returning to baseline on Day 28. The blue animal had a wide peak from Day 5 to Day 11, but always remained below the limit of quantification. The purple animal had slight peaks on Days 8 and 14 before returning to baseline on Day 21.

Overall, across all the groups, there is often a general decrease in IL-5 around Day 3 or 4 before it increases again.

3.3.2.6 IL-8

The IL-8 response also shows a large amount of variability both within and between the groups (Figure 18). All the animals treated with ZMAb + DEF201 have an initial decrease on Day 3, with varying intensity (Figure 18A). The strongest decrease comes from the red animal with an almost 4-log change, going from well above the quantification limit to far below the limit. The response then recovers and remains slightly above the limit of quantification until Day 14 after which it returns to baseline levels. Given its kinetics, it is possible that the dip on Day 3 is not actually as strong since the uncertainty is very high, the upper limit of the uncertainty interval is -1.8 which yields a decrease of about 2 logs. The yellow animal has a weak initial dip and a peak that remains in the low-precision range on Day 9. The green animal reaches a peak on Day 14 about 1.5 log higher than the Day 0 level, decreases on Day 21 and increases again on Day 28. The teal animal appears to increase slightly on Day 6 but remains in the range below the limit of quantification until Day 21, then returns to baseline.

Figure 18: Interleukin 8 concentration in the serum of rhesus macaques after challenge with EBOV/Kikwit and treatment with monoclonal antibodies

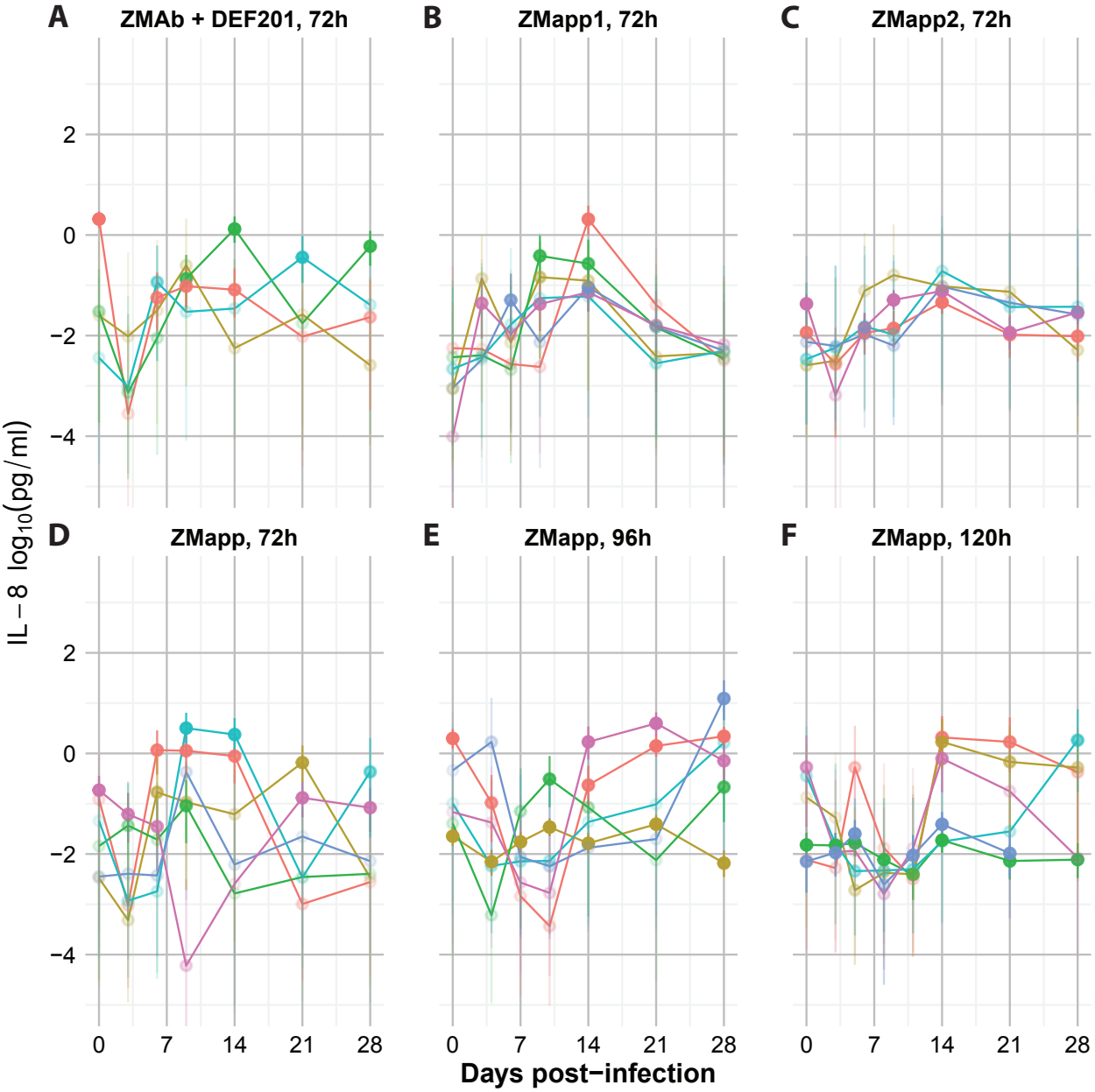

Concentration of interleukin 8 were estimated using an electrochemiluminescent assay. The limit of quantification was about 0.018 pg/ml. The concentrations are calculated from a standard curve using a bayesian multilevel model. The error bars represent the 95% HPDI for the sample. The individual curves were vertically centered for each group using the 4 lowest values (”baseline level”) of each animal’s curve. The transparency of the points reflects the uncertainty of each value, more transparent points have very wide error bars, more opaque points have shorter error bars and are, therefore, more accurate and reliable. The colors within each group represent different animals.

For the ZMapp1-treated animals, four animals peaked on Days 9 and 14 (yellow, green, teal, purple) and returned slowly to baseline by Day 28 (Figure 18B). The red animal peaked on Day 14 only, for an estimated change of about 2.5 logs, and returned to baseline by Day 28. The blue animal had two peaks (Days 6 and 14) and returned to baseline by Day 28.

The animals in that were treated with ZMapp2 showed less dramatic changes in IL-8 concentrations (Figure 18C). The red animal showed little movement over the challenge with a peak approximately 0.8 log above baseline on Day 14, but all samples except Day 3 were close to the limit of quantification. This is supported by uncertainty intervals that are generally less than 1 log-unit wide. The blue animal also had generally well-defined concentrations, again except on Day 3. This animal also showed little variation during the challenge, with the only change of more than 1 log being on Day 3 when the concentration falls below the limit of quantification. All three other animals (yellow, green, and teal) remained below the limit of quantification for the duration of the challenge, as exemplified by uncertainty intervals with a width of about 3 log-units at all time points.

The animals treated with ZMapp at 72 h responded with three different patterns (Figure 18D). The first pattern, including the yellow, green, and blue animals consists of animals with overall concentrations of IL-8 below the limit of quantification. These animals have one or two samples which rise to being close to or slightly above the limit of quantification (Day 9 for green and blue and Day 21 for yellow). All three animals fall back to a similar concentration close to their baseline and Day 0 levels by Day 28. The second pattern includes the red and teal animals and consists of a burst of IL-8 production in the middle of the challenge. It starts with a concentration close to but below the limit of quantification on

Day 0, this is followed by an apparent decline on Day 3, a decrease of almost 2 logs. While the uncertainty is high on both days the estimate of the concentration on Day 0 lies outside of or at the edge of the uncertainty estimate for Day 3, suggesting that there really is a decrease, although the exact intensity is quite uncertain. This decrease is followed by a substantial increase on Day 6 (red) or 9 (teal) of 3 and 3.5 logs, respectively. These increases are close to or above the limit of quantification leading to fairly well-measured concentrations, especially for the teal animal. Both animals remain high through Day 14 and decline on Day 21. The animals diverge on Day 28 when the teal animal appears to be producing more IL-8, whereas the red animal remains at baseline. The third pattern includes a single animal, purple, where concentrations are generally high compared to other animals. Most of the time points for this animal have uncertainty intervals with width ranging from 0.6 to 1.4 logs wide, which is decently precise compared to much of the IL-8 data. The concentrations of IL-8 appear to decline around Day 9, with an apparent effect of 2.8 logs. The uncertainty intervals of Days 6 and 9 are entirely non-overlapping. The response starts increasing on Day 14 and reaches its Day 0 level on Day 21.

The levels of IL-8 in animals treated at 96 h also follow three patterns (Figure 18E). The first two pattern are somewhat similar to the third pattern (purple animal) of the animals treated at 72 h. The first pattern includes the red and purple animals and is almost identical to the 72 h purple animal except that the decrease happens over 6 days (from Day 4 to Day 10) and the recovery to the higher levels happens in 7 days rather than about 14. For both animals, the higher levels of IL-8 are fairly well-defined. The second pattern includes the teal and blue animals and has an extended through. The concentration declines by Day 4 (teal) or 7 (blue) and remains low until Day 28. It is important to note, however, that the

teal animal always has much uncertainty around its concentrations, about 3 logs in width for the uncertainty intervals. Similarly, the only time when the concentration for the blue animal has useful accuracy is the Day 28 concentration. Finally, two animals, yellow and green, appear to have relatively stable concentrations of IL-8 during the challenge. While the green animals has a number of points below the limit of quantification, the yellow animal had well-quantified and stable concentrations of IL-8 throughout the challenge.

Similar groupings can be made for the animals treated at 120 h (Figure 18F). The yellow and purple animals started higher than most, declined and stayed low from Day 3 to Day 11. They recovered and were producing detectable levels of IL-8 by Day 14 with the yellow animal then declining slightly until Day 28 while the purple animal declined to baseline levels. The teal animal also declined from its Day 0 concentration and remained low until Day 21 and then peaked on Day 28. The red animal started at low levels and may have peaked on Day 5 but that is uncertain as the concentration was still below the limit of quantification. The IL-8 levels return to the Day 3 levels and increase on Day 14 to above the limit of quantification. They remain high until Day 21 and go down slightly on Day 28 to the same level as the Day 3 concentration. Finally the blue and green animals had stable IL-8 concentrations that were well-defined throughout the entire challenge period.

Overall, in many cases, IL-8 shows an initial decline around Day 3 and then climbs back to Day 0 levels or higher. However, there exists substantial variation even within groups in the way individual animals appear to respond to the infection and treatment.

3.3.2.7 IL-10

The levels of IL-10 generally remained below the limit of quantification of the assay (Figure 19). The animals treated with ZMAb + DEF201 show little change in their IL-10 concentrations (Figure 19A). The teal animal may have had a slight increase on Days 9 and 14 before returning to baseline on Day 21. The red animal appeared to have been stable and close to the limit of quantification until Day 21, when its IL-10 concentration declined. The green and yellow animals were stable and below the limit of quantification for the duration of the challenge.

The animals treated with ZMapp1 also had generally stable levels of IL-10 (Figure 19B). The red animal had stable and well-defined IL-10 concentrations from Day 0 to Day 21, then dipped on Day 28. The blue animal started below the limit of quantification and increased above it on Day 6 and remained at the same level until Day 28. The teal animal also started low on Days 0 and 3 and increased close to, but below, the limit of quantification on Day 6 until Day 21, then went back down on Day 28. The other three animals (yellow, green, and purple) remained fairly stable and below the limit of quantification for the duration of the challenge.

The animals treated with ZMapp2 showed a more unified pattern (Figure 19C). Except for three points (blue on Day 14, yellow on Days 9 and 21) which were closer, the values were generally below the limit of quantification. The red animal appears to have remained stable for the duration of the experiment. The other four animals all started low and appear to have possibly increased on Day 9 and remained higher until Day 28.

Figure 19: Interleukin 10 concentration in the serum of rhesus macaques after challenge with EBOV/Kikwit and treatment with monoclonal antibodies

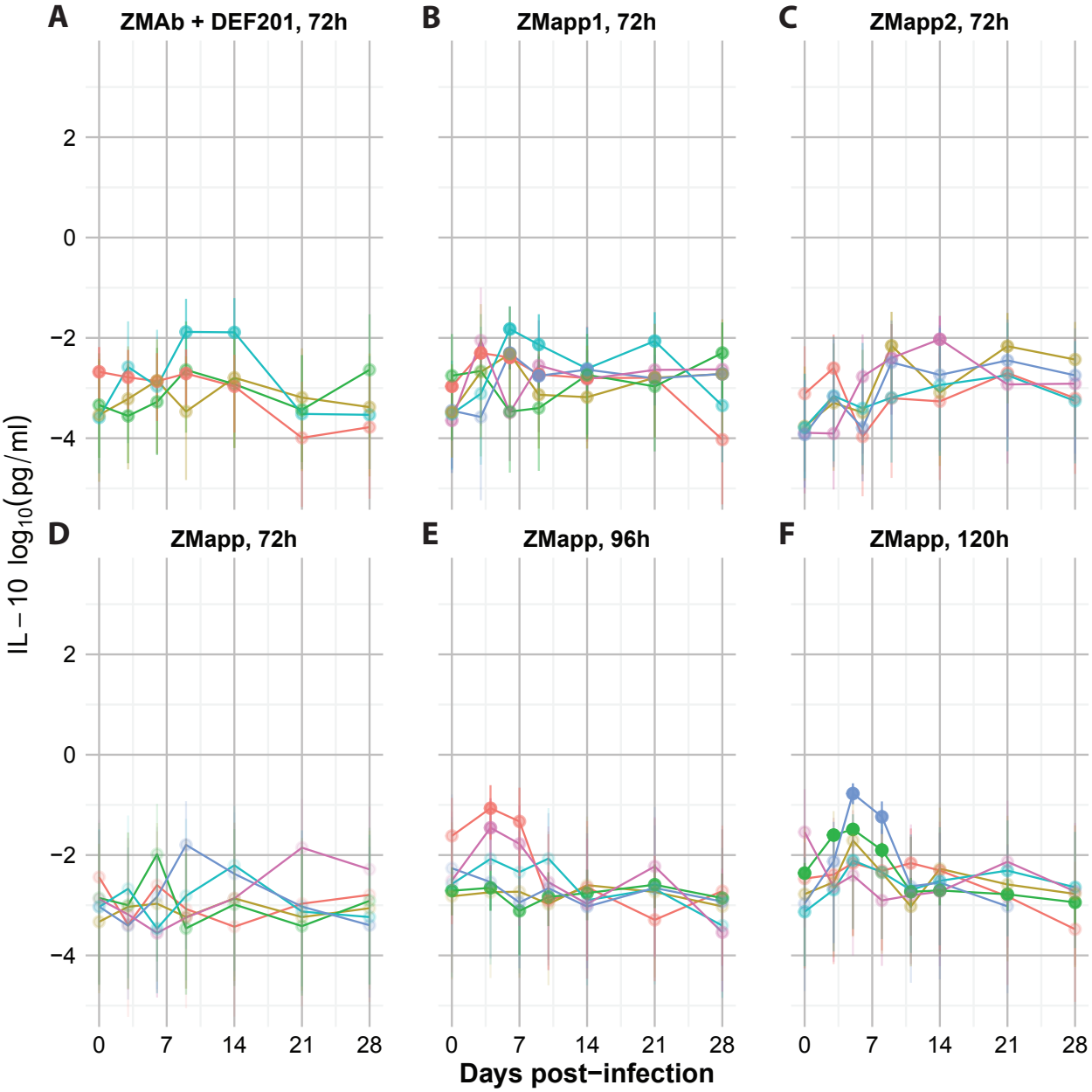

Concentration of interleukin 10 were estimated using an electrochemiluminescent assay. The limit of quantification was about 0.030 pg/ml. The concentrations are calculated from a standard curve using a bayesian multilevel model. The error bars represent the 95% HPDI for the sample. The individual curves were vertically centered for each group using the 4 lowest values (”baseline level”) of each animal’s curve. The transparency of the points reflects the uncertainty of each value, more transparent points have very wide error bars, more opaque points have shorter error bars and are, therefore, more accurate and reliable. The colors within each group represent different animals.

The animals treated with ZMapp at 72 h all remained below the limit of quantification for the duration of the challenge (Figure 19D). The red and yellow animals showed little change over the course of the challenge. The other four animals appear to have had a potential peak when the concentration of IL-10 was higher than baseline, but remained below the limit of quantification. The peaks occurred on Day 6 (green), 9 (blue), 14 (teal), and 21 (purple). The green animal immediately returned to baseline (on Day 9), but the blue and teal animals only returned to baseline on Day 21 (12 and 7 days after the peak, respectively). The purple animal had still not returned completely to baseline by the end of the experiment.

Most of the animals treated at 96 h also generally remain stable throughout the experiment (Figure 19E). Two animals, red and purple, showed a peak on Day 4 when the IL-10 concentration was higher and closer to the limit of quantification, both animals returned to baseline on Day 10. The teal animal appears to have a bump from Day 4 to 10, but given the low intensity and the low precision at those concentrations, it is not possible to be sure the change is real. The blue, green, and yellow animals all showed no changes during the experiment. The green animal had concentrations that varied around the limit of quantification and thus have fairly good precision, increasing the certainty that no meaningful change occurred for this animal.

The animals treated at 120 h appear to have some of the best characterized changes from baseline (Figure 19F). The blue and green animals have peaks around Day 5, with the green animal having good precision throughout the study and the blue animal having good precision on Days 5 and 8. Both animals returned to baseline on Day 11. The yellow and

teal animals, while having concentrations too low for precise estimation, appear to also have a possible peak on Day 5. The red and purple animals appear to have been mostly stable throughout the experiment. It appears possible that the treatment on Day 5 (120 h) is late enough to start seeing immune activation due to the virus in some animals. The treatment with antibodies then controls the antigen and viral loads and leads to reduced activation.

3.3.2.8 IL-12p70

The levels of IL-12p70 observed during the challenge experiment generally remained below the limit of quantification and showed little change over time (Figure 20). In the group treated with ZMAb + DEF201, the red and teal animals showed little change and low concentration for the duration of the challenge (Figure 20A). The green animal, while the concentration remained below the limit quantification, appears to have had increasing levels of IL-12p70 from Day 6 onward. The yellow animal did have a measureable peak on Day 21 with an increase of about 2 logs above Day 0 levels.

The group treated with ZMapp1 shows the most homogeneous IL-12p70 response (Figure 20B). Most animals show an increase from Day 0 to Day 9, and then remain stable until Day 28. Five of the animals had concentrations that remained below the limit of quantification even during the apparently higher plateau at the end of the challenge. The yellow animal had a slightly more measureable peak on Day 9. The red animal had quantifiable concentrations of IL-12p70 during the entire challenge. Its IL-12p70 response increased on Day 3 and decreased slightly (~0.5 log) until Day 28. The trajectory is consistent with that of the other five animals.

Figure 20: Interleukin 12p70 concentration in the serum of rhesus macaques after challenge with EBOV/Kikwit and treatment with monoclonal antibodies

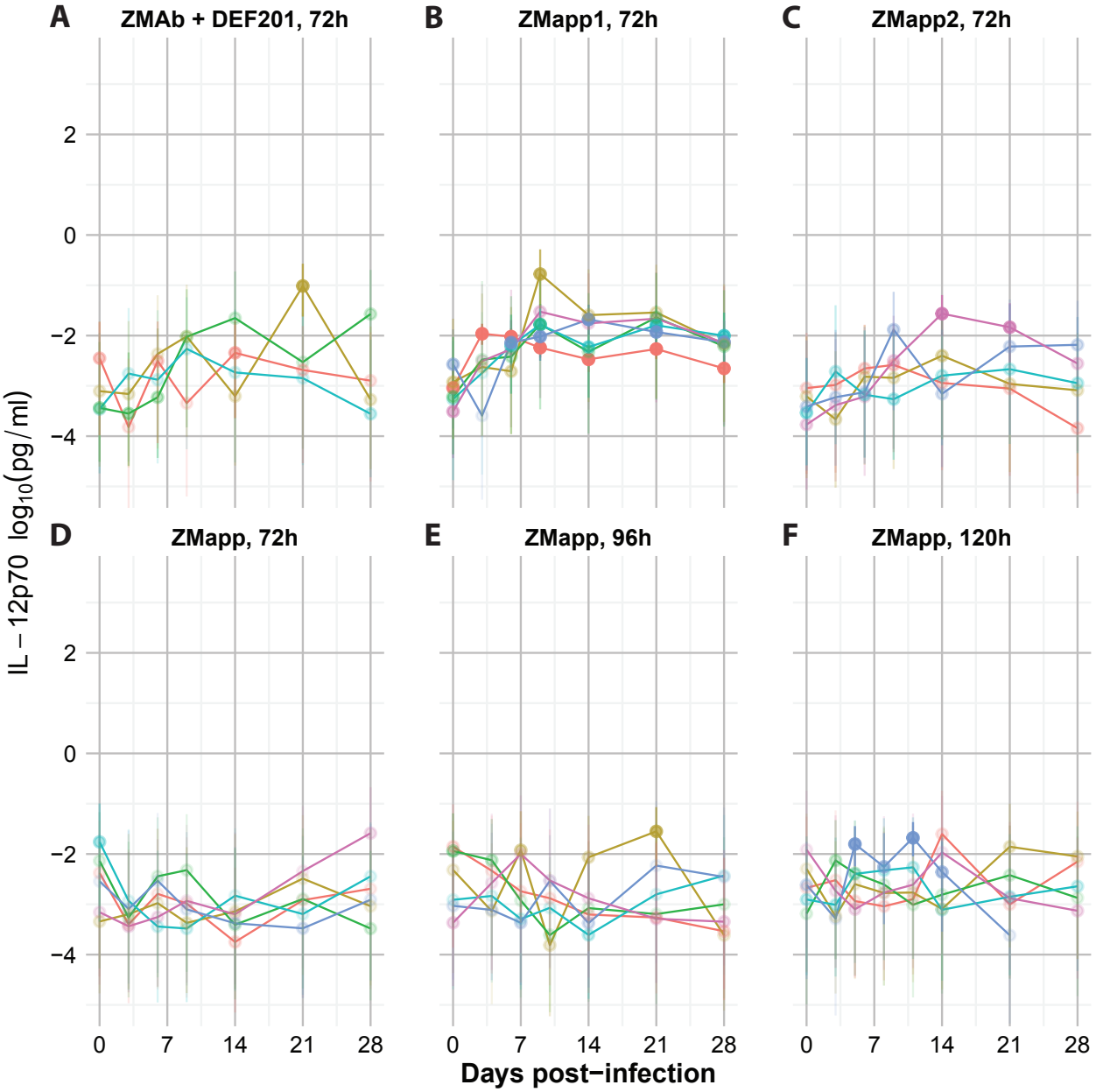

Concentration of interleukin 12p70 were estimated using an electrochemiluminescent assay. The limit of quantification was about 0.044 pg/ml. The concentrations are calculated from a standard curve using a bayesian multilevel model. The error bars represent the 95% HPDI for the sample. The individual curves were vertically centered for each group using the 4 lowest values (”baseline level”) of each animal’s curve. The transparency of the points reflects the uncertainty of each value, more transparent points have very wide error bars, more opaque points have shorter error bars and are, therefore, more accurate and reliable. The colors within each group represent different animals.

Four of the five animals treated with ZMapp2 did not show much change during the challenge (Figure 20C). The blue animal had a potential peak with an increase of about 2 logs on Day 14 with a decrease on Days 21 and 28.

The animals treated with ZMapp at 72 h showed mostly no change throughout the challenge (Figure 20D). The concentrations remained well below the quantification limit. The purple animal appears to have had an increase of slightly over 1 log between Days 14 and 28.

The animals treated at 96 h had more variable responses (Figure 20E). Most of the samples measured had concentrations below the limit of quantification. The yellow animal showed substantial variation over the challenge period with a peak on Day 21 that was close to the limit of quantification. The blue and teal animals oscillated slightly during the challenge but remained below the limit of quantification. The red and green animals appear to have had slightly decreasing levels of IL-12p70 over the duration of the challenge. The purple animal appears to have had a slight increase in IL-12p70 on Day 7 and decreased back to baseline by Day 28.

The animals treated at 120 h also did not show consistent patterns in IL-12p70 levels (Figure 20F). Most animals had levels of IL-12p70 below the limit of quantification. The blue animal was the only animal with well-quantified peaks around Days 5 and 11 before returning to baseline on Day 21. The red animal had an apparent peak on Day 14 and returned to baseline on Day 28. The yellow animal appears to have had higher concentration around the end of the challenge period on Days 21 and 28. The green, purple, and teal animals show no specific pattern.

Figure 21: Tumor Necrosis Factor α concentration in the serum of rhesus macaques after challenge with EBOV/Kikwit and treatment with monoclonal antibodies

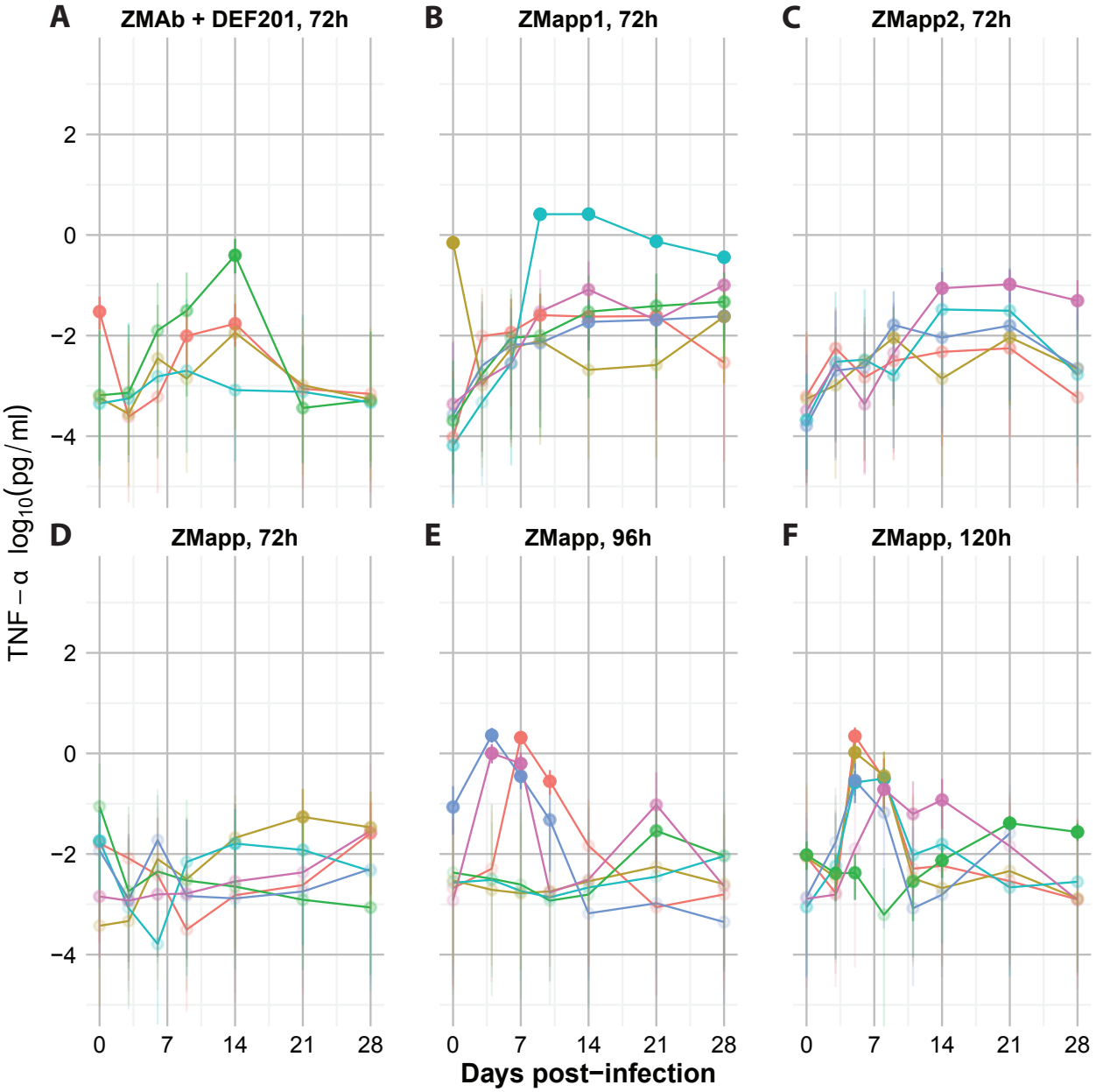

Concentration of Tumor Necrosis Factor α were estimated using an electrochemiluminescent assay. The limit of quantification was about 0.120 pg/ml. The concentrations are calculated from a standard curve using a bayesian multilevel model. The error bars represent the 95% HPDI for the sample. The individual curves were vertically centered for each group using the 4 lowest values (”baseline level”) of each animal’s curve. The transparency of the points reflects the uncertainty of each value, more transparent points have very wide error bars, more opaque points have shorter error bars and are, therefore, more accurate and reliable. The colors within each group represent different animals.

3.3.2.9 TNF-α

The levels of TNF-α showed interesting and moderately consistent patterns during the course of the challenge (Figure 21). Three of the animals treated with ZMAb + DEF201 (red, yellow, and green) showed a peak of TNF-α around Day 14 (Figure 21A). The green animal had an almost 3-log increase, whereas the red and yellow animals had a more modest 1-log increase. The teal animal showed a very slight possible bump earlier than the other animals, around Day 9. Surprisingly, the red animal had levels of TNF-α that were high enough on Day 0 to be measured with accuracy which then dropped off on Day 3.

The animals treated with ZMapp1 followed strikingly consistent trajectories (Figure 21B). Four of the animals followed a very similar trajectory, starting low and increasing by slightly more than 2 logs until Day 14 followed by a plateau until Day 28. The teal animal had the lowest initial estimated concentration, although well within the error of five of the animals, and reached a substantially higher plateau, with an increase of 4 logs between Days 0 and 14. Its response declined by almost 1 log by Day 28. The yellow animal had a stranger trajectory, starting higher than the five other animals, in the range of concentration that is quantified with high precision, and then decreased on Day 3 and remained relatively stable for the rest of the experiment.

The animals treated with ZMapp2 showed less increase in serum TNF-α than the animals treated with ZMapp1 but did show a similar level of consistency (Figure 21C). Four animals had similar kinetics; they remained below the limit of quantification but appeared to increase slightly around Days 14 to 21 before coming back down on Day 28. The blue animal increased to around the limit of quantification by Day 14, representing a 2.5-log increase over Day 0, and remained stable until Day 28. While the pattern is somewhat

similar to the ZMapp1-treated animals, the actual concentrations did not reach the same peaks, as evidenced by the wider uncertainty (also visible as the points being slightly more transparent) compared with the ZMapp1 animals.

The animals treated at 72 h with ZMapp showed little consistency with the patterns of animals treated with ZMAb + DEF201, ZMapp1, or ZMapp2 at the same time (Figure 21D). The responses actually follow highly variable trajectories. The yellow animal is similar to the ZMapp1 and ZMapp 2 groups. The red animal appears to have had a decrease in TNF-α during the challenge with Days 0 and 28 slightly higher than the mid-challenge time points. The green animal had generally decreasing concentrations of TNF-α from Day 0 to Day 28. The purple animal had mostly stable levels of TNF-α with a slight increase on Day 28. The teal animal appears to have had a trough on Days 3 and 6 before returning to its baseline. The blue animal had slightly higher concentrations on Days 0 and 6, it was otherwise relatively stable throughout the challenge.

The animals treated at 96 h are also quite different from the previous groups (Figure 21E). Three of the animals showed an early and strong response, peaking on Days 4 or 7. The blue animal started approximately 1.5 logs higher than other animals on Day 0 and returned to a baseline level on Day 14. The purple animal started around the same level as the other four animals and increased by almost 3 logs on Days 4 and 7, it returned to baseline on Day 10 and had a sudden increase on Day 21 which returned to baseline on Day 28. The red animal peaked on Day 7 after showing no change on Day 3, it slowly returned to a baseline level by Day 21. The teal, yellow, and green animals remained mostly at

baseline during the challenge period, except for the green animal which had a 1-log increase on Day 21 only.

The animals treated at 120 h showed the most consistent pattern of the ZMapp-treated animals (Figure 21F). Four of the animals had a TNF-α peak on Days 5 or 8 with levels reaching well above the limit of quantification. All of these animals returned to baseline levels on Day 11 and remained at or near baseline until Day 28. The purple animal reached a lower peak on Days 8 to 14 and returned to baseline by Day 28. The green animal, while having generally well-defined concentrations, appear to have had a reduction in TNF-α on Day 8 followed by a slight increase over baseline.

Overall the levels of TNF-α during challenge for the animals treated with ZMapp were consistent with increasing effect of virus replication, thus inducing pro-inflammatory responses which peak on the day of the first treatment (in general) and then return to baseline as the virus is cleared.

The picture painted by the serum cytokines reflects, broadly, an initial inflammatory response, mostly T_H1 (from IL-1β and IFN-γ), which appears to be reduced and possibly switched to T_H2 (based on IL-4 and IL-5 responses) by Day 14.

3.3.3 T cell responses

Evaluating the production of cytokines (IFN-γ, IL-2, and IL-4) and the surface expression of CD107a in T cells, it is possible to deduce their T_H1/T_H2 polarization and to assess their ability to produce cytokines or kill cells (CD107a). In order to assess the T cell response, PBMCs were isolated from the NHPs on Day 21. The cells were rested overnight, then stimulated with three peptide pools, plain media, or PMA/Ionomycin for 5 hours in the

presence of GolgiPlug and GolgiStop as well as anti-CD107a antibodies. The cells were then surface-stained for the markers CD3, CD4, and CD8. The samples were fixed and removed from BSL4, then transferred into BD PermWash for intracellular staining. The samples were stained intracellularly for IFN-γ, IL-2, and IL-4. All samples were run on a BD LSR II flow cytometer. The compensation matrix was adjusted in FlowJo vX.6. The gating was performed with the openCyto package running on R 3.4.1 on an Ubuntu 17.09 virtual machine.

The samples from the fall and June experiments, animals treated with ZMapp1, ZMapp2, or ZMapp, were also stained for dead cells. However, since previous experiments did not have this marker, it was ignored in all cases, so that experiments can be compared to each other. The analysis used combinatorial gates (Boolean gating) to define all 16 possible activation profiles based on the 4 activation markers (CD107a, IFN-γ, IL-2, IL-4), from no marker present to all four present for CD4 and CD8 cells separately. The counts were analyzed using a Bayesian multinomial model, which estimated the frequencies of positive cells for all 16 profiles in combination for each stimulation for each group of animals. This ensures that the precision of each observation is taken into account, for example, by accounting for the varying number of CD4 (or CD8) cells present in each sample.

As with the cytokine measurement, very low measurements can appear counterintuitive at first, with values that seem too low. Here the lowest point estimate possible for the frequency is determined by the total number of CD4 or CD8 cells used in the analysis. For example, if no positive events were detected for a particular profile in each of 6 animals with 40,000 CD4 cells, traditionally each animal would be estimated at 0 with an average of

0. But the raw data is summarized at the group-level, under the assumption that the frequency is the same for all members of the group; in that context, this data also suggests that out of 240,000 cells analyzed, none were positive. So the Bayesian analysis will suggest a frequency between 0 and slightly more than 1/240,000 (yielding point estimates at or below 10^{-3}%). Estimates between 10^{-2} and 10^{-3}% represent cases where, for example, 4 or 5 animals have 0 positives in this profile and 1 or 2 animals have 1 positive cell each.

Supplementary Figure 2 shows an example of the posterior predictive check for the data for one animal. In such a check, count data for each profile is generated based on the results from the Bayesian analysis, these histograms are then compared with the actual data (red lines). If the model provides a reasonable estimate, the red lines should, in general but not necessarily always, be near the higher peaks of the histograms. In most cases, the fit is decently good, with the "all negative" and some high count profiles being over-precise but most profiles have estimated frequencies that lead to reasonably good counts.

Due to technical issues and instrument settings, the live/dead discrimination stain created much noise in many stimulation channels for the ZMapp1/ZMapp2 experiment that could not be compensated for, especially in the Brilliant Violet 421 channel used for the marker CD107a. Under normal circumstances, this would not be an issue since any event with more than background staining in the live/dead discrimination channel would be removed from further analysis as a "dead cell". However, since the gating here attempted to ignore that channel, the noise level became unacceptable as it was higher than any expected signal. Therefore, for that experiment a gate was added to remove events that were very high in that channel. While this did not correct the problem completely, the results seem

comparable to those of other experiments. This issue should be kept in mind whenever results from either group (ZMapp1- or ZMapp2-treated animals) are much higher than other groups.

The data from the ZMAb + DEF201 treated animals at 72 h (cynomolgus & rhesus macaques) are reanalyzed from the same raw data as (Xiangguo Qiu et al., 2013).

3.3.3.1 CD4 responses

The CD4 T cell response patterns are presented in Figure 22. The profiles where more activation markers are present are on the left of each graph. Cells with these markers are considered "polyfunctional" in that they secrete more than one cytokine or have more than one role. These cell types are generally considered very useful as they also often produce larger amounts of all the cytokines for which they are positive. The profiles where only one activation marker is present are on the right side of each graph. The points are coded with transparency corresponding to the probability that the group's average frequency is higher than the corresponding "Media" control.

The cynomolgus macaques treated with ZMAb + DEF201 showed better responses against the peptides of Pool 1, which consists mostly of the core of the GP and its receptor binding domain, than to either of the other Pools. While the slight "hockey stick" shape of the results would suggest that the response is mostly from the low functionality phenotypes, it is important to note that the Media stimulation is much higher in those cases, leading to a net increase that is actually very small. Two double positive patterns stand out, IFN-γ + IL-2 and IL-2 + IL-4. The triple combination of IFN-γ + IL-2 + IL4 is also higher than other activation profiles, with almost the same frequency as the single-positive profiles. There is

some signal in the quadruple-positive profile, although the frequency is below 0.01%. In most cases, Pool 3 has the second-highest response, and, in a few cases, has a higher response than Pool 1. Pool 2 shows a generally weak to non-existent response. It only has a higher frequency of positives in the IL-4-only profile of the animals treated at 72 h. Pool 2 contains a large fraction of the glycan cap and the mucin-like domain, the last of which is highly immunogenic in terms of antibody response. Both domains are heavily glycosylated which probably prevents proper T cell responses from forming in the first place. Pool3 contains the end of the mucin-like domain and the GP_2 subunit which includes the internal fusion loops and the transmembrane domain.

The response of the rhesus macaques treated with ZMAb + DEF201 was less focused on one peptide pool. Both Pool 1 and Pool 3 dominated various profiles, unlike the cynomolgus macaques where Pool1 was generally dominant overall. Again, Pool2 did not appear to induce strong responses, especially when it comes to polyfunctional responses. The only polyfunctional pattern with no response at all is the CD107a + IFN-γ + IL-4 pattern. The rhesus macaques had a fairly strong single positive response similar to the cynomolgus macaques with single positive activation patterns not very increased compared to Media.

The rhesus macaques treated with ZMapp1 and ZMapp2 showed a preference for Pool 2, which is more consistent with the cynomolgus than the ZMAb-treated rhesus macaques. However, the ZMapp1- and ZMapp2-treated animals appear to have much more polyfunctional responses than any of the ZMAb-treated animals. Many of the polyfunctional response profiles have higher frequencies than the single-positive profiles, except for

CD107a alone. Also unlike the ZMAb-treated animals, the ZMapp1- and ZMapp2-treated animals have no single-positive IL-4-producing cells. For these two groups, it is important to remember that the noise from the live/dead stain could not be entirely removed from, especially, the CD107a channel and probably contributes to some of the signal, although that should also be the case for the Media-stimulated sample.

The animals treated with the final ZMapp at different times (72, 96, and 120 hours) have highly consistent responses. In all three cases the activation of T cells is dominated by Pool 3. Also, in all three groups two patterns are never detected: CD107a + IFN-γ + IL-4 and IFN-γ + IL-4. The first four response profiles from the left (quadruple-positive, CD107a + IFN-γ + IL-2, CD107a + IFN-γ + IL-4, and CD107a + IL-2 + IL-4) have nearly identical frequencies for the Pool 3 response. Pool 1 and Pool 2 also follow similar shapes for these profiles but their respective ordering changes slightly between groups. In all three cases the CD107a + IL-2 profile is also a prominent feature of the CD4 response, especially, again, with cells stimulated by Pool 3. The same is true for the CD107a alone activation profile (4th from the right). It is interesting to note that, for all of its diversity, the response in ZMapp-treated animals has generally lower frequencies than the other groups. It is a full log (10) lower than the high responses from ZMapp1 and ZMapp2—again, one needs to consider the noise issue for the ZMapp1- and ZMapp2-treated animals.

Overall, there are interesting shifts visible in the CD4 T cell activation profiles as the treatment changes from mouse antibodies to mostly to fully chimeric. Surprisingly, longer delays in treatment do not appear to induce substantial changes in the activation profiles of the CD4 T cells.

Figure 22: CD4 T cell responses

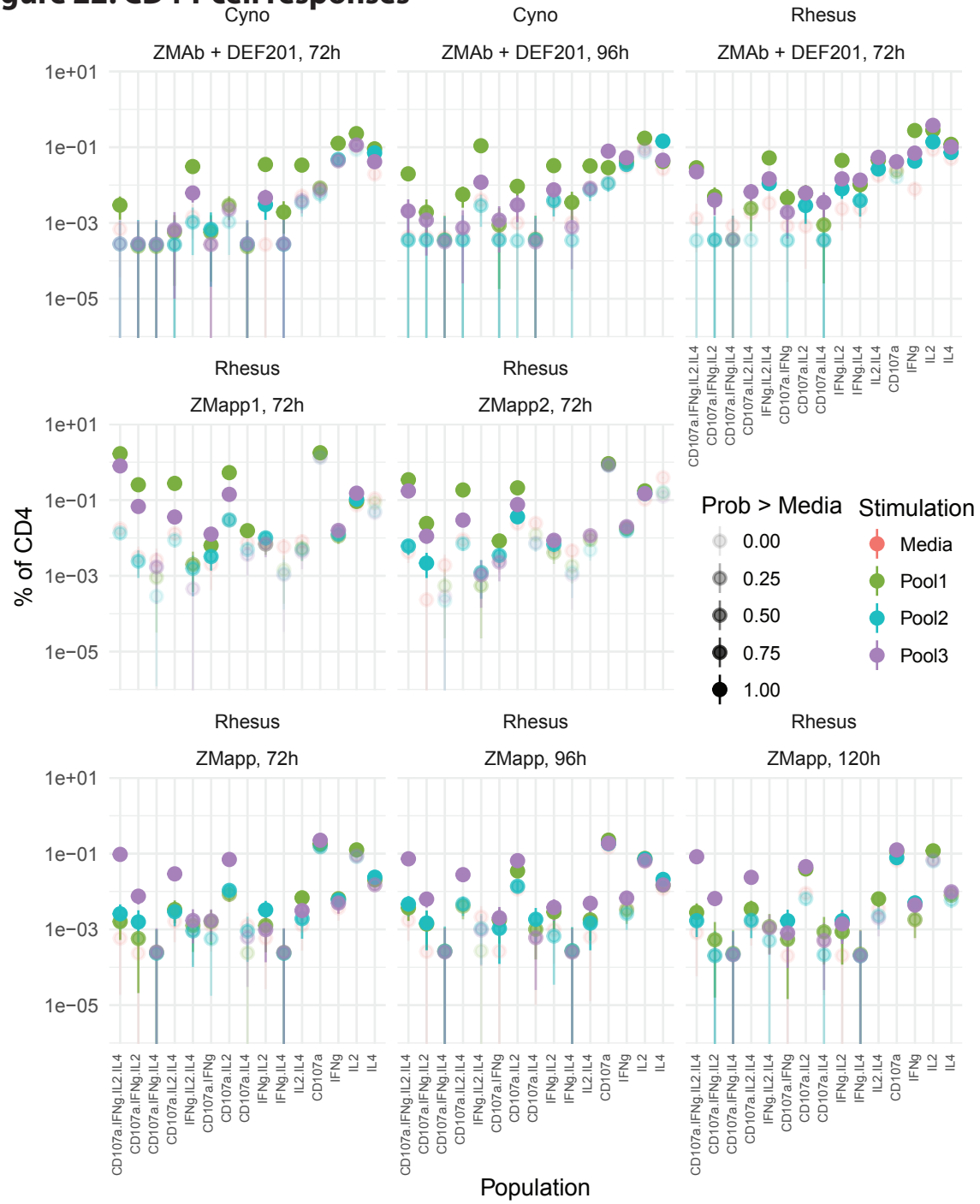

The vertical axis represents $\log_{10}$(% of CD4 cells). The horizontal axis has 15 activation profiles (based on 4 activation markers; total of 16 profiles, not showing the "All Negative" profile for scaling issues) in decreasing order of polyfunctionality from left to right. The colors represent different stimuli applied to the cells. The transparency is linked to the probability that a specific stimulation for a specific activation profile for a group is greater than the corresponding Media control. Nearly invisible points have a probability of being greater than the Media near 0% and completely opaque points are near 100%. The error bars represent the 95% HPDI of the frequency of positive for the group. The data from the Cyno and Rhesus treated with ZMAb + DEF201 at 72 h is reanalyzed from Qiu et al 2013, STM.

Figure 23: CD8 T cell responses

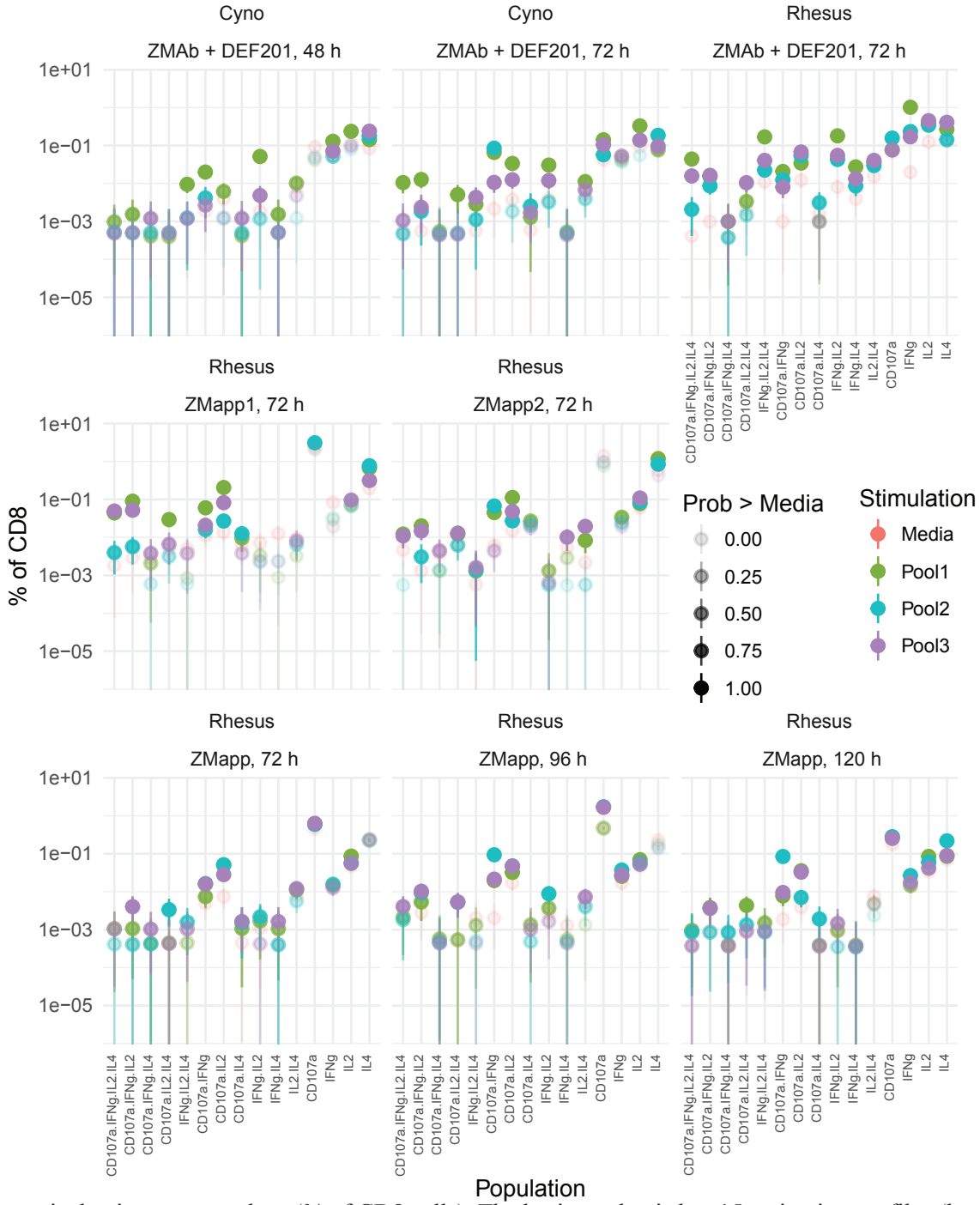

The vertical axis represents $\log_{10}$(% of CD8 cells). The horizontal axis has 15 activation profiles (based on 4 activation markers; total of 16 profiles, not showing the "All Negative" profile for scaling issues) in decreasing order of polyfunctionality from left to right. The colors represent different stimuli applied to the cells. The transparency is linked to the probability that a specific stimulation for a specific activation profile for a group is greater than the corresponding Media control. Nearly invisible points have a probability of being greater than the Media near 0% and completely opaque points are near 100%. The error bars represent the 95% HPDI of the frequency of positive for the group. The data from the Cyno and Rhesus treated with ZMAb + DEF201 at 72 h is reanalyzed from Qiu et al 2013, STM.

3.3.3.2 CD8 responses

The CD8 T cell response patterns are presented in Figure 23. Like the CD4 T cell patterns, the patterns are organized from the most polyfunctional on the left to the least polyfunctional on the right.

The cynomolgus macaques treated with ZMAb + DEF201 have somewhat different responses, unlike the very similar CD4 T cell responses. Both groups have significant frequencies of single-positive cells and while in many cases the frequency was confidently above that of the Media, the biological relevance of such a small increase is not necessarily clear. However, the group treated at 72 h appears to have a stronger polyfunctional response. For many of the polyfunctional profiles, the animals treated at 72 h have frequencies at least 1 log higher than those in the Media control. As for the CD4 T cells, the CD8 T cells appear to react mostly to Pool 1. Pool 3 is often a close second for the animals that received ZMAb at 72 h. These animals also appear to respond slightly better to Pool 2 in the CD107a + IFN-γ profile.

The rhesus macaques treated with ZMAb + DEF201 again showed a more diverse response in terms of the peptide pools to which they respond. In many cases, the intensity of the responses is also higher than they were for the cynomolgus macaques. The frequencies of single-positive cells are also fairly high, but, similar to the cynomolgus macaques, they are not very high above the response of the Media alone, except for IFN-γ. Both Pool 1 and Pool 3 lead to polyfunctional responses, but the responses to Pool 1 are often higher above the responses from the Media control. In the case of the quadruple positive cells, the response to Pool 1 is almost 2 logs higher than Media alone. The response from Pool 3 in the CD107a + IFN-γ + IL-2 profile as about 1 log higher than Media alone. The same is true

for Pool 1 in the following profiles: IFN-γ + IL-2 + IL-4, CD107a + IFN-γ, IFN-γ + IL-2, and IFN-γ alone.

The rhesus macaques treated with ZMapp1 and ZMapp2 showed a similar amount of variation in terms of which peptide pool induces the strongest responses. The animals treated with ZMapp1 had 6 activation profiles which showed virtually no evidence of a response to any of the peptide pools. This includes two triple activation profiles, CD107a + IFN-γ + IL-4 and IFN-γ + IL-2 + IL-4, as well as three double-positive profiles (IFN-γ + IL-2, IFN-γ + IL-4, and IL-2 + IL-4) and one single positive profile (IFN-γ alone). While the animals treated with ZMapp2 had some degree of positive responses, only one of them was at least 1 log higher than the Media control (Pool3 for the IL-2 + IL-4 profile). The only profile where the ZMapp2-treated animals showed no activation at all was the CD107a alone profile. This is also the profile with the highest frequency—but only a small difference from Media—in the animals treated with ZMapp1. Both results might be due to the noise issues coming from the live/dead stain in the neighboring channel. Both sets of animals appeared to have high frequencies of CD107a + IFN-γ and CD107a + IL-2, but the ZMapp1-treated animals showed more difference compared to the Media stimulation. The ZMapp2-treated animals had an approximately 1 log increase in cells co-expressing CD107a and IFN-γ when stimulated with Pool 2, which is similar to the cynomolgus macaques which received ZMAb at 72 h.

The CD8 T cell response of the animals treated with ZMapp was more heterogeneous than the CD4 T cell response of the same animals. Pool 3 appears to be generally better at activating CD8 T cells for these groups, although Pool 1 and Pool 2 are stronger in some of

the profiles. While the single positive responses generally have the highest frequencies, all three groups show little increase compared with the Media control. In most cases, the animals treated at 72 h show no strong increase in the frequency of activated cells compared with the Media control. The exceptions are the CD107a + IL-2 double positive cells where Pool 2 has a frequency about 1 log higher than the Media and the CD107a + IFN-γ + IL-2 profile where Pool 3 is also about 1 log above the Media (although only at an absolute frequency of less than 0.01%). For the animals treated at 96 h, only two profiles show large increases. The CD107a + IL-2 + IL-4 profile has a slightly greater than 1-log increase over the Media for Pool 2 and Pool 3 and the CD107a + IFN-γ profile has an almost 2-log increase over the Media for Pool 2, bringing the latter profile to about 0.1% absolute frequency. The animals treated at 120 h also only show large increases for only two profiles. Similar to the animals treated at 96 h, the CD107a + IFN-γ profile has an increase of almost 2 logs with Pool 2 (absolute frequency of about 0.1%) and the CD107a + IL-2 profile where Pool 1 and Pool 3 show an increase of about 1 log over the Media (absolute frequency of about 0.04%).

Overall the frequency of responding cells appears lower in CD8 T cells than in CD4 T cells. The difference between the frequency of the Media and the peptide pools is also generally smaller for the CD8 T cells. There appears, again, to be a shift in the peptide pool producing the stronger reactions as the treatment shifts from mouse antibodies to chimeric antibodies. There does not appear to be much of a time-course response between the groups of animals treated with ZMapp at different time points.

3.3.4 IgG responses

IgG responses were followed throughout the challenge periods. The antibody response allows us to evaluate the overall kinetics and intensity of the immune response against EBOV, more specifically the glycoprotein. This response is interesting because the glycoprotein is the target of the treatment. Two ELISAs were used to quantify the humoral response. The first assay is a titre-based semi-quantitative assay. This assay has been in use for a long time, but provides limited information as the output is based on last positive dilution. It generally poorly reflects the variation and changes in the amount of antigen-specific IgG present in the serum. A second drawback is that this assay was performed with a horseradish peroxidase (HRP)-labelled Anti-human IgG secondary antibody. The animals treated with various versions of ZMapp (final/1/2) received chimeric antibodies with human F_c regions. In that context, the assay detects the treatment antibodies and it becomes difficult to separate the signal of the treatment and that of the immune response.

The second assay uses pooled positive sera to create a standard (arbitrarily defined to a concentration of 2000 Antibody Units per ml (AU/ml)) to have a fully quantitative assay. This allows the evaluation of the variation between animals and groups and is also more useful in contexts where one might want to model the IgG response (e.g. for using statistical tests or models). This assay is also performed with a mouse monoclonal anti-Rhesus IgG antibody (HRP-labelled) that reacts with the IgG of both rhesus and cynomolgus macaques, but not human antibodies. The major drawback of this assay is that it is more sensitive to optimization parameters. The original, same, anti-human IgG secondary was initially used in this assay and the anti-Rhesus was substituted in. Combined with technical issues,

approximately 10-15% of the samples did not yield useable data, even after multiple re-runs.

3.3.4.1 Titres

The results of the titration assay are presented in Figure 24. The data for the cynomolgus macaques and the rhesus macaques treated at 72 h with ZMAb + DEF201 are adapted from (Xiangguo Qiu et al., 2013). The cynomolgus macaques treated with ZMAb + DEF201 at 48 h started having detectable IgG on Day 6, which is surprisingly early for IgG. The titers increased over the rest of the experiment until Day 28, when two of the three survivors reached titers of 1:1,024,000. The third survivor reached titers of 1:256,000 on Day 28. The cynomolgus macaques treated with ZMAb + DEF201 at 72 h showed similar initial kinetics with a detectable response on Day 6. All three survivors reached titers of 1:1,024,000 by Day 14 and remained at that level until Day 28.

The rhesus macaques treated with ZMAb + DEF201 at 72 h had similar kinetics to the cynomolgus macaques. One animal, teal, had detectable IgG signal on Day 3 at the first dilution tested, although that could be due to either very low and tight (low standard deviation) values in the Day 0 wells (leading to a cut-off that is too low) or to increased noise in the Day 3 wells (leading to an increased OD) or both. The other animals only had detectable IgG starting on Day 6, at which point the teal animal was slightly higher (by 1 dilution) but still very similar to the other animals. Two animals, including the teal animal, reached titers of 1:1,024,000 by Day 14 and remained high. The other animals increased slowly to reach titers of 1:8,000 and 1:64,000.

Figure 24: Antibody titres during challenge

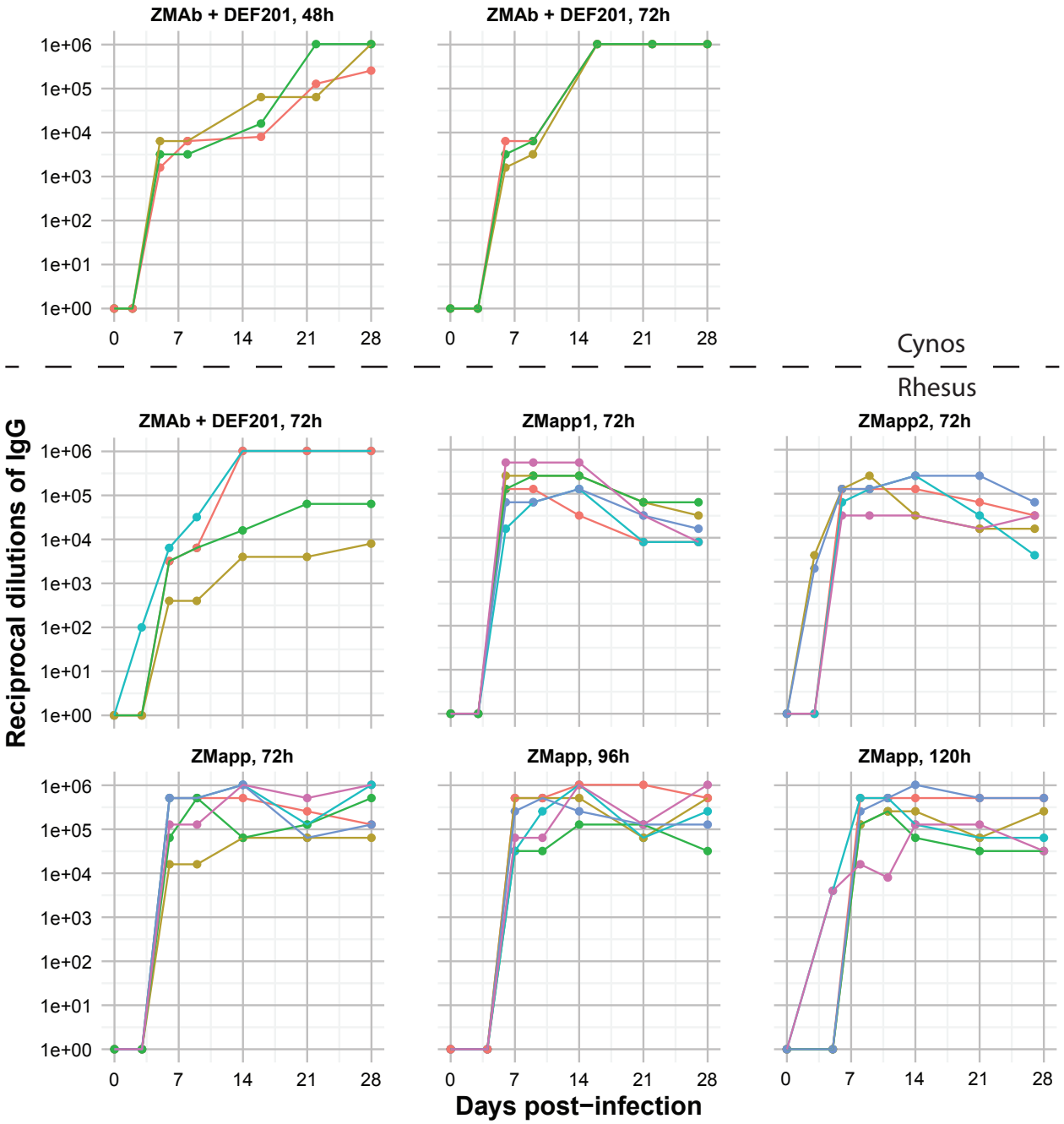

IgG titres over time during the initial challenge. The titre is reported as the reciprocal of the last dilution with signal higher than the Day 0. The data for the cynomolgus and rhesus macaques treated with ZMAb + DEF201 at 72 h are adapted from Qiu et al 2013, STM.

The rhesus macaques treated with ZMapp1 had high levels of detectable IgG from Day 6 to Day 14, in the range of 1:16,000 to 1:512,000. This was expected as this assay is detecting the treatment antibodies administered on Days 3, 6, and 9. It is interesting that the levels reached are so high since only two of the three components of ZMapp1 have human regions, since the 4G7 component was a mouse antibody, hence not detected by the assay. By Day 21, the levels of IgG had approximately stabilized to between 1:8,000 to 1:64,000. These final titers are lower than those of cynomolgus macaques and lower, on average, than those of rhesus macaques treated with ZMAb + DEF201.

The rhesus macaques treated with ZMapp2 did not reach levels as high as those treated with ZMapp 1 between Days 6 and 14 despite all the components of ZMapp2 bearing human regions. Also, there is much less of a difference between the early days after the administration of the treatment and the late time points where most of the treatment antibodies have been eliminated. Most animals, except the blue animal, had slightly lower concentrations on Day 28, ranging from 1:4,000 to 1:64,000. Two animals also had detectable IgG on Day 3, at similar levels to the animals treated with ZMAb + DEF201 on Days 6 and 9. This is most likely, again, due to the threshold method used to calculate the titre.

In almost all cases, the animals treated with ZMapp only had detectable IgG starting after the first treatment. This is expected as the treatment is composed of three human-mouse chimeric antibodies. The two exceptions are probably due to threshold issues. The titer in all animals remained high through Day 14, at least, between 1:8,000 and 1:1,024,000. The Day 28 titers were not changed much, reaching titers between 1:32,000 and 1:1,024,000.

There is no obvious connection between the delay in the start of the treatment and the final titers on Day 28.

3.3.4.2 Quantification

The results of the quantitative assay are presented in Figure 25. Overall, this assay did not detect reliable signs of IgG until Days 10-14. In most cases, the amount of IgG stabilized on Day 21. There are a few interesting features to note.

There appears to be a large amount of variation in the final amounts of IgG present on Day 28. This variation exists within and between the groups. For example, while the animals treated with ZMapp at 72 h mostly have responses above 10^3 AU/ml, one animal appears to have barely increased above background by Day 21. Three animals treated with ZMapp2 have highly consistent responses, but the other two are about 0.5 log lower and 1 log higher. The final concentrations of antibodies are generally in the 10^2-10^5 AU/ml range. Some groups also appear to be responding slightly earlier than others. Groups which respond earlier include: ZMAb + DEF201 72 h (Rhesus), ZMapp1, and ZMapp2. The groups which take more time to respond include: ZMAb 24 h, ZMAb 48 h, ZMAb + DEF201 48 & 72 h (Cynos), and ZMapp 72-120h. Early groups have IgG concentrations on Day 14 that are already substantially above background and remain mostly stable, whereas the Late groups appear to only be starting to respond and only stabilize on Days 21 or later.

The use of a secondary antibody which does not react with human chains shows well how there is no actual IgG response at early time points, unlike some of the results obtained from the titration assay. While the quantitative assay still has a limited range in which quantification is precise, samples above or below the accurate range can still be quantified.

Some of the animals develop extremely high response, reaching possibly as high as 10^5 by Day 28. It is also possible to see variation in animals which reached titers of more than 1:1,024,000 and it appears that titers do not completely correlate with the quantitative assay. For example the yellow and green animals for the rhesus macaques treated with ZMAb + DEF201 have titers 2 and 1 log lower, respectively, than the red and teal animals. However, in the quantitative assay, the yellow and green animals have quantities of IgG intermediate between the red and teal animals.

Figure 25: IgG levels using a quantitative assay

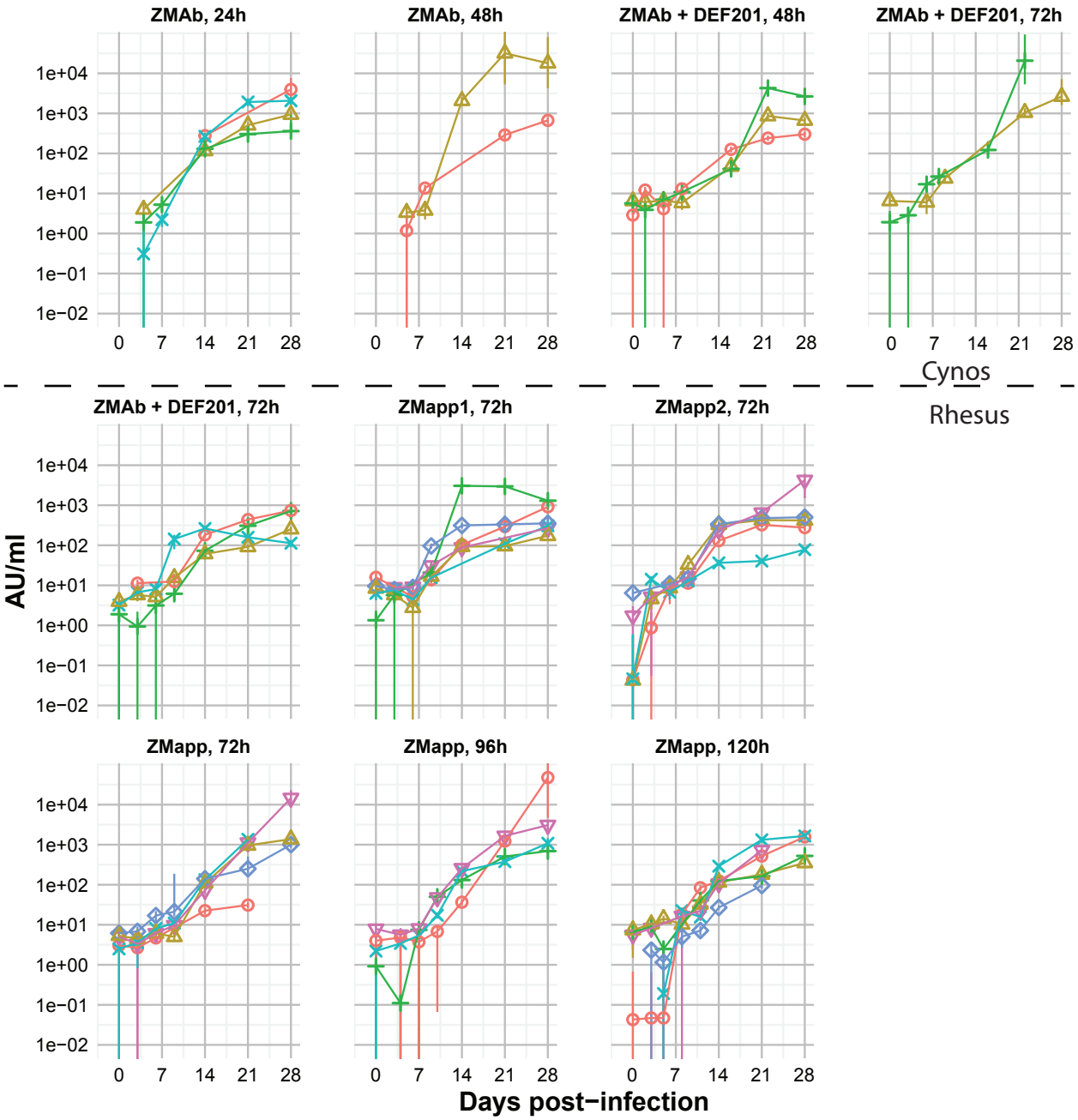

Concentration of IgG (in Antibody Units per ml (AU/ml)). The concentrations were measured using a quantitative assay and a secondary antibody that does not react with the human component of the treatments. The error bars represent the 95% HPDI for the estimate.

CHAPTER: 4 DISCUSSION

4.1 Characteristics of the antibodies

The first hypothesis is about the mechanism of protection of the ZMAb cocktail (and its derivatives). In order to start work on the mechanism of protection, we first need an understanding of some basic properties of the antibodies which compose ZMAb.

The ZMAb cocktail is composed of three mouse antibodies, 1H3, 2G4, and 4G7. These antibodies were derived from mice vaccinated with the VSVΔG-EBOVGP vaccine. (Xiangguo Qiu et al., 2011) The three antibodies were chosen to be part of a cocktail because they were neutralizing and were better at protecting guinea pigs. (Xiangguo Qiu, Fernando, et al., 2012) This ensured that, as the treatment was assessed in species other than mice, there would be at least one mechanism which can still have an effect.

Based on results from Qiu et al the isotype of the antibodies is IgG2a for 1H3 and 4G7, and IgG2b for 2G4. (Xiangguo Qiu et al., 2011)

The variable regions of the antibodies were sequenced. The sequences, for both the heavy and light chains, were aligned (Figure 2). All the heavy chains are quite different, suggesting that the three antibodies are, in fact, from different clones. Interestingly, the light chains of 2G4 and 4G7 share a high degree of homology. This level of homology is slightly lower when considering only the CDRs (67% at the amino acid level, versus 84.5% for the whole variable region), but remains high considering that the two antibodies arose independently. The high level of homology between the light chains is especially interesting in the context of the results of the cross-inhibition assay. Both 2G4 and 4G7 had minimal

effect on the binding of 1H3, suggesting that the epitope of 1H3 was far enough from those of both 2G4 and 4G7 so that their binding did not hinder 1H3 either sterically or by altering the shape of its binding site. However, 2G4 and 4G7 were both able to reduce the signal of the other by at least 34%. This result suggests that either the two antibodies have epitopes close enough for steric hindrance or that each one stabilizes the other's epitope in an "incorrect" conformation for binding.

Further evidence of the closeness of the sites was provided in (Audet et al., 2014) where escape mutants were generated using the VSVΔG-EBOVGP vaccine. Only one escape mutant was found for each of the three mAbs. The escape mutant for 1H3 was found at amino acid position 274 (I274M) placing it in the glycan cap of GP, close to the receptor binding domain. The escape mutants for 2G4 and 4G7 occurred at the same position, amino acid 508, albeit to different amino acids: 2G4 induced a Q508R mutation and 4G7 induced Q508H mutation. It remains unknown whether the escape mutant for 2G4 is also an escape mutant for 4G7 and vice versa. Similar escape mutations were found in one NHP which was treated with the initial ZMAb cocktail at 48 hr post-infection and did not survive. (Xiangguo Qiu, Audet, et al., 2012) Two mutations were found: W275L close to the 1H3 escape mutant found previously (I274M), and Q508R at the same site as 2G4 and 4G7. This animal was the only one to have received a version of ZMAb and developed escape mutations. Additional work supporting overlapping epitopes for 2G4 and 4G7 came as more advanced methods were used to identify the binding locations of the antibodies, including: single-particle electron microscopy (EM) (Murin et al., 2014); alanine scanning (Davidson et al., 2015); and cryo-EM (Tran et al., 2016).

The 2G4 and 4G7 antibodies also share very similar germline genes. Germline genes are the genes passed on from generation to generation which form the basic repertoire of sequences from which the variable regions of antibodies are developed. As B cells mature, mutations accumulate in the germline genes and selection occurs in the lymphatic system to promote the survival and expansion of B cell clones with enhanced affinity and/or specificity for a target. Because some of the germline genes are extremely closely related, it is not always possible to say which gene lead to a specific antibody with certainty. For this reason, tools such as the NCBI's IgBLAST provide the 3 closest germline genes. In the case of the light chains of 2G4 and 4G7, all three top hits are the same. The germline genes 12-41, 12-44, and 12-46 are all closely related to the light variable region of both antibodies.

While the relatedness of the light chains appears to suggest that very few solutions exist to target the $GP_1 - GP_2$ interface, the diversity of the heavy chains suggests that the antibodies arose independently and that some diversity is possible in finding neutralizing antibodies.

While all three antibodies are neutralizing, the level of neutralization varies considerably between 1H3 and 2G4/4G7 (Figure 3). The two antibodies binding the $GP_1 - GP_2$ interface (2G4 and 4G7) appear to be at least 200 times more neutralizing than the antibody which binds the glycan cap (1H3). This is consistent with other studies of the mechanisms of neutralization, which showed that 2G4 and 4G7 are able to bind to the form of GP that is cleaved in the endosome (GP_{cl}). (Tran et al., 2016) The fact that 1H3 binds a location which is cleaved off before receptor contact means it cannot prevent the interaction of the GP_{cl}

and NPC1. (Lee et al., 2008) 1H3 likely neutralizes by preventing the interaction of the virus with the various cell-surface receptors which interact with $GP_{1,2}$.

4.2 Mechanism of action in mice

Antibodies can trigger a number of different mechanisms, depending both on their isotype and on the location of their epitope on the target protein. Two major mechanisms were investigated in mice, antibody-dependent cell-mediated cytotoxicity (ADCC) and complement-mediated toxicity (CMT). Both mechanisms start when many antibodies bind their antigens on the surface of a cell, in close proximity of each other.

4.2.1 ADCC

As NK cells pass through the tissue for immune surveillance, the antibodies interact with F_c receptors (FcγRs) on these cells and the colocalization of these receptors allows intracellular signalling. There are three classes of receptors which recognize IgG, $Fc\gamma RI$ (CD64), $Fc\gamma RII$ (CD32), and $Fc\gamma RIII$ (CD16). (Bruhns & Jönsson, 2015) The CD16 and CD32 receptors have lower affinity for IgG than the CD64 receptor. Also, the CD16 and CD64 receptors require the FcRγ subunit in order to initiate intracellular signalling. Both of these receptors (CD16 and CD64) are activating when triggered. NK cells express only the $Fc\gamma RIII$ which can also be associated with CD3ζ for signal transduction, although knock-out of the FcRγ subunit has been shown to prevent NK-dependent killing of tumour cells. (Clynes, Towers, Presta, & Ravetch, 2000) On the other hand, CD32 contains its own signalling motif, an immunoreceptor tyrosine-based inhibitory motif (ITIM), and inhibits cell activation upon receptor activation. The activation of $Fc\gamma RIII$ activates NK cells and induces cytokine expression (IFN-γ) and target cell killing through the release of granzyme

B and perforin, referred to as ADCC. The activation of $Fc\gamma RI$ and $Fc\gamma RIII$ on macrophages can induce phagocytosis of the target cell.

In order to assess the effect of FcR-mediated mechanisms, mice knocked-out for the Fc$R\gamma$ subunit were infected with MA-EBOV and treated at 48 h with 150 μg of mAb or PBS (Figure 4). The PBS-treated animals showed no difference in time to death or weight loss between the wild-type animals and the knock-out animals. There were also no significant differences in survival between the wild-type and knock-out animals treated with mAbs. Only one knock-out animal died in the 2G4 treatment group, all other groups had complete survival. In fact, the animals knocked-out for the Fc$R\gamma$ subunit appeared, generally, to lose less weight and recover faster than the wild-type animals.

According to Bruhns et al, mice which do not express the Fc$R\gamma$ subunit also lack surface expression of the associated FcγRs. (Bruhns & Jönsson, 2015) The weight loss data might suggest that, while the antibodies are preventing death, they still contribute, albeit slightly, to the disease. This could happen as the antibodies bind the virus and become bound by FcγRIII on macrophages and dendritic cells. They could thus promote close contact between the virus and the target cells and slightly increase the infection rate. However, given that the antibodies are protective, their antiviral activity must be much greater than any enhancing effect. Because the weight data comes from group weights, it is possible that a few extreme observations are skewing the means in one direction or the other. While this is an interesting observation, it needs to be confirmed with a new experiment properly designed to study the change in the intensity and timing of the weight loss. Ideally such an experiment should also include wild-type mice treated with a mutant antibody which

cannot bind to FcγRs, for example using the LALA mutation. (Arduin et al., 2015) Also, due to the number of mice received for the experiment, the knock-out group treated with 4G7 only had 3 mice. This could hide a difference in efficacy.

The main goal in using FcRγ knock-out mice was to evaluate the effect of ADCC. Antibodies can also mediate phagocytosis by binding the FcγRIII on macrophages; however, ADCC is expected to be a more effective means of clearing infected cells. Macrophages are targets of EBOV and could conceivably be infected through phagocytosis, whereas the NK cells which carry out most of the ADCC activity are not target cells.

In order to confirm the FcRγ knock-out results, mice deficient in NK cells were also challenged and treated under the same conditions (1000 LD_{50}, treatment at 2 Days post-infection). These mice have the gene encoding the transcription factor Nfil3 (also known as E4BP4) knocked-out. This transcription factor is necessary for the development of NK cells. (Gascoyne et al., 2009) Thus, mice knocked-out for this gene do not have peripheral NK cells (identified as NK1.1- and CD122-positive cells by flow cytometry).

Given the results obtained with the FcRγ subunit–deficient mice, the results for 4G7 were quite surprising (Figure 5). The animals treated with PBS or 2G4 showed no changes in survival rates, although the PBS-treated Nfil3-deficient animals appeared to succumb to disease slightly earlier than the wild-type animals. The Nfil3-deficient animals treated with 1H3 showed slightly lower survival (67% vs 100% for wild-type), but the difference was not statistically significant (p = 0.138). The 4G7-treated animals, however, showed a substantial decrease in survival in Nfil3-deficient mice (20% vs 100% for wild-type). This difference was statistically significant (p = 0.0072) and very interesting biologically. Unlike

the FcRγ subunit knock-out mice, the Nfil3-deficient mice appear to have had a level of morbidity as severe as or worse than the wild-type animals, based on weight loss.

One possible mechanism for the effect on the efficacy of 4G7 is that NK cells are capable of signalling from CD16 through both the FcRγ subunit (which was knocked-out previously) and the CD3ζ co-receptor. It is possible that in the absence of the FcRγ subunit, the CD3ζ co-receptor could provide enough functionality to maintain the level of ADCC needed for protection. However, removing the peripheral NK cells entirely leads to a more complete absence of ADCC and possibly other mechanisms, unrelated to antibodies, which promote survival.

4.2.2 The complement

Another mechanism by which antibodies can help to clear pathogens is through complement-mediated toxicity (CMT). This mechanism is triggered when antibodies can fix the C1q component. (K. Murphy, 2012) C1q is part of the C1 complex with C1r and C1s and is better recruited by large numbers of antibodies in close proximity. Once C1q is fixed to the antibodies, the conformational change activates C1r which activates C1s. Cleaved C1s cleaves C2 and C4 into C2a + C2b and C4a + C4b. Together, the C2a and C4b products form the C3 convertase. This C3 convertase cleaves C3 into C3a, which attracts lymphocytes, and C3b (the C5 convertase), which continues the cleavage chain until multiple C9 components are inserted in the membrane to form a pore.

In order to evaluate the importance of complement-based activity, two different models were used. In the first model, the mice have had the gene for C1q knocked-out preventing proper assembly of the C1 complex and its binding to IgG. The second model uses cobra

venom factor to deplete the components downstream of C3b. Cobra venom factor has the same activity as C3b without the need to be fixed on a cell (i.e. the reaction occurs in the fluid phase) and it cannot be inactivated by normal complement controls. (Cochrane, Müller-Eberhard, & Aikin, 1970; Lachmann & Halbwachs, 1975)

The C1q knock-out mice did not show any meaningful difference in survival compared to the wild-type animals (Figure 6). In the case of 4G7, the knock-out mice even had slightly better survival than the wild-type mice (100% vs 83.3%). Overall, the results suggest that the complement may have only minimal involvement in mediating the protection provided by the antibodies of ZMAb. There was also very little difference between the weight loss curves of wild-type and knock-out mice (Figure 8). The most interesting difference appears to be that the knock-out animals have a more variable course of disease than the wild-type animals.

The effect of depleting the complement in wild-type mice was similar to the knock-out of C1q (Figure 9). The C3 animals treated with PBS did succumb to infection slightly later than the non-depleted animals, although the difference was not significant ($p = 0.17$). Similar to the C1q knock-out mice, the animals depleted of complement and treated with 4G7 showed slightly better survival (100% vs 80%). It is surprising to find the same effect twice under similar circumstances. However, the odd result, if one can call it that, is that 4G7 has partial protection in the wild-type mice in the complement experiments. In all other mouse experiments reported here (FcRγ, Nfil3 knock-outs and the F_{ab} experiment), the 4G7 antibody always completely protects wild-type mice. The weight loss curves support the

absence of an effect from the complement as the curves for the complement-depleted animals are very similar to those of the wild-type animals.

4.2.3 Impact of neutralization

All the mechanisms of action of antibodies that involve the host immune system are initiated by the F_c fragment. (Bruhns & Jönsson, 2015; Kapur et al., 2014) Cutting antibodies with papain cleaves the F_{ab} fragments from the F_c fragment. The F_{ab} fragment contains the regions of the antibody involved in binding to the target, it is called the fragment, antigen binding or F_{ab}. The other fragment contains a highly conserved and tightly folded region which is easy to crystallize, it is called the fragment, crystallizable F_c. The F_c fragment can be removed from the mixture (result of the cut with papain) by using Protein A. The F_{ab} produced cannot activate cell-based receptors or the complement. Unfortunately, the F_c fragment is also responsible for binding to the FcRn receptor and the recycling of IgG antibodies. (L. Liu, 2017) This means that F_{ab} fragments have a much shorter half-life than normal species-matched antibodies, e.g. hours rather than days. Covell et al estimated that the serum half-life of F_{ab} is about 35 times shorter than that of the full antibody. (Covell et al., 1986)

In order to assess the effect of neutralization, it is necessary to remove all other functions of the antibodies. Producing $F_{ab}s$ from the antibodies is one way to remove those other functions. Because the F_c fragment is essential for the long half-life of antibodies, the dosing schedule for the two treatments, full IgG and F_{ab} fragments, is not the same. Multiple injections of mAbs, beyond using reagents and increasing the number of injections the mice receive, are of little benefit since a single injection is already known to be protective. On the

other hand, a single injection of F_{ab} to a healthy mouse (~100 μg) would be reduced to undetectable levels very quickly. In the presence of antigen, the removal of F_{ab} from the circulation would be even faster.

In every case, the F_{ab} was less effective than the full IgG (Figure 10). This is supported by the weight loss, where the F_{ab}-treated animals lost more weight than the animals treated with full IgG (Figure 11). However, the fact that any protection could be achieved with $F_{ab}s$ alone suggest that neutralization could be the only mechanism that is required, with a sufficiently high dose. The protection rates appear related to the neutralization efficiency of the antibodies. This is supported by additional work in rodents by Zheng et al where horse $F_{ab}2$ fragments were protective at doses of 1 or 2 mg/mouse/treatment under the same schedule as was done here. (Zheng et al., 2016) The dose used was fairly high, in part because the $F_{ab}2$ were derived from anti-serum, not purified monoclonal antibodies. The horse $F_{ab}2$ fragments would also not be able to trigger F_c-mediated mechanisms and probably have a similar half-life to the mouse $F_{ab}s$.

mAb 1H3 is the least neutralizing, with an IC_{50} of about 40 $\frac{\mu g}{ml}$ versus approximately 0.16 and 0.11 $\frac{\mu g}{ml}$ for 2G4 and 4G7, respectively. This makes sense if the half-life comes into play as 1H3 would drop below its IC_{50} long before 2G4 and 4G7. In the absence of antigen, it would approximately take an extra 7-8 half-lives before 2G4 and 4G7 would dip below their $IC_{50}s$ compared with 1H3. If we take into account that the $F_{ab}s$ likely diffuse in at least some tissues, it is possible that the peak concentration of 1H3 is actually below its IC_{50}.

These results are not all that surprising. The antibodies in ZMAb were chosen because they were neutralizing. While this does not imply that neutralization is the main mechanism, it does suggest that it should be important for these mAbs.

This experiment had two flaws. First, due to the difference in half-lives, it is difficult to assign the reason for the decreased efficacy of the $F_{ab}s$, whether it is due to the short half-life or the need for additional mechanisms. This could be resolved by using antibodies bearing the LALA mutation discussed earlier, they should have the same half-life without binding to FcγRs. The second flaw is that the IgG-treated animals received a single treatment, while the F_{ab}-treated animals received six. Ideally, the IgG-treated animals should have received PBS injections when the other animals were being treated. For example, the mouse which died on Day 4 in the 4G7 F_{ab}-treated group was found dead in its cage minutes after treatment, suggesting that the intraperitoneal injection, rather than the virus, was the cause of death. Removing this animal from the experiment would increase the survival rate for 4G7 F_{ab} from 60 to 67% (6 of 10 to 6 of 9 survivors).

Other studies support weak ADCC activity for 2G4 and 4G7. Liu et al used a pseudotyped lentivirus system expressing the EBOV GP as a surface protein and inducing the expression of both EBOV GP and Firefly luciferase in infected cells. (Q. Liu et al., 2017) By injecting the mice with antibodies and then performing *in vivo* imaging, they were able to assess the efficacy of different antibodies to trigger the elimination of the infected cells. They found that MIL77 (a chimeric version of ZMapp containing the mAbs c13C6, c2G4, and c4G7) induced very little ADCC *in vivo* in mice when injected 1 day post-infection. They attributed the lack of effect, in part, to the human F_c of MIL77. However, Overdijk et al showed that

human IgG, especially IgG1 as used for MIL77, could activate ADCC in mice, although not as well as mouse IgG. (Overdijk et al., 2012)

4.2.4 Mechanisms in mice: conclusions

Overall, the data presented suggest that, in mice, the antibodies of ZMAb appear to mediate their effect by preventing the infection of new cells rather than by removing already-infected cells. The dramatically different results between FcRγ– and Nfil3–knock-out mice are more difficult to reconcile. The interaction between NK cells and antibodies is generally considered to happen through FcγRs signalling through the FcRγ subunit. It is possible that the CD3ζ subunit can replace enough functionality to rescue the activity of FcγRIII for 4G7 to mediate its effect. On the other hand, the protective efficacy of ZMAb in NHPs, where mouse antibodies have no binding with FcγRs, also suggests that neutralization is sufficient for protection.

4.3 Immune responses during treatment with antibodies

4.3.1 Cytokine response

Because antibodies interact with many components of the innate immune system and these components can affect the development of the adaptive response, the immune responses of NHPs which survived the EBOV challenge was evaluated. One important way in which innate cells influence the adaptive response is by the cytokines being secreted. In order to evaluate this aspect of the immune response 9 cytokines, especially related to the T_h1/T_h2 polarization of CD4 T cells were measured in every available serum sample from survivors (Figures 12-20).

The cytokine data is only reported for the rhesus macaques. All cynomolgus macaques were treated with ZMAb and preliminary screens showed high levels of anti-mouse IgG antibodies (close to 1:1,000,000). The samples were run but all animals showed elevated cytokines starting between Days 10 and 14 which generally remained high through Day 28. Two of the animals which were rechallenged 9 weeks later (week 13 post-infection) still had levels of all measured cytokines at the same level as Day 28 from Week 13 through Week 17. It was concluded that the anti-mouse IgG reacted with the antibodies used in the cytokine assay. The rhesus macaques treated with ZMAb are presented because they do not show responses suggesting this kind of interference, either because they did not develop anti-mouse IgG or because these antibodies did not cross-react with the assay.

In order to get a sense of the viral antigen load present in the blood, the RT-qPCR–based viral loads are presented (Figure 12). The genome copies are reported rather than infectious virus because defective particles can be detected by this method (if they contain a genome), but would not be detected by the $TCID_{50}$ method. While non-infectious, these particles would still count towards the amount of antigen visible to the immune system. The genome copies do not necessarily correlate with the amounts of sGP, VP40, or NP present in the blood but should still be related, roughly, to the timing of antigen presence and elimination.

One of the first cytokines to peak and decline is IFN-γ (Figure 13). In many cases, such as for ZMAb + DEF201 and ZMapp1/ZMapp2-treated animals, IFN-γ starts to increase or even peaks on Day 3. Surprisingly, none of the animals treated with ZMapp on Day 3 have a notable increase until Day 6. In the ZMapp-treated animals, the intensity and the number of

animals with an increase increases with additional delays in treatment. In general, T cell responses do not peak until Days 10 to 14, by which time almost all the animals have returned to baseline. The early production of IFN-γ suggests that it is not produced by T cells, but most likely by cells part of the innate immune system. NK cells and macrophages could be releasing IFN-γ in response to the presence of infected cells.

The inter-individual variation is very evident in the concentrations of IFN-γ on Day 3. Most animals already have increased IFN-γ over the Day 0 sample, except for one animal (green) treated with ZMAb + DEF201, all animals treated with ZMapp at 72 h, and 4 of the 6 animals treated at 96 h. The difference between the Day 3 change over Day 0 between the animals treated with ZMapp at 72 and 120 h is surprising. While the animals show much variation, one would not expect this variation to neatly cluster with the group since no experimental manipulation had been done before that time point. The animals treated at 120 h also show an interesting pattern in the decline of the IFN-γ response, five of them peak on Day 8 and have completely returned to baseline by Day 11. In two cases, this represents a decrease of about 4 logs in 3 days. In some cases the decrease in IFN-γ happens just after a peak of IL-4, but most animals do not have much change in the serum concentrations of IL-4 (Figure 16).

The intensity of the change in IFN-γ is stronger than has been seen for vaccines in humans. For example, Cohen et al studied the cytokine profiles of individuals receiving smallpox vaccination and found that serum IFN-γ peaked on Days 8-9 and increased from ~1 pg/ml to 14 pg/ml, an increase of 1.15 logs. (Cohen et al., 2010) On the other hand, NHPs generally peaked on Days 3-8 with total increases as high as 5 logs over baseline. Even if

we restrict ourselves to comparing increases between well-defined points, some animals still show 2-3 logs of increase over 3 days. Some studies have been done with the VSVΔG-EBOVGP vaccine, which is at least a live virus, for example Dahlke et al. (Dahlke et al., 2017) However, the results are generally not reported in a way that can be compared with the current results. Dahlke et al only report the correlations between cytokines, for example. Cohen et al, studying smallpox vaccination, do not even provide error bars on the average concentrations measured.

The fact that IFN-γ is often already elevated by the time the first treatment is administered strongly suggests that ZMAb and ZMapp are not the cause of the increase. Additionally, the fact that the animals treated with ZMAb + DEF201 have a relatively short-lived IFN-γ burst suggests that the DEF201 may not be having a very strong effect. However, EVD often results in a cytokine storm which includes elevated IFN-γ. (Younan et al., 2017) A number of the animals with strong IFN-γ peaks, but not all of them, show a peak of IL-4 before or as the IFN-γ is going down. For almost all the animals which do have a measureable IL-4 peak, the peak happens after at least one treatment with antibodies. IL-4 is able to suppress the expression of cytokines associated with T_h1 responses, such as IFN-γ. (K. M. Murphy & Reiner, 2002) IL-4 is also involved in wound healing; it is possible that its presence helps to deal with the damage done by viral replication and the associated immune response. (Salmon-Ehr et al., 2000)

The cytokine IL-12 is a T_h1-polarizing cytokine for CD4 T cells. It is also able to counter the IL-4–mediated suppression of T_h1 cytokines. During the challenge, the vast majority of animals show no defined concentration of IL-12 (Figure 20). Only one group shows a clear

pattern, the animals treated with ZMapp 1, which only consists of all the animals appearing to have slightly higher levels of IL-12 starting on Day 9 than before. The red animal in this group is the only animal with multiple samples where there is enough IL-12 for accurate quantification and it shows mostly no change. IL-12 is generally secreted by antigen-presenting cells, mostly macrophages and dendritic cells. As such, it is likely that the late peaks (yellow animals treated with ZMAb or ZMapp (96 h) and purple animal treated with ZMapp2) are due to natural variation rather than to EVD or the treatments.

IL-2 follows strange patterns (Figure 15). It is generally produced only by T cells, but appears to increase soon after challenge in the animals treated with ZMAb, ZMapp1, and ZMapp2. In most cases, IL-2 starts to increase on Day 3 post-challenge and plateaus by Days 3 or 6. At that point the concentrations remain stable through Day 28, except for three animals (1 for each group) which have higher concentrations than the other animals in the same group. The internal consistency within each group is very strange and inconsistent with the variation seen for all other cytokines. IL-2 is an expansion signal for T cells, one would expect it to go down by Days 10-15, as the T cell response has generally started contracting by Day 21. This pattern is also definitely different from the ZMapp-treated animals. Contrary to the ZMapp1-treated animals, the animals treated at 72 h with ZMapp show no discernable pattern in IL-2 serum concentrations. The two cocktails are very similar, with the sole difference that ZMapp1 contained mouse 4G7 whereas ZMapp contains chimeric 4G7. It is unlikely that the strange pattern is due to anti-mouse IgG antibodies, as with the cynomolgus macaques, since the increased signal starts before the animals are exposed to the treatment. Additionally, the pattern is just as strong with ZMapp2, composed of the chimerics for 13C6, 1H3, and 2G4 suggesting that the presence of

a mouse antibody is not the trigger of this IL-2 response. The anti-mouse IgG antibody response would only start to be detectable around Day 10-14 when there has been enough time to produce large amounts of anti-treatment antibodies. The animals treated with ZMapp at 96 h do show a peak around Day 7 with most animals returning to some baseline level. The animals treated with ZMapp at 120 h have much variation in the first part of the challenge and settle in the upper range of their variation starting on Day 21. It is difficult to explain the behavior of IL-2 in this context.

The cytokine IL-5 can be secreted by T_h2 CD4 T cells, mast cells and eosinophils. In eosinophils, IL-5 can be released from granules upon stimulation of the cells by IgG-based immune complexes. (Dubucquoi et al., 1994) IL-5 is also important for the recruitment and development of eosinophils. Additionally, eosinophils are capable of secreting many cytokines, including IL-2, IL-4, IL-8, IL-10, and TNFα. (Hogan et al., 2008; Moqbel, Levi-Schaffer, & Kay, 1994) Many animals appear to have increases in IL-5 after receiving the ZMAb or ZMapp treatments (Figure 17). However, it is difficult to establish any clear pattern of activation. The ZMAb + DEF201-treated animals show well-defined peaks of IL-5 after receiving the first or second treatment despite the treatment being mouse IgG, which should not bind to NHP FcγRs. Some of the animals treated with ZMapp1 and with ZMapp at 72 and 96 h show a peak between Days 6-10. Overall, IL-5 may not be necessary for protection against the acute phase of the disease, until approximately Day 9-10 when animals that are still alive are very likely to survive. This is supported by the wide array of patterns at early times, with some animals having decreases (e.g. green in ZMapp treated at 120 h) and others showing little to no change, while some, as described above, do show

increases. IL-5 might play a role in the final clearance of virus and infected cells from the tissues.

Another granulocyte attracting cytokine is IL-8; it attracts neutrophils to sites of inflammation. IL-8 showed a very wide array of patterns in animals which survived a challenge, suggesting that, like serum IL-5, it also may not be a determinant of protection (Figure 18). The most surprising pattern consists of animals with high baseline levels of IL-8, such as the purple animals treated with ZMapp, the red animal treated with ZMapp at 96 h, and the yellow and teal animals treated with ZMapp at 120 h. All of these NHPs had levels of serum IL-8 above the limit of quantification and dipped below that limit around Days 7-11 only to come back to the higher baseline around Days 14 or 21. Also, a number of animals treated with ZMapp2 (red and purple), ZMapp at 96 h (yellow), and ZMapp at 120 h (green and blue) have levels of serum IL-8 that are high enough to be quantified accurately but which did not change during entire challenge experiment. IL-8 concentrations, like IL-5, do not appear to correlate with viremia. For example, both the groups treated with ZMapp at 96 and 120 h show a very high degree of internal consistency with regards to viremia, but a very high level of variation in the levels of IL-8 and IL-5.

IL-1β is a pro-inflammatory cytokine secreted by macrophages. (K. Murphy, 2012) IL-1β is secreted in the serum in a "bump" pattern, but mostly in ZMapp-treated animals (Figure 14). Only two other animals have meaningful changes in serum IL-1β, the green animal treated with ZMAb + DEF201 and the purple animal treated with ZMapp2. Four animals treated with ZMapp1 have well-defined IL-1β but with little to no change during the challenge. Again, there is a disconnection between the profiles of the ZMapp1- and ZMapp-

treated animals (at 72 h). As with IFN-γ, the response of IL-1β is unlikely to be due to the treatment as it often starts before the first treatment is administered and often resolved before the last treatment is administered. The peak occurs between Days 3 and 5, around the time when the animals would normally start to show mild symptoms of infection, which is consistent with the role of IL-1β as a general, pro-inflammatory signal.

The other pro-inflammatory cytokine measured, TNFα shows peaks consistent with an early inflammatory response in some groups (Figure 21). In animals treated with ZMAb, the TNFα response peaks around Day 14 for the three animals with any change in concentration. The intensity of the peaks appears unrelated to viral load, as all the animals have a similar viremia profile but the teal animal shows no TNFα response. The animals treated with ZMapp1, and ZMapp2 to a lesser extent, have a TNFα profile somewhat reminiscent of IL-2, starting low and reaching an upper plateau around Day 9. As with IL-2, the ZMapp1-treated teal animal has higher concentrations than the others. It is possible that the same, or a similar, process is involved in the response for these animals, for example eosinophils can secrete both cytokines. Based on the reaction of IL-2 to both ZMAb and ZMapp1, which both contain mouse antibodies, it would be tempting to suggest that the mouse mAbs are the reason for the strange patterns. However, the ZMapp2-treated animals have similar patterns and were treated with a purely chimeric treatment. The ZMapp-treated animals show a correlation between the number of animals with TNFα peaks and the delay of the first treatment; however, the intensity of the TNFα response, in responders, does not appear to follow the same trend. This is consistent with TNFα being produced in response to viral replication and possible tissue damage rather than the treatment.

The last cytokine measured during the challenge is IL-10. This cytokine can promote T_h2 responses and is also anti-inflammatory. IL-10 can prevent the activation of the TNFα converting enzyme (TACE also known as ADAM-17). (Brennan et al., 2008) Most animals show no changes in serum IL-10 concentrations (Figure 19). Overall, 6 animals have some pattern which appears like a possible response to the infection. The teal animal treated with ZMAb and the purple animal treated with ZMapp2 show an increase around Days 9 and 14. The ZMapp1-treated animals do not show much change in IL-10, but with TNFα levels increasing, a counter-response would be expected. Although, throughout the entire experiment TNFα levels never pass above 30 pg/ml which may remain safe even after almost 3 weeks, as with the teal ZMapp1-treated animal. The IL-10 levels of the ZMapp-treated animals (72 h) are consistent with the results of the ZMapp1-treated animals, which suggest that the single mouse antibody in ZMapp1 does not affect IL-10 secretion. The red and purple animals treated at 96 h, as well as the green and blue animals treated at 120 h both show a slight increase early after infection which disappears by Day 10. The green animal treated at 120 h shows a similar profile for both IL-10 and IL-4, with both cytokine at a level that is well-defined for the duration of the challenge. The peaks in the ZMapp-treated animals start before the treatment is administered, again suggesting that the initiation of the IL-10 response could be caused by the treatment.

Overall, it appears possible that the antibodies help to prevent the cytokine storm phenotype, most likely by reducing the GP antigen load and preventing the infection of new cells. Among other things, the cytokine storm appears to be triggered by the binding of TIM-1 on T cells to phosphatidylserine in the viral membrane. (Younan et al., 2017) This activates the T cells in a non-specific manner, stimulating them to secrete large amounts of

cytokines. The antibodies possibly sequester the virions into immune complexes and prevent the interaction of TIM-1 and the viral membrane. Additionally, these immune complexes might also trigger cells like eosinophils to secrete IL-4 and IL-10, thereby reducing the inflammatory response. Even in the case of mouse antibodies, the immune complexes may contain enough proteins to overcome the lack of affinity of human (or primate) FcγRs for mouse antibodies. Iampietro et al have shown that GP is also able to induce T cell death without infecting them. (Iampietro et al., 2017) The mechanism involves the interaction of GP and TLR4, it is possible that antibody-coated virions cannot interact well with TLR4 and thus do not induce T cell apoptosis.

Another interesting point is the strong increase in the production of IL-4 in animals receiving DEF201. IFN-α and adenoviruses would generally be expected to induce a T_h1 polarization. Either the rhesus macaques do not respond to the consensus human IFN-α or the antibodies—even the mouse antibodies—might induce a T_h2 signal strong enough to counter the effect of DEF201.

The results from the cytokine profiling support the conclusions obtained in mice that the antibodies (even the chimeric antibodies) work mostly through neutralization, not by activating cell killing and phagocytosis by NK cells and macrophages, respectively. The antibodies might also be able to promote a T_h2-friendly environment by forming immune complexes that stimulate granulocytes and macrophages.

4.3.2 T cell response on Day 21

The status of T cell–mediated responses was assessed on Day 21. Day 21 was chosen because the T cell response is already contracting from its peak on Day 14, but it remains

detectable. In order to assess cytokine production from T cells, peripheral blood mononuclear cells were isolated and allowed to rest overnight. The cells were stimulated in the presence of a CD107a antibody labelled with Brilliant Violet 421 to assess degranulation (related to the release of preformed granules containing cytokines or perforin and granzyme B). The cells were then stained for surface expression of CD3, CD4, and CD8 (labelled with Alexa Fluor 700, PerCP-Cy5.5, and PE-Cy7, respectively). After permeabilization, the cells were stained intracellularly for the cytokines IL-2, IL-4, and IFN-γ (labelled with Alexa Fluor 488, PE, and APC, respectively).

The counts of CD4 (or CD8, separately) T cells which fit in each of 16 activation profiles (based on 4 activation markers each of which can be positive or negative) were fit to a multinomial distribution for each group. This approach allows accounting for the total number of T cells considered in the analysis, which can range from about 20 to 70 thousand even within one group. It also ensures that the total frequencies for all 16 populations sum to 1 (or 100%) of the T cells. The procedure does have the drawback of overestimating the precision of activation profiles which have high counts relative to the others. The estimated rate for each activation profile (except the "All negative" profile, which would throw off the scale) are plotted by group and by stimulation in Figures 21 and 22.

First, the cynomolgus and rhesus macaques appear to respond to different pools when treated with ZMAb. The cynomolgus macaques respond most strongly to Pool 1, which contains the core and receptor-binding domain of GP. On the other hand, the rhesus macaques respond to Pools 1 and 3, which contains part of the mucin domain and GP_2. The response in the cynomolgus macaques is mostly polyfunctional. While the single-positive

profiles (on the right hand side of each graph) have higher frequencies, they also are much less increased over the Media stimulation than the more polyfunctional profiles (polyfunctionality increases towards the left). This is also true for the rhesus macaques except that they also respond well with IFN-γ alone. The switch to chimeric treatments also appears to have altered the response. The rhesus macaques treated with ZMapp1 and ZMapp2 respond to both Pools 1 and 3. It is possible that Pool 2 does not produce a good response because the peptides presented during the challenge would be heavily glycosylated, if they are presented at all, whereas the peptides used in the stimulation are not. Here, the high polyfunctionality is even more evident as the profiles with few activation markers have frequencies mostly equal to the Media and the corresponding points are transparent. Another interesting aspect is the higher frequencies of cells which show polyfunctional profiles compared with the ZMAb-treated animals. The immune complexes formed with chimeric antibodies might be better at stimulating antigen-presenting cells, resulting in better immune responses.

The rhesus macaques treated with ZMapp show fairly similar profiles, despite the delay in the initiation of the treatment. These animals are far more Pool 3–dominant than the rhesus macaques treated with ZMAb, ZMapp1, or ZMapp2. Given that the difference between ZMapp1 and ZMapp is that ZMapp1 contain mouse 4G7 while ZMapp contains chimeric 4G7, it is possible that the antibodies are directing some of the immune targeting. However, it would make more sense for antibodies to stimulate the targeting of proteins, not necessarily of epitopes within proteins. The ZMapp-treated animals also have some activation profiles that are expressed in response to Pool 2, although generally at lower frequencies than Pool3. Again, as before the response is mostly polyfunctional. In the

animals treated with chimeric antibodies, IFN-γ and IL-4 are only produced by the same cells in the context of the quadruple-positive CD107a + IL-2 + IL-4 + IFN-γ profile, suggesting that most cells have probably committed to a T_h1 or T_h2 response. Some of the profiles which include both IL-4 and IFN-γ remain present in the animals treated with ZMAb, which could indicate that some cells retain the T_h0 phenotype. None of the cytokines measured shows a pattern of variation consistent with this result, i.e. different between ZMAb- vs chimeric-treated animals. Either the effect is due to a cytokine that was not measured or the cytokine was not produced in large enough amounts to be detected in the serum. It is possible that DEF201 could be responsible for this difference; however, it would have done so without significantly affecting the measured cytokines, which is improbable.

The pattern of response to the different peptide pools is mostly conserved in CD8 T cells. The exception is that there is more response towards Pool 2 than in CD4 T cells, although Pool 2 still only occasionally induces the stronger response. The largest difference is that the increase in the frequency of the activation patterns is almost never greater than 1 log over the Media stimulation, whereas CD4 T cells had many responses with increases of 2 logs or more. This may be the effect of the IL-4 production in many of the animals that was seen during the challenge. Despite CD4 T cells which produce IFN-γ and an initial IFN-γ spike early after infection, the CD8 T cell response appears very weak. Naive CD8 T cells require that antigen-presenting cells be primed by CD4 T cells in order to receive all of the co-stimulation signals they require to mature. It is possible that the combination of Il-4, IL-5, and IL-10 seen during the challenge prevented these antigen-presenting cells from expressing sufficient level of co-stimulatory signals. Unfortunately, there is no data

indicating the level of CD8 T cell response needed for protection and virtually no data showing the relationship between different intensities of CD8 T cell response and survival. Even if such data existed, it is highly unlikely that the results could be compared with those presented here, due to technical and gating differences.

Overall, like the cytokines, the balance of the response in CD4 and CD8 cells is consistent with the antibodies performing 2 roles: 1) neutralization of the virus rather than elicitation of innate cell-mediated responses (which would result in the production of IFN-γ rather than IL-4); and 2) favoring a T_h2-polarized response, as seen by the low frequencies of responding CD8 T cells.

4.3.3 Antibody responses

The antibody response was assessed using two different methods. Historical data using a legacy titration assay is presented first (Figure 25). The semi-quantitative nature of the assay means that variation is difficult to detect as small and large changes may or may not affect the titres. Another assay was developed based on the one published by Vu et al, this assay is fully quantitative, allowing us to see the normal variation in responses. (Vu et al., 2016) Unfortunately, technical issues made it impossible to obtain usable data for all serum samples tested using the quantitative assay.

Overall, all animals had detectable IgG responses by the end of the challenge, according to both assays. The titration assay appears to have been overly sensitive with the cynomolgus macaques as IgG should not be detectable by Day 5. This is supported by the results from the quantitative assay where the first noticeable increase happens on Day 16. Both assays confirm that the yellow and green animals reach high anti-EBOV IgG levels for both of the

groups treated with ZMAb + DEF201. The titers for the animals treated with ZMAb alone are not reported because they used a virus-like particle–based assay rather than one using purified recombinant EBOV GP. Both of these groups also show strong responses, reaching IgG concentrations similar to those of the ZMAb + DEF201 animals in the quantitative assay.

The rhesus macaques treated with ZMAb + DEF201 did not all reach titers as high as the cynomolgus macaques receiving the same treatment. This is consistent with the quantitative assay where the rhesus macaques do not reach a concentration greater than 1000 AU/ml. Most likely, these differences are due to differences in the immune responses of rhesus vs cynomolgus macaques

The titration assay used an anti-human IgG polyclonal antibody conjugated to horseradish peroxidase for detection of the serum IgG. After the switch to chimeric antibody–based treatments, this assay also detects the treatment antibodies. On the other hand, the quantitative assay uses a monoclonal anti-rhesus IgG antibody (also conjugated) to perform detection. This monoclonal cross-reacts with cynomolgus IgG, but not human IgG. That allows the quantitative assay to detect only the IgG that is part of the NHPs' immune response.

All animals treated with chimeric IgG (ZMapp1, ZMapp2, and ZMapp) show very high titers starting from the sample after the first treatment. In some cases there is a decrease by Day 28, but it is not possible to confirm whether all human IgG has been eliminated based on the titration data. The quantitative assay confirms that all animals have an IgG response before Day 28 (Figure 26). This response generally does not start before Day 9 and often

reaches a plateau by Day 14 or 21. There does not appear to be a relationship between delay of treatment and intensity of the antibody response. The additional 2 days which add to the amount of antigen facing the immune system does not appear to affect the intensity of the antibody response, unlike what was observed for the IFN-γ and TNFα responses.

The teal animal treated with ZMapp2 had a very low antibody response. This animal also had no response in any of the cytokines measured. This animal appears to have been able to survive the infection with a treatment that is less neutralizing than ZMAb or ZMapp (ZMapp2 is composed of c13C6, c1H3, and c2G4 of which only 2G4 is a good neutralizer) and without much immune activation.

4.4 Mechanisms not directly addressed

It is possible for neutrophils to perform cell killing. While their contribution has not been individually evaluated here, they also require the FcR γ subunit to trigger Fc-mediated mechanisms in mice. Therefore, the γ subunit-knock out mice would also not have been able to trigger cell killing by neutrophils. On the other hand, neutrophils were still present and functional in the Nfil3$^{-/-}$ model and appear not to have been able to replace the effect of NK cells for 4G7, although it does remain unclear whether they had any effect for 1H3 and 2G4.

Another mechanism not explicitly studied here is the phagocytosis of infected cells, by macrophages and neutrophils for example. Like neutrophils and NK cells, the activating Fc receptors on macrophages require the FcR γ subunit to trigger intracellular signalling and, like cell-mediated cytotoxic responses, the γ subunit-knock out mice would have been unable to trigger phagocytosis. However, the NK-deficient mice were still able to trigger Fc-

dependent phagocytosis. This could be one explanation for the discrepancy between the γ subunit-knock out and the NK-deficient mice for 4G7. With NK cells absent more infected cells are phagocytosed. Given that macrophages, unlike NK cells, are permissive to infection by EBOV, they could contribute to virus spreading rather than virus control. This effect of phagocytosis might also be supported by the F_{ab} experiment, where for 4G7, having no ADCC and no phagocytosis at all, due to the absence of Fc regions, yielded a 60% (6 of 10) survival rate as opposed to a 20% (1 of 5) survival rate when NK cells were absent. It also appears that, in the absence of NK cells, neutrophils were unable to replace their effect, although this could also be due to different Fc-independent effects of NK cells such as killing cells displaying stress signals.

4.5 Other antibodies used to treat filovirus infections

Since the initial publications on ZMAb and ZMapp, a number of new antibodies have been generated or discovered that are protective in animal-based models of EVD. Many of those mAbs were chosen specifically for their high neutralizing activity. A recent find, isolated from an EVD survivor, is capable of neutralizing EBOV, Bundibugyo virus, and Sudan virus. (Gilchuk et al., 2018) This cross-neutralizing antibody is protective in smaller animal models (where they exist for the respective viruses). Experiments using a LALA-mutated antibody suggest, as the results presented here for ZMAb, that this antibody's neutralizing effect is sufficient to protect mice from lethal disease.

In 2012-2013, a consortium was formed to systematically evaluate the protective efficacy of all anti-EBOV mAbs that had been produced to date. The consortium evaluated the protective efficacy in mice and guinea pigs, but also used *in vitro* assays to evaluate the

ability of the various antibodies to trigger phagocytosis (by neutrophils and macrophages separately) and NK-mediated functions (degranulation and cytokine secretion). Their results, published in August 2018, show that protection can be a complicated phenomenon, with strongly neutralizing antibodies often being protective (defined as 60% protection under their chosen conditions) but not always. (Gunn et al., 2018; Saphire et al., 2018) Partial and non-neutralizing antibodies could also be protective (as in the MB-003 cocktail for example) and, in these cases, the protective efficacy was strongly correlated with recruitment of Fc-mediated mechanisms.

Another interesting development over the last few years is the development of equine $F(ab')_2$ fragments. Like F_{ab} fragments, $F(ab')_2$ fragments are proteolytically cleaved from full IgG, but the cut happens closer to the F_c region leaving the two F_{ab} fragments bound by a disulfide bond. Also like F_{ab} fragments, $F(ab')_2$ fragments do not trigger Fc-mediated mechanisms. Qiu et al showed that, once pharmacokinetic issues are overcome, equine $F(ab')_2$ can also be protective in mice and guinea pigs. (Zheng et al., 2016)

Overall, research into new antibodies and systematic large-scale study of existing mAbs suggest that neutralization may be sufficient for protection, but importantly, that neutralization is not strictly required for protection.

CHAPTER: 5 CONCLUSION

In order to assess the mechanism of action implicated in mediating the protection provided by the antibodies that compose ZMAb, mice bearing various immune defects were used to systematically remove certain components of the response. Neither the removal of the complement component C1q nor depletion of the complement components downstream of C3 produced meaningful reductions in efficacy. The removal of the FcRγ subunit, preventing FcγR signalling, also did not eliminate the protective efficacy of the antibodies. The removal of NK cells by knocking-out the transcription factor Nfil3 did appear to have a profound effect on 4G7 only. It is possible, since NK cells interact with antibodies through FcγRs and that they express CD3ζ, that an alternate signalling mechanism can rescue 4G7 if NK cells are still present. However, the use of $F_{ab}s$, which removed all F_c-mediated mechanisms, still provided the mice with a degree of protection that was inversely proportional to the IC_{50} of the antibodies. Considering the fact that the mouse antibodies were still quite protective in NHPs, where their F_c-mediated effects would be almost non-existent, the most important mechanism for the ZMAb antibodies is likely to be neutralization.

Because antibodies can be used by the host immune system to recognize pathogens and can affect cell activation patterns and cytokine secretion, the effect of different versions of the ZMAb treatment (ZMAb + DEF201, ZMapp1, ZMapp2, ZMapp) on the immune response during and after infection were compared. The immune responses developed can inform us, indirectly, on the nature of some of the interactions of the antibodies with the immune

system. Most serum cytokine patterns appear to have been dependent on the antibodies mostly in that there was no cytokine storm in survivors. Possibly, the immune complexes formed by the antibodies and the virus can trigger the secretion of T_h2-polarizing cytokines by cells like eosinophils and macrophages. This T_h2 polarization is apparent in the low levels of activation of CD8 T cells on Day 21. The host antibody response does not seem to be very strongly affected by the nature of the treatment. While some small variation appears to be present between different treatments, these changes are often less than the variation within the groups. These results are also consistent with neutralization being the major mechanism of protection for both ZMAb and ZMapp.

Overall, the results presented and those developed in the literature suggest a potential course to develop new mAb-based therapies against new and emerging viruses. An initial rapid search can be done to find neutralizing antibodies, these antibodies are likely to be effective regardless of host receptor and can be screened for rapidly with generally well-characterized assays. Such initial cocktails provide the additional time required for more in-depth studies of useful and important F_c-mediated mechanisms. The understanding of the contribution of various mechanisms can then be used to develop cocktails that recruit a wider array of effector functions and may have enhanced efficacy.

CHAPTER: 6 FUTURE DIRECTIONS

Now that the mechanism of ZMAb, and its derivatives, is known, it would be interesting to study the mechanisms involved in the protection of mice by non-neutralizing antibodies. Some of these non-neutralizing antibodies had better early protection profiles in mice. Additionally, the MB-003 cocktail was protective and did not contain antibodies that were strongly neutralizing. Knowing that we can use neutralizing antibodies to protect NHPs from EBOV gives an advantage in developing and evolving therapies. However, we should ensure that other mechanisms would not add to the efficacy of the treatments we are developing.

Members of the Special Pathogens group have been working on developing new reporter viruses that should be useable for *in vivo* imaging. It would be interesting to develop mouse models that use those viruses to evaluate ADCC and neutralization *in vivo*. For example, by seeing whether new cells are being infected (neutralization) or if the signal is being cleared (ADCC). Such tools combined with knock-out and humanized (expressing human receptors) mice might allow us to figure out the mechanisms involved in the protection of larger panels of antibodies.

The Viral hemorrhagic fever Immunotherapy Consortium (VIC) has also developed a number of *in vitro* assays related to various F_c-mediated mechanisms as well as predictive computer models that might highlight potentially protective antibodies before moving into animal experiments.

Another interesting avenue of research would be to evaluate the utility of various mechanisms when treatment is started at different phases of the infection. For example, if antibodies are administered very early after exposure, neutralizing mAbs have too little virus available for neutralization and rapid killing (or phagocytosis) of infected cells may be more useful. On the other hand, late during infection, when viremia is high, new cells are infected too rapidly for ADCC and phagocytosis to have much impact; at that point, neutralizing antibodies help to reduce the infection rate and allow other mechanisms (F_c-mediated mAbs and the host immune response) time to have their full effect. Eventually, it might be found that the composition of the cocktail should take into account the viremia of the patient.

CHAPTER: 7 REFERENCES

Abbink, P., Lemckert, A. A. C., Ewald, B. A., Lynch, D. M., Denholtz, M., Smits, S., … Barouch, D. H. (2007). Comparative Seroprevalence and Immunogenicity of Six Rare Serotype Recombinant Adenovirus Vaccine Vectors from Subgroups B and D. *Journal of Virology*. https://doi.org/10.1128/JVI.02696-06

Aleksandrowicz, P., Marzi, A., Biedenkopf, N., Beimforde, N., Becker, S., Hoenen, T., … Schnittler, H.-J. (2011). Ebola Virus Enters Host Cells by Macropinocytosis and Clathrin-Mediated Endocytosis. *The Journal of Infectious Diseases*, *204*(suppl 3), S957–S967. https://doi.org/10.1093/infdis/jir326

Alimonti, J., Leung, A., Jones, S., Gren, J., Qiu, X., Fernando, L., … Kobinger, G. (2014). Evaluation of transmission risks associated with in vivo replication of several high containment pathogens in a biosafety level 4 laboratory. *Scientific Reports*, *4*, 1–7. https://doi.org/10.1038/srep05824

Alvarez, C. P., Lasala, F., Carrillo, J., Muñiz, O., Corbí, A. L., & Delgado, R. (2002). C-Type Lectins DC-SIGN and L-SIGN Mediate Cellular Entry by Ebola Virus in *cis* and in *trans*. *Journal of Virology*, *76*(13), 6841–6844. https://doi.org/10.1128/JVI.76.13.6841-6844.2002

Annunziato, F., & Romagnani, S. (2009). Heterogeneity of human effector CD4+ T cells. *Arthritis Research & Therapy*, *11*(6), 257. https://doi.org/10.1186/ar2843

Arduin, E., Arora, S., Bamert, P. R., Kuiper, T., Popp, S., Geisse, S., … Kovarik, J. (2015). Highly

reduced binding to high and low affinity mouse Fc gamma receptors by L234A/L235A and N297A Fc mutations engineered into mouse IgG2a. *Molecular Immunology*, *63*(2), 456–463. https://doi.org/10.1016/j.molimm.2014.09.017

Audet, J., & Kobinger, G. P. (2015). Immune evasion in ebolavirus infections. *Viral Immunology*, *28*(1), 10–18. https://doi.org/10.1089/vim.2014.0066

Audet, J., Wong, G., Wang, H., Lu, G., Gao, G. F., Kobinger, G., & Qiu, X. (2014). Molecular Characterization of the Monoclonal Antibodies Composing ZMAb: A Protective Cocktail Against Ebola Virus. *Scientific Reports*, *4*, 6881. https://doi.org/10.1038/srep06881

Beniac, D. R., Melito, P. L., Devarennes, S. L., Hiebert, S. L., Rabb, M. J., Lamboo, L. L., … Booth, T. F. (2012). The organisation of Ebola virus reveals a capacity for extensive, modular polyploidy. *PloS One*, *7*(1), e29608. https://doi.org/10.1371/journal.pone.0029608

Borisevich, I. V, Mikhaĭlov, V. V, Krasnianskiĭ, V. P., Gradoboev, V. N., Lebedinskaia, E. V, Potryvaeva, N. V, & Timan'kova, G. D. (1995). [Development and study of the properties of immunoglobulin against Ebola fever]. *Voprosy Virusologii*, *40*(6), 270–273. Retrieved from http://www.ncbi.nlm.nih.gov/pubmed/8686265

Bornholdt, Z. A., Ndungo, E., Fusco, M. L., Bale, S., Flyak, A. I., Crowe, J. E., … Saphire, E. O. (2016). Host-primed Ebola virus GP exposes a hydrophobic NPC1 receptor-binding pocket, revealing a target for broadly neutralizing antibodies. *MBio*, *7*(1), 1–11. https://doi.org/10.1128/mBio.02154-15

Bray, M., & Geisbert, T. W. (2005). Ebola virus: the role of macrophages and dendritic cells in the pathogenesis of Ebola hemorrhagic fever. *The International Journal of*

Biochemistry & Cell Biology, *37*(8), 1560–1566. https://doi.org/10.1016/j.biocel.2005.02.018

Brennan, F. M., Green, P., Amjadi, P., Robertshaw, H. J., Alvarez-Iglesias, M., & Takata, M. (2008). Interleukin-10 regulates TNF-α-converting enzyme (TACE/ADAM-17) involving a TIMP-3 dependent and independent mechanism. *European Journal of Immunology*, *38*(4), 1106–1117. https://doi.org/10.1002/eji.200737821

Bruhns, P., & Jönsson, F. (2015). Mouse and human FcR effector functions. *Immunological Reviews*, *268*(1), 25–51. https://doi.org/10.1111/imr.12350

Burke, J., Declerq, R., & Ghysebrechts, G. (1978). Ebola haemorrhagic fever in Zaire, 1976. Report of an international commission. *Bulletin of the World Health Organization*, *56*(2), 271–293. https://doi.org/1978;56(2):271-293.

Centers for Disease Control and Prevention. (2014). Signs and Symptoms. Retrieved November 15, 2017, from https://www.cdc.gov/vhf/ebola/symptoms/index.html

Clynes, R. a, Towers, T. L., Presta, L. G., & Ravetch, J. V. (2000). Inhibitory Fc receptors modulate in vivo cytoxicity against tumor targets. *Nature Medicine*, *6*(4), 443–446. https://doi.org/10.1038/74704

Cochrane, C. G., Müller-Eberhard, H. J., & Aikin, B. S. (1970). Depletion of plasma complement in vivo by a protein of cobra venom: its effect on various immunologic reactions. *J Immunol*, *105*(1), 55–69. https://doi.org/10.1016/0041-0101(71)90016-X

Cohen, J. I., Hohman, P., Fulton, R., Turk, S.-P., Qin, J., Thatcher, K., & Hornung, R. L. (2010). Kinetics of Serum Cytokines after Primary or Repeat Vaccination with the Smallpox

Vaccine. *The Journal of Infectious Diseases*, *201*(8), 1183–1191. https://doi.org/10.1086/651453

Covell, D. G., Barbet, J., Holton, O. D., Black, C. D. V, Parker, R. J., & Weinstein, J. N. (1986). Pharmacokinetics of Monoclonal Immunoglobulin G 1 , F (ab ′) 2 , and Fab ′ in Mice Pharmacokinetics of Monoclonal Immunoglobulin d , F (ab ') 2 , and Fab ' in Mice. *Cancer Res*, *46*(August), 3969–3978.

Dahlke, C., Kasonta, R., Lunemann, S., Krähling, V., Zinser, M. E., Biedenkopf, N., … Lapujade, O. (2017). Dose-dependent T-cell Dynamics and Cytokine Cascade Following rVSV-ZEBOV Immunization. *EBioMedicine*, *19*, 107–118. https://doi.org/10.1016/j.ebiom.2017.03.045

Davidson, E., Bryan, C., Fong, R. H., Barnes, T., Pfaff, J. M., Mabila, M., … Doranz, B. J. (2015). Mechanism of Binding to Ebola Virus Glycoprotein by the ZMapp, ZMAb, and MB-003 Cocktail Antibodies. *Journal of Virology*, *89*(21), 10982–10992. https://doi.org/10.1128/JVI.01490-15

Dubucquoi, S., Desreumaux, P., Janin, A., Klein, O., Goldman, M., Tavernier, J., … Capron, M. (1994). Interleukin 5 synthesis by eosinophils: association with granules and immunoglobulin-dependent secretion. *The Journal of Experimental Medicine*, *179*(2), 703–708. https://doi.org/10.1084/jem.179.2.703

Dye, J. M., Herbert, A. S., Kuehne, A. I., Barth, J. F., Muhammad, M. A., Zak, S. E., … Pratt, W. D. (2012). Postexposure antibody prophylaxis protects nonhuman primates from filovirus disease. *Proceedings of the National Academy of Sciences of the United States of*

America, *109*(13), 5034–5039. https://doi.org/10.1073/pnas.1200409109

Ebihara, H., Theriault, S., Neumann, G., Alimonti, J. B., Geisbert, J. B., Hensley, L. E., … Feldmann, H. (2007). In vitro and in vivo characterization of recombinant Ebola viruses expressing enhanced green fluorescent protein. *The Journal of Infectious Diseases*, *196 Suppl*(335405), S313-22. https://doi.org/10.1086/520590

Feldmann, H., & Geisbert, T. W. (2011). Ebola haemorrhagic fever. *Lancet*, *377*(9768), 849–862. https://doi.org/10.1016/S0140-6736(10)60667-8

Feldmann, H., Jones, S. M., Daddario-DiCaprio, K. M., Geisbert, J. B., Ströher, U., Grolla, A., … Geisbert, T. W. (2007). Effective post-exposure treatment of Ebola infection. *PLoS Pathogens*, *3*(1), e2. https://doi.org/10.1371/journal.ppat.0030002

Finak, G., Frelinger, J., Jiang, W., Newell, E. W., Ramey, J., Davis, M. M., … Gottardo, R. (2014). OpenCyto: An Open Source Infrastructure for Scalable, Robust, Reproducible, and Automated, End-to-End Flow Cytometry Data Analysis. *PLoS Computational Biology*, *10*(8), e1003806. https://doi.org/10.1371/journal.pcbi.1003806

Formenty, P., Libama, F., Epelboin, A., Allarangar, Y., Leroy, E., Moudzeo, H., … Grein, T. (2003). [Outbreak of Ebola hemorrhagic fever in the Republic of the Congo, 2003: a new strategy?]. *Medecine Tropicale : Revue Du Corps de Sante Colonial*, *63*(3), 291–295.

Francica, J. R., Varela-Rohena, A., Medvec, A., Plesa, G., Riley, J. L., & Bates, P. (2010). Steric shielding of surface epitopes and impaired immune recognition induced by the ebola virus glycoprotein. *PLoS Pathogens*, *6*(9), e1001098. https://doi.org/10.1371/journal.ppat.1001098

Gascoyne, D. M., Long, E., Veiga-Fernandes, H., de Boer, J., Williams, O., Seddon, B., … Brady, H. J. M. (2009). The basic leucine zipper transcription factor E4BP4 is essential for natural killer cell development. *Nature Immunology*, *10*(10), 1118–1124. https://doi.org/10.1038/ni.1787

Gatherer, D. (2014). The 2014 Ebola virus disease outbreak in West Africa. *The Journal of General Virology*, *95*(Pt 8), 1619–1624. https://doi.org/10.1099/vir.0.067199-0

Geisbert, T. W., Hensley, L. E., Jahrling, P. B., Larsen, T., Geisbert, J. B., Paragas, J., … Vlasuk, G. P. (2003). Treatment of Ebola virus infection with a recombinant inhibitor of factor VIIa/tissue factor: a study in rhesus monkeys. *Lancet*, *362*(9400), 1953–1958. https://doi.org/10.1016/S0140-6736(03)15012-X

Geisbert, T. W., Lee, A. C. H., Robbins, M., Geisbert, J. B., Honko, A. N., Sood, V., … Maclachlan, I. (2010). Postexposure protection of non-human primates against a lethal Ebola virus challenge with RNA interference: a proof-of-concept study. *Lancet*, *375*(9729), 1896–1905. https://doi.org/10.1016/S0140-6736(10)60357-1

Geisbert, T. W., Pushko, P., Anderson, K., Smith, J., Davis, K. J., & Jahrling, P. B. (2002). Evaluation in nonhuman primates of vaccines against Ebola virus. *Emerging Infectious Diseases*. https://doi.org/10.3201/eid0805.010284

Geisbert, T. W., Young, H. A., Jahrling, P. B., Davis, K. J., Kagan, E., & Hensley, L. E. (2003). Mechanisms underlying coagulation abnormalities in ebola hemorrhagic fever: overexpression of tissue factor in primate monocytes/macrophages is a key event. *The Journal of Infectious Diseases*, *188*(11), 1618–1629. https://doi.org/10.1086/379724

Geisbert, T. W., Young, H. a, Jahrling, P. B., Davis, K. J., Larsen, T., Kagan, E., & Hensley, L. E. (2003). Pathogenesis of Ebola hemorrhagic fever in primate models: evidence that hemorrhage is not a direct effect of virus-induced cytolysis of endothelial cells. *The American Journal of Pathology*, *163*(6), 2371–2382. https://doi.org/10.1016/S0002-9440(10)63592-4

Gelman, A., Chew, G. L., & Shnaidman, M. (2004). Bayesian analysis of serial dilution assays. *Biometrics*, *60*(2), 407–417. https://doi.org/10.1111/j.0006-341X.2004.00185.x

Georges, A., Leroy, E. M., Renaut, A. A., Benissan, C. T., Nabias, R. J., Ngoc, M. T., … Georges-Courbot, M. (1999). Ebola Hemorrhagic Fever Outbreaks in Gabon, 1994–1997: Epidemiologic and Health Control Issues. *The Journal of Infectious Diseases*, *179*(s1), S65–S75. https://doi.org/10.1086/514290

Gilchuk, P., Kuzmina, N., Ilinykh, P. A., Huang, K., Gunn, B. M., Bryan, A., … Crowe, J. E. (2018). Multifunctional Pan-ebolavirus Antibody Recognizes a Site of Broad Vulnerability on the Ebolavirus Glycoprotein. *Immunity*, *49*(2), 363–374.e10. https://doi.org/10.1016/j.immuni.2018.06.018

Gunn, B. M., Yu, W. H., Karim, M. M., Brannan, J. M., Herbert, A. S., Wec, A. Z., … Alter, G. (2018). A Role for Fc Function in Therapeutic Monoclonal Antibody-Mediated Protection against Ebola Virus. *Cell Host and Microbe*, *24*(2), 221–233.e5. https://doi.org/10.1016/j.chom.2018.07.009

Henao-Restrepo, A. M., Camacho, A., Longini, I. M., Watson, C. H., Edmunds, W. J., Egger, M., … Kieny, M.-P. (2017). Efficacy and effectiveness of an rVSV-vectored vaccine in

preventing Ebola virus disease: final results from the Guinea ring vaccination, open-label, cluster-randomised trial (Ebola Ça Suffit!). *The Lancet*, *389*(10068), 505–518. https://doi.org/10.1016/S0140-6736(16)32621-6

Hensley, L. E., Stevens, E. L., Yan, S. B., Geisbert, J. B., Macias, W. L., Larsen, T., … Geisbert, T. W. (2007). Recombinant human activated protein C for the postexposure treatment of Ebola hemorrhagic fever. *The Journal of Infectious Diseases*, *196 Suppl*, S390-9. https://doi.org/10.1086/520598

Hoenen, T., Jung, S., Herwig, A., Groseth, A., & Becker, S. (2010). Both matrix proteins of Ebola virus contribute to the regulation of viral genome replication and transcription. *Virology*, *403*(1), 56–66. https://doi.org/10.1016/j.virol.2010.04.002

Hogan, S. P., Rosenberg, H. F., Moqbel, R., Phipps, S., Foster, P. S., Lacy, P., … Rothenberg, M. E. (2008). Eosinophils: biological properties and role in health and disease. *Clinical and Experimental Allergy : Journal of the British Society for Allergy and Clinical Immunology*, *38*(5), 709–750. https://doi.org/10.1111/j.1365-2222.2008.02958.x

Iampietro, M., Younan, P., Nishida, A., Dutta, M., Lubaki, N. M., Santos, R. I., … Bukreyev, A. (2017). Ebola virus glycoprotein directly triggers T lymphocyte death despite of the lack of infection. *PLoS Pathogens*, *13*(5), 1–27. https://doi.org/10.1371/journal.ppat.1006397

Jaax, N., Jahrling, P., Geisbert, T., Geisbert, J., Steele, K., McKee, K., … Peters, C. (1995). Transmission of Ebola virus (Zaire strain) to uninfected control monkeys in a biocontainment laboratory. *Lancet (London, England)*, *346*(8991–8992), 1669–1671.

Retrieved from http://www.ncbi.nlm.nih.gov/pubmed/8551825

Jahrling, P. B., Geisbert, J., Swearengen, J. R., Jaax, G. P., Lewis, T., Huggins, J. W., … Peters, C. J. (1996). Passive immunization of Ebola virus-infected cynomolgus monkeys with immunoglobulin from hyperimmune horses. *Archives of Virology. Supplementum*, *11*, 135–140. Retrieved from http://www.ncbi.nlm.nih.gov/pubmed/8800795

Jahrling, P. B., Geisbert, T. W., Geisbert, J. B., Swearengen, J. R., Bray, M., Jaax, N. K., … Peters, C. J. (1999). Evaluation of immune globulin and recombinant interferon-alpha2b for treatment of experimental Ebola virus infections. *The Journal of Infectious Diseases*, *179 Suppl*, S224-34. https://doi.org/10.1086/514310

Jahrling, P. B., Geisbert, T. W., Johnson, E. D., Peters, C. J., Dalgard, D. W., & Hall, W. C. (1990). Preliminary report: isolation of Ebola virus from monkeys imported to USA. *The Lancet*, *335*(8688), 502–505. https://doi.org/10.1016/0140-6736(90)90737-P

Jones, S. M., Feldmann, H., Ströher, U., Geisbert, J. B., Fernando, L., Grolla, A., … Geisbert, T. W. (2005). Live attenuated recombinant vaccine protects nonhuman primates against Ebola and Marburg viruses. *Nature Medicine*, *11*(7), 786–790. https://doi.org/10.1038/nm1258

Kapur, R., Einarsdottir, H. K., & Vidarsson, G. (2014). IgG-effector functions: "The Good, The Bad and The Ugly." *Immunology Letters*, 1–6. https://doi.org/10.1016/j.imlet.2014.01.015

Khan, a S., Tshioko, F. K., Heymann, D. L., Le Guenno, B., Nabeth, P., Kerstiëns, B., … Ksiazek, T. G. (1999). The reemergence of Ebola hemorrhagic fever, Democratic Republic of the

Congo, 1995. *The Journal of Infectious Diseases*, *179 Suppl*, S76–S86. https://doi.org/10.1086/514306

Khanna, M., Sharma, S., Kumar, B., & Rajput, R. (2014). Protective immunity based on the conserved hemagglutinin stalk domain and its prospects for universal influenza vaccine development. *BioMed Research International*, *2014*, 0–2. https://doi.org/10.1155/2014/546274

Kimberlin, C. R., Bornholdt, Z. a, Li, S., Woods, V. L., MacRae, I. J., & Saphire, E. O. (2010). Ebolavirus VP35 uses a bimodal strategy to bind dsRNA for innate immune suppression. *Proceedings of the National Academy of Sciences of the United States of America*, *107*(1), 314–319. https://doi.org/10.1073/pnas.0910547107

Kondratowicz, A. S., Lennemann, N. J., Sinn, P. L., Davey, R. A., Hunt, C. L., Moller-Tank, S., … Maury, W. (2011). T-cell immunoglobulin and mucin domain 1 (TIM-1) is a receptor for Zaire Ebolavirus and Lake Victoria Marburgvirus. *Proceedings of the National Academy of Sciences*, *108*(20), 8426–8431. https://doi.org/10.1073/pnas.1019030108

Krasnianskiĭ, V. P., Mikhaĭlov, V. V, Borisevich, I. V, Gradoboev, V. N., Evseev, A. A., & Pshenichnov, V. A. (1994). [The isolation of hyperimmune horse serum to the Ebola virus]. *Voprosy Virusologii*, *39*(2), 91–92. Retrieved from http://www.ncbi.nlm.nih.gov/pubmed/8017064

Kratz, T., Roddy, P., Oloma, A. T., Jeffs, B., Ciruelo, D. P., De La Rosa, O., & Borchert, M. (2015). Ebola virus disease outbreak in Isiro, democratic Republic of the Congo, 2012: Signs and symptoms, management and outcomes. *PLoS ONE*, *10*(6), 1–18.

https://doi.org/10.1371/journal.pone.0129333

Krishnan, A., Miller, E. H., Herbert, A. S., Ng, M., Ndungo, E., Whelan, S. P., … Chandran, K. (2012). Niemann-Pick C1 (NPC1)/NPC1-like1 chimeras define sequences critical for NPC1's function as a flovirus entry receptor. *Viruses*, *4*(11), 2471–2484. https://doi.org/10.3390/v4112471

Kühl, A., Banning, C., Marzi, A., Votteler, J., Steffen, I., Bertram, S., … Pöhlmann, S. (2011). The Ebola Virus Glycoprotein and HIV-1 Vpu Employ Different Strategies to Counteract the Antiviral Factor Tetherin. *The Journal of Infectious Diseases*, *204 Suppl*(Suppl 3), S850-60. https://doi.org/10.1093/infdis/jir378

Kuhn, J. H., Bao, Y., Bavari, S., Becker, S., Bradfute, S., Brister, J. R., … Nichol, S. T. (2013). Virus nomenclature below the species level: a standardized nomenclature for laboratory animal-adapted strains and variants of viruses assigned to the family Filoviridae. *Archives of Virology*, *158*(6), 1425–1432. https://doi.org/10.1007/s00705-012-1594-2

Lachmann, P. J., & Halbwachs, L. (1975). The influence of C3b inactivator (KAF) concentration on the ability of serum to support complement activation. *Clinical and Experimental Immunology*, *21*(1), 109–114. Retrieved from http://www.ncbi.nlm.nih.gov/pubmed/52423

Lee, J. E., Fusco, M. L., Hessell, A. J., Oswald, W. B., Burton, D. R., & Saphire, E. O. (2008). Structure of the Ebola virus glycoprotein bound to an antibody from a human survivor. *Nature*, *454*(7201), 177–182. https://doi.org/10.1038/nature07082

Lennemann, N. J., Herbert, A. S., Brouillette, R., Rhein, B., Bakken, R. A., Perschbacher, K. J., … Maury, W. (2017). Vesicular stomatitis virus pseudotyped with Ebola virus glycoprotein serves as a protective, non-infectious vaccine against Ebola virus challenge in mice. *Journal of Virology*, *91*(17), JVI.00479-17. https://doi.org/10.1128/JVI.00479-17

Leung, D. W., Shabman, R. S., Farahbakhsh, M., Prins, K. C., Borek, D. M., Wang, T., … Amarasinghe, G. K. (2010). Structural and functional characterization of Reston Ebola virus VP35 interferon inhibitory domain. *Journal of Molecular Biology*, *399*(3), 347–357. https://doi.org/10.1016/j.jmb.2010.04.022

Liu, L. (2017). Pharmacokinetics of monoclonal antibodies and Fc-fusion proteins. *Protein & Cell*. https://doi.org/10.1007/s13238-017-0408-4

Liu, Q., Fan, C., Li, Q., Zhou, S., Huang, W., Wang, L., … Wang, Y. (2017). Antibody-dependent-cellular-cytotoxicity-inducing antibodies significantly affect the post-exposure treatment of Ebola virus infection. *Scientific Reports*, *7*(2), 45552. https://doi.org/10.1038/srep45552

Liu, X., Pop, L. M., & Vitetta, E. S. (2008). Engineering therapeutic monoclonal antibodies. *Immunological Reviews*, *222*, 9–27. https://doi.org/10.1111/j.1600-065X.2008.00601.x

Lubaki, N. M., Ilinykh, P., Pietzsch, C., Tigabu, B., Freiberg, A. N., Koup, R. A., & Bukreyev, A. (2013). The lack of maturation of Ebola virus-infected dendritic cells results from the cooperative effect of at least two viral domains. *Journal of Virology*, *87*(13), 7471–

7485. https://doi.org/10.1128/JVI.03316-12

Lupton, H. W., Lambert, R. D., Bumgardner, D. L., Moe, J. B., & Eddy, G. A. (1980). INACTIVATED VACCINE FOR EBOLA VIRUS EFFICACIOUS IN GUINEAPIG MODEL. *The Lancet*. https://doi.org/10.1016/S0140-6736(80)92352-1

Mahanty, S., & Bray, M. (2004). Pathogenesis of filoviral haemorrhagic fevers. *The Lancet Infectious Diseases*, *4*(8), 487–498. https://doi.org/10.1016/S1473-3099(04)01103-X

Mahnke, Y. D., Brodie, T. M., Sallusto, F., Roederer, M., & Lugli, E. (2013). The who's who of T-cell differentiation: human memory T-cell subsets. *European Journal of Immunology*, *43*(11), 2797–2809. https://doi.org/10.1002/eji.201343751

Mandal, A., & Viswanathan, C. (2015). Natural killer cells: In health and disease. *Hematology/Oncology and Stem Cell Therapy*, *8*(2), 47–55. https://doi.org/10.1016/j.hemonc.2014.11.006

Marzi, A., Reinheckel, T., & Feldmann, H. (2012). Cathepsin B & L are not required for ebola virus replication. *PLoS Neglected Tropical Diseases*, *6*(12), e1923. https://doi.org/10.1371/journal.pntd.0001923

Marzi, A., Yoshida, R., Miyamoto, H., Ishijima, M., Suzuki, Y., Higuchi, M., … Takada, A. (2012). Protective efficacy of neutralizing monoclonal antibodies in a nonhuman primate model of Ebola hemorrhagic fever. *PloS One*, *7*(4), e36192. https://doi.org/10.1371/journal.pone.0036192

McElreath, R. (2015). *Statistical Rethinking: A Bayesian Course with Examples in R and Stan* (1st ed.). Chapman and Hall/CRC. Retrieved from

https://www.crcpress.com/Statistical-Rethinking-A-Bayesian-Course-with-Examples-in-R-and-Stan/McElreath/p/book/9781482253443

Mehedi, M., Falzarano, D., Seebach, J., Hu, X., Carpenter, M. S., Schnittler, H.-J., & Feldmann, H. (2011). A new Ebola virus nonstructural glycoprotein expressed through RNA editing. *Journal of Virology*, *85*(11), 5406–5414. https://doi.org/10.1128/JVI.02190-10

Mikhaĭlov, V. V, Borisevich, I. V, Chernikova, N. K., Potryvaeva, N. V, & Krasnianskiĭ, V. P. (1994). [The evaluation in hamadryas baboons of the possibility for the specific prevention of Ebola fever]. *Voprosy Virusologii*, *39*(2), 82–84. Retrieved from http://www.ncbi.nlm.nih.gov/pubmed/8017061

Miranda, M. E., Ksiazek, T. G., Retuya, T. J., Khan, a S., Sanchez, a, Fulhorst, C. F., … Peters, C. J. (1999). Epidemiology of Ebola (subtype Reston) virus in the Philippines, 1996. *The Journal of Infectious Diseases*, *179 Suppl*(Suppl 1), S115-9. https://doi.org/10.1086/514314

Mohan, G. S., Li, W., Ye, L., Compans, R. W., & Yang, C. (2012). Antigenic subversion: a novel mechanism of host immune evasion by Ebola virus. *PLoS Pathogens*, *8*(12), e1003065. https://doi.org/10.1371/journal.ppat.1003065

Montero, M., van Houten, N. E., Wang, X., & Scott, J. K. (2008). The membrane-proximal external region of the human immunodeficiency virus type 1 envelope: dominant site of antibody neutralization and target for vaccine design. *Microbiology and Molecular Biology Reviews*, *72*(1), 54–84. https://doi.org/10.1128/MMBR.00020-07

Moqbel, R., Levi-Schaffer, F., & Kay, A. B. (1994). Cytokine generation by eosinophils. *The*

Journal of Allergy and Clinical Immunology, *94*(6 Pt 2), 1183–1188. https://doi.org/10.1016/0091-6749(94)90330-1

Mühlberger, E. (2007). Filovirus replication and transcription. *Future Virology*, *2*(2), 205–215. https://doi.org/10.2217/17460794.2.2.205

Mühlberger, E. M., Weik, M., Volchkov, V. E., Klenk, H.-D., & Becker, S. (1999). Comparison of the Transcription and Replication Strategies of Marburg Virus and Ebola Virus by Using Artificial Replication Systems. *Journal of Virology*, *73*(3), 2333–2342.

Mupapa, K., Massamba, M., Kibadi, K., Kuvula, K., Bwaka, A., Kipasa, M., … Muyembe-Tamfum, J. J. (1999). Treatment of Ebola hemorrhagic fever with blood transfusions from convalescent patients. International Scientific and Technical Committee. *The Journal of Infectious Diseases*, *179 Suppl*, S18-23. https://doi.org/10.1086/514298

Murin, C. D., Fusco, M. L., Bornholdt, Z. A., Qiu, X., Olinger, G. G., Zeitlin, L., … Saphire, E. O. (2014). Structures of protective antibodies reveal sites of vulnerability on Ebola virus. *Proceedings of the National Academy of Sciences*, *111*(48), 17182–17187. https://doi.org/10.1073/pnas.1414164111

Murphy, K. (2012). *Janeway's Immunobiology* (8th ed.). New York, NY: Garland Science. Retrieved from http://garlandscience.com/product/isbn/9780815342434

Murphy, K. M., & Reiner, S. L. (2002). Decision making in the immune system: The lineage decisions of helper T cells. *Nature Reviews Immunology*, *2*(12), 933–944. https://doi.org/10.1038/nri954

Nfon, C. K., Leung, A., Smith, G., Embury-Hyatt, C., Kobinger, G., & Weingartl, H. M. (2013).

Immunopathogenesis of Severe Acute Respiratory Disease in Zaire ebolavirus-Infected Pigs. *PLoS ONE*, *8*(4). https://doi.org/10.1371/journal.pone.0061904

Nwanegbo, E., Vardas, E., Gao, W., Whittle, H., Sun, H., Rowe, D., … Gambotto, A. (2004). Prevalence of neutralizing antibodies to adenoviral serotypes 5 and 35 in the adult populations of The Gambia, South Africa, and the United States. *Clinical and Diagnostic Laboratory Immunology*, *11*(2), 351–357. Retrieved from http://www.ncbi.nlm.nih.gov/pubmed/15013987

Okumura, A., Pitha, P. M., Yoshimura, A., & Harty, R. N. (2010). Interaction between Ebola virus glycoprotein and host toll-like receptor 4 leads to induction of proinflammatory cytokines and SOCS1. *Journal of Virology*, *84*(1), 27–33. https://doi.org/10.1128/JVI.01462-09

Olinger, G. G., Pettitt, J., Kim, D., Working, C., Bohorov, O., Bratcher, B., … Zeitlin, L. (2012). Delayed treatment of Ebola virus infection with plant-derived monoclonal antibodies provides protection in rhesus macaques. *Proceedings of the National Academy of Sciences of the United States of America*, *109*(44), 18030–18035. https://doi.org/10.1073/pnas.1213709109

Oswald, W. B., Geisbert, T. W., Davis, K. J., Geisbert, J. B., Sullivan, N. J., Jahrling, P. B., … Burton, D. R. (2007). Neutralizing antibody fails to impact the course of Ebola virus infection in monkeys . *PLoS Pathogens*, *3*(1), e9. https://doi.org/10.1371/journal.ppat.0030009

Overdijk, M. B., Verploegen, S., Ortiz Buijsse, A., Vink, T., Leusen, J. H. W., Bleeker, W. K., &

Parren, P. W. H. I. (2012). Crosstalk between Human IgG Isotypes and Murine Effector Cells. *The Journal of Immunology*, *189*(7), 3430–3438. https://doi.org/10.4049/jimmunol.1200356

Parren, P. W. H. I., Geisbert, T. W., Maruyama, T., Jahrling, P. B., & Burton, D. R. (2002). Pre- and Postexposure Prophylaxis of Ebola Virus Infection in an Animal Model by Passive Transfer of a Neutralizing Human Antibody. *Journal of Virology*, *76*(12), 6408–6412. https://doi.org/10.1128/JVI.76.12.6408-6412.2002

Pettitt, J., Zeitlin, L., Kim, D. H., Working, C., Johnson, J. C., Bohorov, O., … Olinger, G. G. (2013). Therapeutic intervention of Ebola virus infection in rhesus macaques with the MB-003 monoclonal antibody cocktail. *Science Translational Medicine*, *5*(199), 199ra113. https://doi.org/10.1126/scitranslmed.3006608

Plotkin, S. A. (2010). Correlates of protection induced by vaccination. *Clinical and Vaccine Immunology*, *17*(7), 1055–1065. https://doi.org/10.1128/CVI.00131-10

Presta, L. G. (2008). Molecular engineering and design of therapeutic antibodies. *Current Opinion in Immunology*, *20*(4), 460–470. https://doi.org/10.1016/j.coi.2008.06.012

PREVAIL II Writing Group, Multi-National PREVAIL II Study Team, Davey, R. T., Dodd, L., Proschan, M. A., Neaton, J., … Malvy, D. (2016). A Randomized, Controlled Trial of ZMapp for Ebola Virus Infection. *The New England Journal of Medicine*, *375*(15), 1448–1456. https://doi.org/10.1056/NEJMoa1604330

ProMED-mail. (2007). Ebola hemorrhagic fever—Congo DR. Retrieved November 30, 2017, from http://www.promedmail.org/pls/apex/f?p=2400:1000

Qiu, X., Alimonti, J. B., Melito, P. L., Fernando, L., Ströher, U., & Jones, S. M. (2011). Characterization of Zaire ebolavirus glycoprotein-specific monoclonal antibodies. *Clinical Immunology (Orlando, Fla.)*, *141*(2), 218–227. https://doi.org/10.1016/j.clim.2011.08.008

Qiu, X., Audet, J., Wong, G., Pillet, S., Bello, A., Cabral, T., … Kobinger, G. P. (2012). Successful treatment of ebola virus-infected cynomolgus macaques with monoclonal antibodies. *Science Translational Medicine*, *4*(138), 138ra81. https://doi.org/10.1126/scitranslmed.3003876

Qiu, X., Fernando, L., Alimonti, J. B., Melito, P. L., Feldmann, F., Dick, D., … Jones, S. M. (2009). Mucosal immunization of cynomolgus macaques with the VSVDeltaG/ZEBOVGP vaccine stimulates strong ebola GP-specific immune responses. *PloS One*, *4*(5), e5547. https://doi.org/10.1371/journal.pone.0005547

Qiu, X., Fernando, L., Melito, P. L., Audet, J., Feldmann, H., Kobinger, G., … Jones, S. M. (2012). Ebola GP-Specific Monoclonal Antibodies Protect Mice and Guinea Pigs from Lethal Ebola Virus Infection. *PLoS Neglected Tropical Diseases*, *6*(3), e1575. https://doi.org/10.1371/journal.pntd.0001575

Qiu, X., Wong, G., Audet, J., Bello, A., Fernando, L., Alimonti, J. B., … Kobinger, G. P. (2014). Reversion of advanced Ebola virus disease in nonhuman primates with ZMapp. *Nature*, *514*(7520), 47–53. https://doi.org/10.1038/nature13777

Qiu, X., Wong, G., Fernando, L., Audet, J., Bello, A., Strong, J., … Kobinger, G. P. (2013). mAbs and Ad-Vectored IFN- Therapy Rescue Ebola-Infected Nonhuman Primates When

Administered After the Detection of Viremia and Symptoms. *Science Translational Medicine*, *5*(207), 207ra143-207ra143. https://doi.org/10.1126/scitranslmed.3006605

R Core Team. (2017). R: A Language and Environment for Statistical Computing. Vienna, Austria. Retrieved from https://www.r-project.org/

Raphael, I., Nalawade, S., Eagar, T. N., & Forsthuber, T. G. (2015). T cell subsets and their signature cytokines in autoimmune and inflammatory diseases. *Cytokine*, *74*(1), 5–17. https://doi.org/10.1016/j.cyto.2014.09.011

Riera Romo, M., Pérez-Martínez, D., & Castillo Ferrer, C. (2016). Innate immunity in vertebrates: an overview. *Immunology*, *148*(2), 125–139. https://doi.org/10.1111/imm.12597

Roels, T. H., Bloom, A. S., Buffington, J., Muhungu, G. L., Mac Kenzie, W. R., Khan, A. S., … Ksiazek, T. G. (1999). Ebola hemorrhagic fever, Kikwit, Democratic Republic of the Congo, 1995: risk factors for patients without a reported exposure. *The Journal of Infectious Diseases*, *179 Suppl*, S92-7. https://doi.org/10.1086/514286

Salmon-Ehr, V., Ramont, L., Godeau, G., Birembaut, P., Guenounou, M., Bernard, P., & Maquart, F. X. (2000). Implication of interleukin-4 in wound healing. *Laboratory Investigation; a Journal of Technical Methods and Pathology*, *80*(8), 1337–1343. Retrieved from http://www.ncbi.nlm.nih.gov/pubmed/10950124

Sanchez, a, Trappier, S. G., Mahy, B. W., Peters, C. J., & Nichol, S. T. (1996). The virion glycoproteins of Ebola viruses are encoded in two reading frames and are expressed

through transcriptional editing. *Proceedings of the National Academy of Sciences of the United States of America*, *93*(8), 3602–3607. Retrieved from http://www.pubmedcentral.nih.gov/articlerender.fcgi?artid=39657&tool=pmcentrez&rendertype=abstract

Saphire, E. O., Schendel, S. L., Fusco, M. L., Gangavarapu, K., Gunn, B. M., Wec, A. Z., … Dye, J. M. (2018). Systematic Analysis of Monoclonal Antibodies against Ebola Virus GP Defines Features that Contribute to Protection. *Cell*, *174*(4), 938–952.e13. https://doi.org/10.1016/j.cell.2018.07.033

Stan Development Team. (2013). *Stan Modeling Language User's Guide and Reference Manual*. Retrieved from http://mc-stan.org/

Stan Development Team. (2016). RStan: the R interface to Stan. Retrieved from http://mc-stan.org/

Sullivan, N. J., Geisbert, T. W., Geisbert, J. B., Xu, L., Yang, Z.-Y., Roederer, M., … Nabel, G. J. (2003). Accelerated vaccination for Ebola virus haemorrhagic fever in non-human primates. *Nature*, *424*(6949), 681–684. https://doi.org/10.1038/nature01876

Sullivan, N. J., Hensley, L., Asiedu, C., Geisbert, T. W., Stanley, D., Johnson, J., … Nabel, G. J. (2011). CD8(+) cellular immunity mediates rAd5 vaccine protection against Ebola virus infection of nonhuman primates. *Nature Medicine*, *17*(9), 1128–1131. https://doi.org/10.1038/nm.2447

Sullivan, N. J., Martin, J. E., Graham, B. S., & Nabel, G. J. (2009). Correlates of protective immunity for Ebola vaccines: implications for regulatory approval by the animal rule .

Nature Reviews.Microbiology, *7*(5), 393–400. https://doi.org/10.1038/nrmicro2129; 10.1038/nrmicro2129

Sullivan, N. J., Sanchez, A., Rollin, P. E., Yang, Z., & Nabel, G. J. (2000). Development of a preventive vaccine for Ebola virus infection in primates. *Nature*, *408*, 605–609.

Towner, J. S., Sealy, T. K., Khristova, M. L., Albariño, C. G., Conlan, S., Reeder, S. A., … Nichol, S. T. (2008). Newly discovered Ebola virus associated with hemorrhagic fever outbreak in Uganda. *PLoS Pathogens*, *4*(11), 3–8. https://doi.org/10.1371/journal.ppat.1000212

Tran, E. E. H., Nelson, E. A., Bonagiri, P., Simmons, J. A., Shoemaker, C. J., Schmaljohn, C. S., … White, J. M. (2016). Mapping of Ebolavirus Neutralization by Monoclonal Antibodies in the ZMapp Cocktail Using Cryo-Electron Tomography and Studies of Cellular Entry. *Journal of Virology*, *90*(17), 7618–7627. https://doi.org/10.1128/JVI.00406-16

Twenhafel, N. A., Mattix, M. E., Johnson, J. C., Robinson, C. G., Pratt, W. D., Cashman, K. A., … Honko, A. N. (2013). Pathology of experimental aerosol Zaire ebolavirus infection in rhesus macaques. *Veterinary Pathology*, *50*(3), 514–529. https://doi.org/10.1177/0300985812469636

Vogel, G., & Kupferschmidt, K. (2015). In setback for potential Ebola drug, company halts trial. Retrieved November 3, 2017, from http://www.sciencemag.org/news/2015/06/setback-potential-ebola-drug-company-halts-trial

Vu, H., Shulenin, S., Grolla, A., Audet, J., He, S., Kobinger, G., … Holtsberg, F. W. (2016). Quantitative serology assays for determination of antibody responses to Ebola virus

glycoprotein and matrix protein in nonhuman primates and humans. *Antiviral Research*, *126*, 55–61. https://doi.org/10.1016/j.antiviral.2015.11.012

Wang, H., Shi, Y., Song, J., Qi, J., Lu, G., Yan, J., & Gao, G. F. (2016). Ebola Viral Glycoprotein Bound to Its Endosomal Receptor Niemann-Pick C1. *Cell*, *164*(1–2), 258–268. https://doi.org/10.1016/j.cell.2015.12.044

Warren, T. K., Warfield, K. L., Wells, J., Swenson, D. L., Donner, K. S., Van Tongeren, S. A., … Bavari, S. (2010). Advanced antisense therapies for postexposure protection against lethal filovirus infections. *Nature Medicine*, *16*(9), 991–994. https://doi.org/10.1038/nm.2202

Warren, T. K., Wells, J., Panchal, R. G., Stuthman, K. S., Garza, N. L., Van Tongeren, S. a., … Bavari, S. (2014). Protection against filovirus diseases by a novel broad-spectrum nucleoside analogue BCX4430. *Nature*, *508*(7496), 402–405. https://doi.org/10.1038/nature13027

Watanabe, S., Takada, A., Watanabe, T., Ito, H., Kida, H., & Kawaoka, Y. (2000). Functional Importance of the Coiled-Coil of the Ebola Virus Glycoprotein. *Journal of Virology*, *74*(21), 10194–10201. https://doi.org/10.1128/JVI.74.21.10194-10201.2000.Updated

Weingartl, H. M., Embury-Hyatt, C., Nfon, C., Leung, A., Smith, G., & Kobinger, G. (2012). Transmission of Ebola virus from pigs to non-human primates. *Scientific Reports*, *2*, 811. https://doi.org/10.1038/srep00811

Wong, G., Richardson, J. S., Pillet, S., Patel, A., Qiu, X., Alimonti, J., … Kobinger, G. P. (2012). Immune parameters correlate with protection against ebola virus infection in rodents

and nonhuman primates. *Science Translational Medicine*, *4*(158), 158ra146. https://doi.org/10.1126/scitranslmed.3004582

World Health Organisation. (1978). Ebola haemorrhagic fever in Sudan, 1976. Report of a WHO/International Study Team. *Bulletin of the World Health Organization*, *56*(2), 247–270. https://doi.org/1978;56(2):247-270.

World Health Organization. (2003). Outbreak(s) of Ebola haemorrhagic fiver, Congo and Gabon, October 2001- July 2002. *Weekly Epidemiological Record*, *78*(26), 223–228.

World Health Organization. (2004). Ebola haemorrhagic fever in the Republic of the Congo - update 6. Retrieved November 30, 2017, from http://www.who.int/csr/don/2004_01_06/en/

World Health Organization. (2015). Reported deaths Data by country.

Xu, L., Sanchez, A., Yang, Z., Zaki, S. R., Nabel, E. G., Nichol, S. T., & Nabel, G. J. (1998). Immunization for Ebola virus infection. *Nature Medicine*, *4*(1), 37–42. Retrieved from http://www.ncbi.nlm.nih.gov/pubmed/9427604

Ye, J., Ma, N., Madden, T. L., & Ostell, J. M. (2013). IgBLAST: an immunoglobulin variable domain sequence analysis tool. *Nucleic Acids Research*, *41*(Web Server issue), W34-40. https://doi.org/10.1093/nar/gkt382

Younan, P., Iampietro, M., & Nishida, A. (2017). Ebola Virus Binding to Tim-1 on T Lymphocytes Induces a Cytokine Storm. *Mbio*, *8*(5), 1–20. https://doi.org/10.1128/mBio.00845-17

Zheng, X., Wong, G., Zhao, Y., Wang, H., He, S., Bi, Y., … Xia, X. (2016). Treatment with hyperimmune equine immunoglobulin or immunoglobulin fragments completely protects rodents from Ebola virus infection. *Scientific Reports*, *6*(1), 24179. https://doi.org/10.1038/srep24179

Zipeto, D., & Beretta, A. (2012). HLA-C and HIV-1: Friends or foes? *Retrovirology*, *9*, 1–9. https://doi.org/10.1186/1742-4690-9-39

CHAPTER: 8 ANNEX I: SUPPLEMENTARY FIGURES

8.1 Supplementary Figure 1

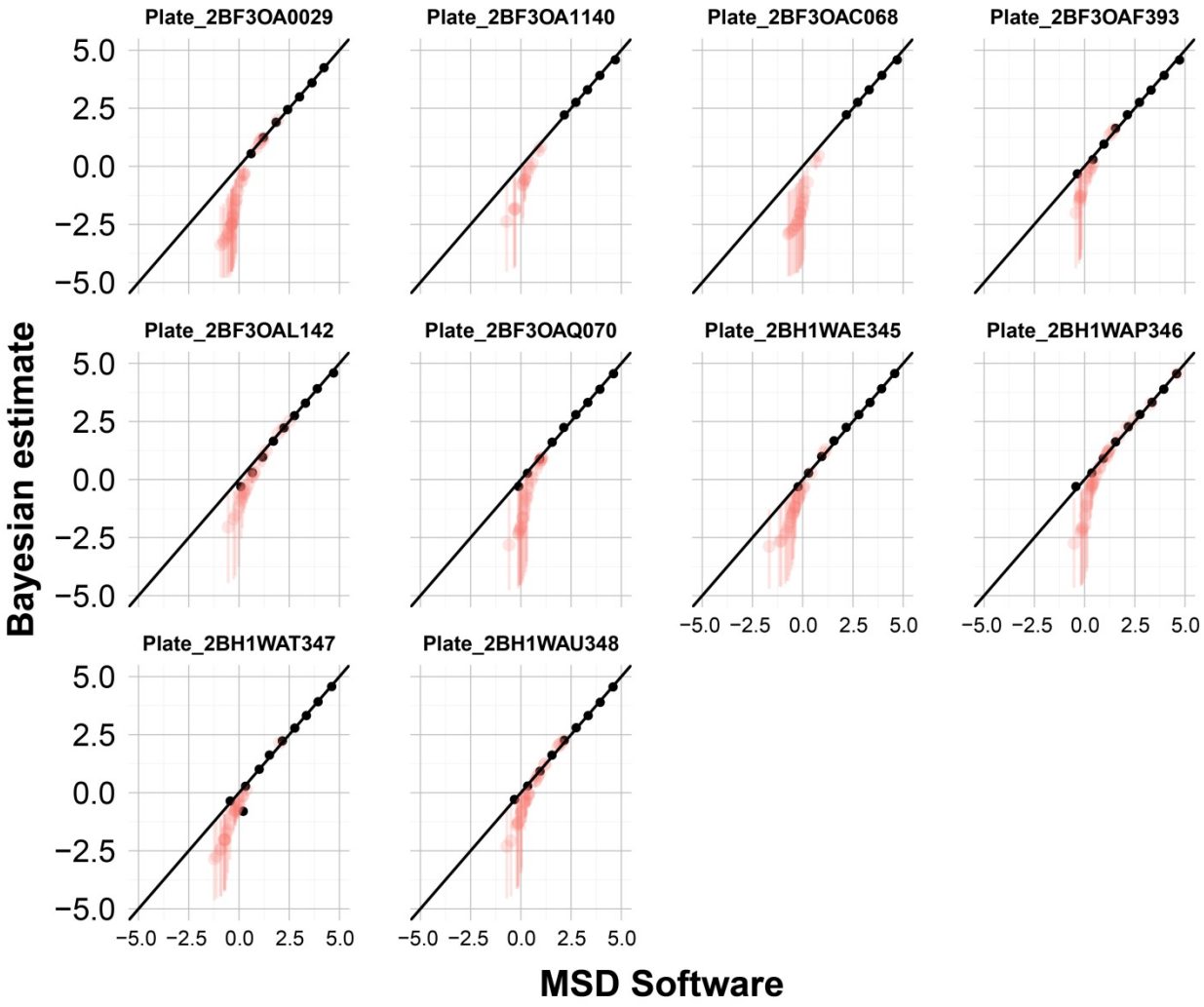

Correlation of the software-derived sample concentrations for IFN-γ and the estimates provided by the Bayesian model separated by plate. The red points are samples (with associated uncertainties) and the black points are standards. The black line represents the ridge along which both values are equal.

8.2 Supplementary Figure 2

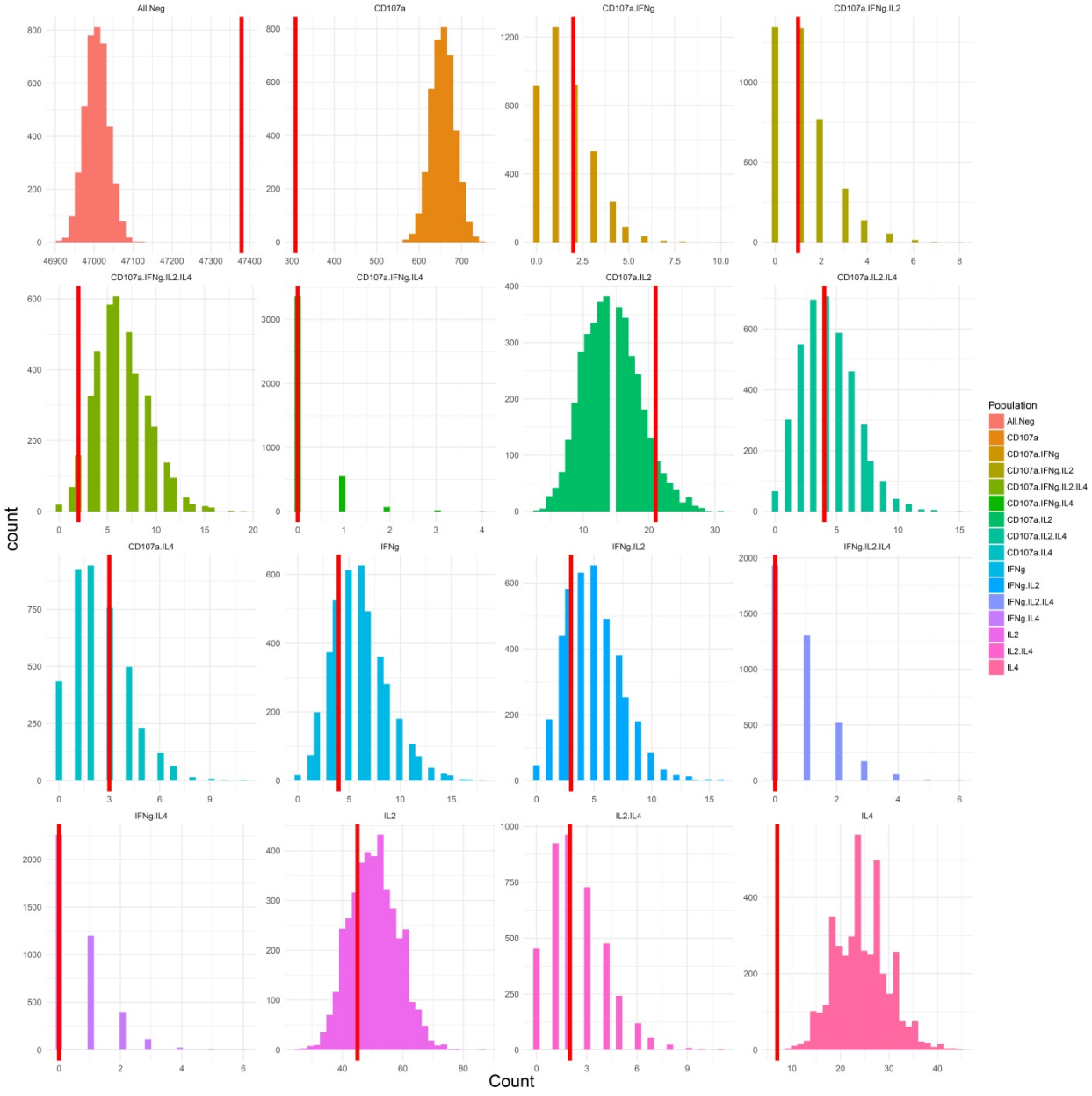

Posterior prediction of the count of positive cells for one of the samples analyzed. The posterior distribution of the group-level frequency estimate for each activation profile was used to simulate data for a specific animal from that group. The vertical red lines represent the count of each profile from this animal.